Experimental determination of field output factors and detector specific output correction factors in small fields of megavoltage radiotherapy beams

Casar, Božidar

Faculty of Science

Department of Physics

Božidar Casar

EXPERIMENTAL DETERMINATION OF FIELD OUTPUT FACTORS AND DETECTOR SPECIFIC OUTPUT CORRECTION FACTORS IN SMALL FIELDS OF MEGAVOLTAGE RADIOTHERAPY BEAMS

DOCTORAL DISSERTATION

Supervisors:

Assist. Prof. Dr. Slaven Jurković

Prof. Dr. Robert Jeraj

Zagreb, 2019

Sveučilište u Zagrebu

Prirodoslovno matematički fakultet

Fizički odsjek

Božidar Casar

EKSPERIMENTALNO ODREĐIVANJE FAKTORA POLJA I SPECIFIČNIH KOREKCIJSKIH FAKTORA ODZIVA DETEKTORA U MALIM POLJIMA MEGAVOLTNIH RADIOTERAPIJSKIH SNOPOVA

DOKTORSKI RAD

Mentori:

Doc. dr. Slaven Jurković

Prof. dr. Robert Jeraj

Zagreb, 2019

Information on supervisors

Dr. Slaven Jurković is a Head of Medical Physics Department at the Clinical Hospital Center Rijeka (http://kbc-rijeka.hr/radiofizika/?lang=en) and Assisstant Professor at the Faculty of medicine of University of Rijeka. He is also a member of Council of the Doctoral study of Physics at the University of Rijeka. Dr. Jurković is an author of over 25 published papers (https://bib.irb.hr/lista-radova?autor=254636). In the last ten years he leaded/coordinated six international projects funded by the International Atomic Energy Agency. He is also reviewer for Croatian Science Foundation and for several international scientific journal in the field of medical physics.

Dr. Robert Jeraj is a Professor of Medical Physics, Human Oncology, Radiology and Biomedical Engineering at the University of Wisconsin, Madison, where he leads the Imaging and Radiation Sciences Program at the University of Wisconsin Carbone Cancer Center. He is the Director of the Translational Imaging Research Program that oversees concept development, protocol design, and implementation of imaging in trials incorporating novel anti-cancer drugs, and the Director of the Wisconsin Oncology Network of Imaging eXcellence (WONIX), a regional clinical trial network that focuses on extensive imaging and molecular biomarker endpoints. Dr. Jeraj is also a Professor at the University of Ljubljana, Slovenia, where he leads a research group of medical physics. Among other duties, Dr. Jeraj is the chair of the Working Group on the Future of Medical Physics Research and Academic Training at AAPM, the largest medical physics organization, and a member of the Biomarker and Experimental Imaging Sciences Committees at ECOG-ACRIN, the largest cooperative clinical trials group in the USA. He also serves as a member of the Medical Imaging Drug Advisory Committee at Food and Drug Administration (FDA), USA, as a member of the External Advisory Board of the Metrology for Medical Physics Centre of the National Physics Laboratory (NPL), UK and a member of the International Advisory Board of the National Research Center for Radiotherapy (DCCC Radiotherapy), Denmark. Dr. Jeraj is an author of over 120 published papers, text books and book chapters, and is a frequent invited lecturer and presenter on the use of molecular imaging in therapeutic interventions and general applications of medical physics in radiation and medical oncology.

Moji dragi mami za vso ljubezen,
zaupanje in požrtvovalnost,
ter mojemu očetu za podporo,
ko sem jo najbolj potreboval.

Acknowledgments

This thesis would not have been accomplished without support, contribution, assistance, and encouragement from a number of colleagues and friends.

First of all, I would like to thank my supervisors, Assist. Prof. Slaven Jurković and Prof. Robert Jeraj, for their continuous support during the preparation and finalization of the thesis.

A special thanks go to my colleagues and friends, Dr. Eduard Gershkevitsh, Dr. Ignasi Mendez, and Prof. Saiful Huq. Without their support and contribution, this work would not have been completed. I would also like to thank my colleagues from the Institute of Oncology, Aljoša, David, and Denis, for their occasional assistance during the experimental part of this work.

Finally, I would like to express my gratitude to my daughter Larisa and my son Bine for giving the meaning to my life, and to all those who have enriched my life with their love and made my journey easier.

I dedicate this work also to my dear friend and first mentor in my professional career, Prof. Ervin Podgoršak, who showed me that the discipline toward our work should be one of our strongest guiding attributes.

Abstract of doctoral thesis

The goal of this work was to determine field output factors, $\Omega_{Q_{clin},Q_{ref}}^{f_{clin},f_{ref}}$, using EBT3 radiochromic films and W1 plastic scintillator as reference detectors on two different linear accelerators. Secondly, we aimed to provide a large and consistent set of data for detector specific output correction factors, $k_{Q_{clin},Q_{ref}}^{f_{clin},f_{ref}}$, for small static fields for seven solid state detectors and seven small ionization chambers. In the case of ionization chambers, $k_{Q_{clin},Q_{ref}}^{f_{clin},f_{ref}}$ were determined in two orientations – parallel and perpendicular, to test the hypothesis, that $k_{Q_{clin},Q_{ref}}^{f_{clin},f_{ref}}$ are lower and therefore advantageous for parallel orientation.

$\Omega_{Q_{clin},Q_{ref}}^{f_{clin},f_{ref}}$ were determined for 6 and 10 MV photon beams with and without flattening filter and for nine fields ranging from 0.5 x 0.5 cm^2 to 10 x 10 cm^2. Signal readings obtained with EBT3 radiochromic films and W1 plastic scintillator were fitted by an analytical function. $k_{Q_{clin},Q_{ref}}^{f_{clin},f_{ref}}$ were determined empirically for 14 clinically used small detectors, under the same experimental conditions.

It has been found that, for a given linear accelerator, $\Omega_{Q_{clin},Q_{ref}}^{f_{clin},f_{ref}}$ need to be determined for every combination of photon beam energy, filtration, and field size as the differences between them can be statistically significant ($p < 0.05$). Further, it has been demonstrated, that the parallel orientation of ionization chamber is advantageous over the perpendicular, which is an important contribution to the present international dosimetry protocol for small fields IAEA TRS-483. Use of two reference detectors for the determination of field output factors for small static fields in MV photon beams is a novel approach and has been justified in our thesis.

Large set of $k_{Q_{clin},Q_{ref}}^{f_{clin},f_{ref}}$ data for seven solid-state detectors and seven ionization chambers in four MV beams determined on two linear accelerators by a single group of researchers can be considered a valuable supplement to the literature and the IAEA TRS-483 dataset. Recommendation on the orientation of ionization chambers is the last significant outcome of our work.

Key words: W1 scintillator, EBT3 films, diodes, ionization chambers, small fields, field output factors

Sažetak doktorske disertacije

Uvod

Novi međunarodni protokol za dozimetriju uskih snopova fotona visokih energija (dalje mala polja) IAEA TRS-483 je objavljen prije nešto više od godinu dana. Njime su dane preporuke vezano za referentnu i relativnu dozimetriju malih polja, koje se temelje na vrlo opsežnim istraživanjima velikog broja istraživačkih grupa koje se bave dozimetrijom malih polja. Nedostatak izvornih podataka koji su objavljeni u protokolu je određena nekonzistentnost, odnosno njihova raspršenost, što je posebice navedeno i u samom dozimetrijskom protokolu TRS-483. One se očituju u načinu određivanja specifične veličine polja (posebno veličine najmanjih polja), korištenoj radnoj udaljenosti, dubini u vodi na kojoj se mjeri ili računa, te mjestu definiranja veličine polja (na površini fantoma ili na referentnoj dubini). Unatoč tome što je značajan broj istraživanja proveden korištenjem različitih vrsta detektora (diode, male i mikro ionizacijske komore, dijamantni detektori, plastični scintilacijski detektori, alanin i radiokromski filmovi) u objavljenim podacima često nedostaje odgovarajuća procjena nesigurnosti svakog od koraka u određivanju, kako faktora polja, tako i korekcijskih faktora.

U svrhu nadopune i poboljšanja protokola za dozimetriju malih polja postavljene su hipoteze doktorskog rada:

Hipoteza 1: Na temelju mjerenja pomoću referentnih detektora (plastični scintilacijski detektor i radiokromski film) i određivanja faktora polja moguće je eksperimentalno odrediti ukupne korekcijske faktore za diode i ionizacijske komore u uskim snopovima X-zraka visokih energija proizvedenih linearnim akceleratorima.

Hipoteza 2: Korekcijski faktori polja za male i mikro ionizacijske komore su manji ukoliko su određeni u tzv. paralelnoj orijentaciji ionizacijskih komora. Tako određeni faktori predstavljaju poboljšanje u odnosu na one određene u okomitoj orijentaciji ionizacijskih komora koja je preporučena u dozimetrijskom protokolu TRS-483.

Materijali i metode

Eksperimentlani dio rada je proveden u Ljubljani i Talinu na dva različita linearna akceleratora elektrona, Elekta Versa HD i Varian TrueBeam. Mjerenja na oba linearna akceleratora provedena su u megavoltnim snopovima X-zraka od 6 MV i 10 MV, s filterom (WFF) i bez filtera (FFF) za homogenizaciju snopa.

Mjerenja su provedena u izocentričnoj mjernoj postavi, na udaljenosti od fokusa do površine fantoma SSD = 90 cm. Detektori su bili postavljani na dubinu od 10 cm. Istraživanje je provedeno za devet polja zračenja od 0.5 × 0.5 cm^2 do 10 × 10 cm^2, s tim da je polje 10 × 10 cm^2 odabrano kao referentno polje za izračun faktora polja i za svaki detektor specifičnih korekcijskih faktora. Istraživanjem je obuhvaćeno 16 detektora: plastični scintilacijski detektor Exradin W1 (W1 PSD), radiokromski film EBT3, šest dioda (IBA SFD dioda, IBA Razor dioda, PTW 60008 Diode P, PTW 60012 Diode E, PTW 60018 Diode SRS i SN EDGE dioda), jedan dijamantni detektor (PTW 60019 microDiamond) i sedam malih ionizacijskih komora (IBA CC04, IBA Razor, PTW 31016 3D PinPoint, PTW 31021 3D Semiflex, PTW 31022 3D PinPoint, PTW 31023 PinPoint i SI Exradin A16). Svi detektori su odabarani sukladno preporukama danim u dozimetrijskom protokolu TRS-483 i na temelju njihove široke uporabe za relativnu dozimetriju. Kao referentni detektori odabrani su scintilacijski detektor (W1 PSD) i radiokromski film EBT3. Razlog za to je što su po svojim fizikalnim karakteristikama gotovo ekvivalentni vodi te pokazuju zanemarivu energijsku ovisnost. Pomoću njih su određeni faktori polja $\Omega_{Q_{clin},Q_{ref}}^{f_{clin},f_{ref}}$.

Uprosječeni odzivi $M_{Q_{clin}}^{f_{clin}}$ izmjereni filmom EBT3 i detektorom W1 PSD su korigirani za efekt volumnog usrednjenja k_{vol} i normirani na odziv $M_{Q_{ref}}^{f_{ref}}$ izmjeren u referentnom polju. Na taj način su određeni diskretni faktori polja $\Omega_{Q_{clin},Q_{ref}}^{f_{clin},f_{ref}}$ za mala polja koja se koriste klinički.

$$\Omega_{Q_{clin},Q_{ref}}^{f_{clin},f_{ref}} = \frac{M_{Q_{clin}}^{f_{clin}}}{M_{Q_{ref}}^{f_{ref}}} k_{vol}$$

Vrijednosti $\Omega_{Q_{clin},Q_{ref}}^{f_{clin},f_{ref}}$, određene na temelju mjerenja pomoću referentnih detektora, su usklađene pomoću analitičke funkcije koju su predložili Sauer i Wilbert:

$$\Omega(S_{clin}) = P_{\infty} \frac{S_{clin}^n}{l^n + S_{clin}^n} + S_{\infty}\left(1 - e^{-b \cdot S_{clin}}\right)$$

Za sve detektore i sva polja zračenja S_{clin} obuhvaćena ovim istraživanjem izračunate su diskretne vrijednosti specifičnih korekcijskih faktora:

$$k_{Q_{clin},Q_{ref}}^{f_{clin},f_{ref}}(S_{clin}) = \frac{\Omega_{Q_{clin},Q_{ref}}^{f_{clin},f_{ref}}}{M_{Q_{clin}}^{f_{clin}} / M_{Q_{ref}}^{f_{ref}}}$$

gdje $k_{Q_{clin},Q_{ref}}^{f_{clin},f_{ref}}(S_{clin})$ predstavlja ukupni korekcijski faktor za pojedini detektor u ovisnosti o veličini kliničkog polja S_{clin}.

Rezultati i rasprava

Faktori polja i korekcijski faktori $k_{Q_{clin},Q_{ref}}^{f_{clin},f_{ref}}$ za detektore obuhvaćene istraživanjem su prikazani kao analitičke funkcije te kao diskretne vrijednost. Utvrđeno je da su razlike u faktorima statistički značajne ($p < 0.05$). Zbog toga za svaki linearni akcelerator faktori malih polja trebaju biti eksperimentalno određeni za sve veličine polja i u svakoj od kombinacija snopa X-zraka sa i bez filtracije.

U slučaju dioda i dijamantnog detektora utvrđeno je da se vrijednosti $k_{Q_{clin},Q_{ref}}^{f_{clin},f_{ref}}$ za većinu najmanjih polja (< 1.5 cm) statistički značajno ($p < 0.05$) razlikuju od vrijednosti publiciranih u dozimetrijskom protokolu. Za PTW microDiamond detektor je utvrđena statistički značajna razlika ($p < 0.05$) za $k_{Q_{clin},Q_{ref}}^{f_{clin},f_{ref}}$ za sve snopove manje od 1.5 × 1.5 cm^2 proizvedene linearnim akceleratorom Elekta Versa HD. Na istom akceleratoru je utvrđena statistički značajna razlika između korekcijski faktora malih polja ovisno o tome je li snop filtriran ili nije. Kod istog detektora utvrđene su razlike u ovisnost $k_{Q_{clin},Q_{ref}}^{f_{clin},f_{ref}}$ i do 6% za nominalno jednake snopove na dva korištena linearna akceleratora. Isti trend je uočen i kod dioda, što ukazuje da različiti sustavi za kolimaciju snopa mogu značajno utjecati na veličinu korekcijskih faktora najmanjih polja $S_{clin} < 0.8$ cm.

U slučaju ionizacijskih komora, naši rezultati za korekcijske faktore polja $k_{Q_{clin},Q_{ref}}^{f_{clin},f_{ref}}$ su uspoređeni s podacima za tri ionizacijske komore istog tipa objavljenim u dozimetrijskom protokolu TRS-483. Vrijednosti korekcijskih faktora za ionizacijske komore IBA CC04, PTW 31016 PinPoint 3D i SI Exradin A16, dobivene u sklopu ovog istraživanja, potvrdile su vrijednosti objavljene u dozimetrijskom protokolu TRS-483. Publicirane vrijednosti za

$k_{Q_{clin},Q_{ref}}^{f_{clin},f_{ref}}$ su dobivene samo za okomitu orijentaciju ionizacijskih komora pa usporedba s našim rezultatima za $k_{Q_{clin},Q_{ref}}^{f_{clin},f_{ref}}$ dobivenim za paralelnu orijentaciju za spomenute tri ionizacijske komore nije bila moguća. Korekcijski faktori za ostale četiri ionizacijske komore IBA Razor IC, PTW 31021 3D Semiflex, PTW 31022 PinPoint 3D and PTW 31023 PinPoint, prikazani u ovom istraživanju, se mogu smatrati vrijednom nadopunom dozimetrijskog protokola TRS-483.

Nadalje, naši eksperimentalni podaci su potvrdili pretpostavku da su korekcijski faktori za ionizacijske komore manji ukoliko se mjerenje provodi tako da je glavna os ionizacijske komore postavljenja paralelno u odnosu na središnju os snopa (paralelna orijentacija), nego li kad je glavna os ionizacijske komore postavljena okomito na središnju os snopa (okomita orijentacija). Pošto su $k_{Q_{clin},Q_{ref}}^{f_{clin},f_{ref}}$ uvijek manji kod paralelne orijentacije statistička značajnost razlika je ispitana koristeći Studentov t-test. Ovisno o orijentaciji ionizacijske komore, utvrđena je statistički značajna razlika ($p < 0.05$) kod korekcijskih faktora $k_{Q_{clin},Q_{ref}}^{f_{clin},f_{ref}}$ za najmanja polje. Drugim riječima vrijednosti $k_{Q_{clin},Q_{ref}}^{f_{clin},f_{ref}}$ za najuže snopove X-zraka dobivene u okomitoj orijentaciji su u pravilu statistički značajno veće od onih dobivenih u paralelnoj orijentaciji. Jedinu iznimku predstavlja ionizacijska komora IBA CC04 kod koje nije utvrđena statistički značajna razlika kod $k_{Q_{clin},Q_{ref}}^{f_{clin},f_{ref}}$ u ovisnosti o orijentaciji ionizacijske komore niti u jednom od osam korištenih snopova X-zraka na dva linearna akceleratora. Razlog tome je što IBA CC04 ionizacijska komora ima približno jednake dimenzije efektivnog volume u dva ispitivana smjera (promjer šupljine je 4.0 mm, a njezina dužina u smjeru centralne elektrode je 3.6 mm) što rezultira priližno jednakim volumnim usrednjavanjem odziva u dvije orijentacije, koje u najvećoj mjeri doprinosi vrijednosti $k_{Q_{clin},Q_{ref}}^{f_{clin},f_{ref}}$. Vrijedi napomenuti da je za ionizacijsku komoru PTW 31021 Semiflex 3D utvrđena statistički značajna razlika vezana za orijentaciju samo kod najmanjeg polja zračenja (0.5×0.5 cm^2) u dva snopa X-zraka (10 MV WFF i FFF) linearnog akceleratora Elekta Versa HD dok to nije utvrđeno niti kod jednog od četiri snopa X-zraka linearnog akceleratora Varian TrueBeam. Stoga možemo zaključiti da i kod te ionizacijske komore, zbog njene konstrukcije, možemo očekivati približno jednaku vrijednost odziva u obje orijentacije.

Ukratko, vrijednosti korekcijskih faktora $k_{Q_{clin},Q_{ref}}^{f_{clin},f_{ref}}$ ionizacijskih komora obuhvaćenih ovim istraživanjem su bile manje u slučaju kada je ionizacijska komora bila postavljena na način da njena glavna os bude paralelna sa središnjom osi snopa X-zraka. Zbog toga preporučujemo da

se za određivanje korekcijskih faktora malih polja $k_{Q_{clin},Q_{ref}}^{f_{clin},f_{ref}}$ koristi paralelna orijentacija ionizacijskih komora, što je u suprotnosti s preporukom u dozimetrijskom protokolu TRS-483.

Zaključak

Primjena dva referentna detektora, EBT3 radiokromskog filma i W1 plastičnog scintilacijskog detektora, kao i primjena analitičke funkcije predstavljaju novi i potpuno opravdan pristup određivanju faktora polja uskih snopova X-zraka visokih energija, čime je potvrđena prva hipoteza. Nadalje, određen je značajan skup korekcijskih faktora $k_{Q_{clin},Q_{ref}}^{f_{clin},f_{ref}}$ za šest dioda, jedan dijamantni detektor te sedam ionizacijskih komora u po četiri snopa X-zraka različitih veličina polja zračenja na dva linearna akceleratora. To je napravljeno slijedeći stroge eksperimentalne zahtjeve pa se može smatrati vrijednom nadopunom recentnog dozimetrijskog protokola za dozimetriju malih polja TRS-483.

Nadalje, rezultati provedenog istraživanja vezani za određivanje korekcijskih faktora $k_{Q_{clin},Q_{ref}}^{f_{clin},f_{ref}}$ ionizacijskih komora, unatoč tome što su u suprotnosti s preporukama danim u dozimetrijskom protokolu TRS-483, potvrđuju našu drugu hipotezu. Dakle, korekcijski faktori $k_{Q_{clin},Q_{ref}}^{f_{clin},f_{ref}}$ su manji ukoliko se mjerenje ionizacijskom komorom provodi u paralelnoj orijentaciji. Zbog toga se mjerenje ionizacijskim komorama malog volumena u paralelnoj orijentaciji preporuča kao metoda izbora za određivanje korekcijskih faktora $k_{Q_{clin},Q_{ref}}^{f_{clin},f_{ref}}$. To također predstavlja važnu nadopunu dozimetrijskog protokola TRS-483 u kojem je preporučena isključivo okomita orijentacija ionizacijske komore za određivanje faktora polja.

Ključne riječi: dozimetrija malih polja, W1 scintilator, EBT3 film, diode, ionizacijske komore, faktori polja

TABLE OF CONTENTS

1 INTRODUCTION

1.1 Background and thesis rationale

Radiotherapy is one of the three main modalities for cancer treatment, the other two being surgery and systemic therapy with drugs, e.g., chemotherapy and hormonal drug therapy. The objective of radiotherapy is to deliver a lethal dose of ionizing radiation to tumor tissue while at the same time minimizing the dose to the surrounding normal tissues and organs at risk. To realize this objective, we need to precisely deliver required dose to the predefined target volume (tumor), which is one of the most important clinical tasks for medical physicists. To achieve this, we need to measure radiation, and we need to fully understand dosimetry methodology and its limitations. Many dosimetry protocols have been developed in the past for reference dosimetry in external radiotherapy and brachytherapy, including detail guidelines for dosimetric measurements, and remain a backbone for successful and predictive outcome of radiotherapy treatment.

The reference dosimetry of megavoltage (MV) photon beams used in conventional external radiotherapy using linear accelerators is currently based on various international dosimetry protocols, such as, TRS-398 Code of Practice (CoP)[1] published by the International Atomic Energy Agency (IAEA) and TG-51 protocol[2] with its Addendum[3] published by the American Association of Physicists in Medicine (AAPM). These protocols provide a guidance on clinical reference dosimetry using ionization chambers that have been calibrated in terms of absorbed dose to water in a reference beam of quality Q_0 (usually ^{60}Co) and reference field size 10×10 cm^2. Having a calibration coefficient of the ionization chamber one can determine the absorbed dose to water $D_{w,Q}$ in the beam quality Q under reference conditions following guidelines from those dosimetry protocols. Beam calibrations are done under conditions that are very close to the real situation of a conventional radiotherapy treatment, for example, 3D conformal radiotherapy, with respect to the field sizes as well as the calibration depth. In general, we can say that in conventional radiotherapy absorbed dose is determined for broad beams comparable to the size of clinically used radiation fields and at depth where charged-particle equilibrium exists.

In the last two decades, the availability and wide utilization of modern technologies has facilitated the use of radiotherapy techniques such as intensity modulated radiation therapy

(IMRT), volumetric modulated arc therapy (VMAT), stereotactic radiosurgery (SRS) and stereotactic body radiation therapy (SBRT) for the treatment of cancer patients using external beam radiation therapy. These techniques use many non-standard photon fields for the planning and delivery of the prescribed dose. Non-standard fields can be small and used for the treatment of small tumors e.g. in the case of SRS, or can be composed from many small fields for treatments of irregularly shaped larger lesions or tumors in the vicinity of organs at risk. Several dedicated treatment units such as and GammaKnife® (Elekta Instrument AB, Stockholm, Sweden), Tomotherapy® (Accuray, Sunnyvale, CA, USA) and CyberKnife® (Accuray, Sunnyvale, CA, USA), use small or composite fields for the delivery of complex radiotherapy treatments, although conventional linear accelerators (linacs) have very similar capabilities. In this respect, it should be noted that the IAEA TRS-398 or AAPM TG-51 and TG-51 Addendum protocols provided guidance for reference and relative dosimetry in conventional (broad) fields and do not provide guidance for dosimetry in small fields. Misunderstanding of this basic concept and its limitations, as well as the absence of a suitable dosimetry protocol for small fields resulted in the occurrence of dosimetric errors in clinical practice and several accidents and erroneous patient treatments involving the incorrect use of small fields were reported in the literature.[4,5] For example, use of too large ionization chamber resulted in incorrectly determined (too low) output factors for small fields and subsequently wrong calculation of number of monitor units, resulting in fatal outcomes. Already two decades ago, Das et al.[6] found difference up to 12% in output factors measured at different institutions for stereotactic photon fields having a size bellow 2.0 cm. All that has contributed to the publication of several documents on dosimetry of small MV photon beams: IPEM Report Number 103 published by the Institute of Physics and Engineering in Medicine,[7] formalism for small field dosimetry published by Alfonso et al.[8] and ICRU Report 91 published by the International Commission on Radiation Units and Measurements.[9] However, until the recent joint publication of the International CoP TRS-483 for reference and relative dosimetry of small static fields in external beam radiotherapy published by the IAEA and the AAPM,[10,11] no national or international guidance for performing reference and relative dosimetry in small fields was available to the practicing medical physicists.

New international dosimetry protocol for small fields TRS-483 provides several recommendations regarding the reference and relative dosimetry of small static fields for high energy photon beams up to 10 MV based on published data from research studies conducted until 2015.[12] However, we need to read and use the TRS-483 protocol with awareness of

difficulties with which were authors of this protocol confronted and were explicitly pointed out: *"Unfortunately, the published data are rather scattered for certain field sizes, especially for the smallest fields, and lack homogeneity with regard to the SSD or SDD used, the depth of measurement or calculation, the definition of field size at the surface or at a reference depth, etc."*[10] Although a considerable amount of research was done on small megavoltage photon beams using various types of detectors: diodes, small (sometimes denoted as mini) and micro ionization chambers, diamond detectors, plastic scintillators, alanine and radiochromic films, to mention only few, most of the published data also lack a proper estimation of the uncertainty in the various steps involved.[10] Those research efforts were not limited only to the necessary physical characterization of various detectors but were predominantly focused on the determination of field output factors and associated detector specific output correction factors, which are also central issues in the present thesis, since they are the most important dosimetric quantities in small field dosimetry. If output factors for small photon fields are not correctly determined and introduced in the treatment planning systems (TPS), serious complications can occur during radiotherapy treatments with unfavorable and even fatal outcome for patients.

To derive field output factors for small fields from the data published in the literature, TRS-483 considered three types of datasets. One of these datasets includes the reference detectors which are perturbation free except for volume averaging (the other two being detectors with known output correction factors and detectors with Monte Carlo calculated output correction factors). Main characteristics of these detectors are their near water equivalency, with radiological properties close to the corresponding values for water, which also have weak or negligible energy dependence in the MV radiotherapy photon beams. Examples are some passive detectors such as alanine and radiochromic films. The only commercially available active dosimeter with properties close to that of water and weak energy dependence is plastic scintillator detector. In our study, plastic scintillator and radiochromic film were utilized as reference detectors for the determination of field output factors.

Response of detectors in small fields and the determination of detector specific output correction factors has been extensively investigated for a range of detectors by several research groups, using one of the following three techniques: (i) empirical approach, where uncorrected signal ratios were determined and compared to the field output factors determined with reference detectors,[13–38] numerical approach, where output correction factors or chamber properties were determined with Monte Carlo (MC) simulations,[39–46] and (iii) semi-empirical approach which combines both, measurements and numerical/analytical calculations, and

where output correction factors were most commonly determined through the comparison of measured uncorrected detector's signal ratios with MC calculated field output factors.[47,48,49,50] There are advantages and disadvantages of each of these approaches.[51] However, since the numerical MC calculations have to be verified and validated with measurements, in this study an empirical (experimental) approach for the determination of field output factors using two reference detectors was used. Also detector specific output correction factors for a large number of different types of detectors were determined using an experimental approach following the guidelines from TRS-483.

Experimental determination of field output factors in small fields is challenging because detectors that can be used to accurately determine field output factors, without requiring corrections for non-water equivalency of their sensitive measuring volume and volume averaging due to their finite size, are presently not commercially available. Furthermore, for very small fields with dimensions below about 2.0×2.0 cm^2, small positional uncertainties can lead to significant uncertainties in the measurement results. This means that there are no ideal detectors for measurements of field output factors in small fields. Although a large amount of experimental and numerical data for field output factors and output correction factors for different detectors are available in the literature, there is considerable scatter of such data for the smallest field sizes; additionally, lack of homogeneity in the measurement set-up (SSD or SDD), the definition of field size and different procedures for positioning the detector in the central beam axis makes the interpretation of such data very challenging.[10]

1.2 Thesis hypotheses and objectives

Based on present theoretical knowledge on small field dosimetry, a formalism published in the TRS-483 Code of Practice, a lack of published data for field output factors and detector specific output correction factors for many detectors presently used in clinical dosimetry, especially for smallest fields below 1.0×1.0 cm^2 and 10 MV photon energy, among other issues, lead us to the two central hypothesis and subsequent objectives of our thesis.

HYPOTHESIS 1: Total detector specific output correction factors can be determined experimentally for solid state detectors and ionization chambers suitable for relative dosimetry in small fields, considering radiochromic films and plastic scintillator as reference detectors for the determination of field output factors in small megavoltage beams from linear accelerators.

The hypothesis was tested through the following two objectives:

Objective 1: to develop a novel empirical method for the determination of field output factors on two different linear accelerators for 6 and 10 MV photon beams with and without flattening filters using radiochromic films and plastic scintillators as reference detectors and to provide specific datasets for field output factors for nine square fields ranging from 0.5×0.5 to 10×10 cm^2 for all investigated beam energies. Since these two detectors are referred to as perturbation free, except for volume averaging,[10] later was studied in particular, aiming to develop an analytical approach for the calculation of corresponding volume averaging correction factors.

Objective 2: to provide a large set of data for detector specific output correction factors, based on the obtained field output factors from Objective 1, for seven solid state detectors and seven ionization chambers with small sensitive volumes, suitable for small field dosimetry. The purpose was to provide detector specific output correction factors in the form of an analytical function as well as in the form of discrete values based on the experimental data, using consistent measurement conditions and methodology and following the recommendations given in the TRS-483 and ICRU Report 91.[9] Such compilation of mostly unpublished data is considered as a valuable supplement to the literature and served to validate the data sets given in TRS-483.

HYPOTHESIS 2: Detector specific output correction factors for small and micro ionization chambers are smaller and therefore advantageous if they are determined for parallel orientation of the ionization chamber with respect to the beam axis compared to the perpendicular orientation as advised in the TRS-483 CoP.

This hypothesis was tested in one specific objective:

Objective 3: to obtain detector specific output correction factors for seven small and micro ionization chambers utilizing parallel orientation with respect to the beam axis, where an ionization chamber is positioned with its main axis parallel to the central axis of the beam. This approach does not follow the specific advice given in the TRS-483 where perpendicular orientation is recommended. We aimed to present comprehensive set of results along with statistical analysis and provide alternative and justified recommendation for the orientation of ionization chambers for the determination of output correction factors, and hopefully resolve the ambiguities and dilemmas on this particular challenging issues in small field dosimetry.

Throughout the study, the same experimental set-up was used for all measurements for all detectors, following the recommendations given in TRS-483. Field output correction factors and detector specific output correction factors, presented in analytical form in this study, may serve as a reference dataset for comparison with other studies, and for small fields not used explicitly in our measurements, considering similar or comparable experimental set-up and conditions.

1.3 Thesis outline

Chapter 1 provides a background of the thesis and presents some challenges in small field dosimetry of megavoltage photon beams, followed by the hypotheses and objectives of the thesis. Chapter 2 describes basic physics of small beams, while chapter 3 presents a TRS-483 formalism for relative and absolute dosimetry in small fields, which was applied in the thesis. A brief description of basic properties for five different types of detectors used in the study is given in chapter 4. Chapters 5, 6 and 7 cover original contribution of our work and encompass a description of the theoretical and experimental methodology and equipment used, a comprehensive report on the obtained results with subsequent analysis and comparison with the datasets from TRS-483. Final Chapter 8 presents a summary of our findings and provides recommendations on measurements of small field output factors and on the orientation of the ionization chambers in the megavoltage photon beams, among others.

The thesis is mainly based on the published paper Casar B, Gershkevitsh E, Mendez I, Jurković S, Huq MS. A novel method for the determination of field output factors and output correction factors for small static fields for six diodes and a microdiamond detector in megavoltage photon beams. *Med Phys*. 2018; https://doi.org/10.1002/mp.13318,[52] published presentation at conferences and unpublished work with small and micro ionization chambers.

2 BASIC PHYSICS OF SMALL FIELDS

There are three main physical conditions, which determine if a megavoltage (MV) photon beam can be considered as small:

i. a loss or lack of lateral charged-particle equilibrium (LCPE);
ii. partial occlusion of the primary radiation source by the machine collimating devices;
iii. the size of the detector is comparable to the field dimensions

First two conditions are beam related conditions, while the last one is detector related. If at least one of previous three conditions is fulfilled, an external megavoltage photon beam can be designated as small.

2.1 Beam related small field conditions

2.1.1 Loss of lateral charged particle equilibrium

In broad megavoltage photon beams charged particle equilibrium (CPE) exists in both directions, in longitudinal and in lateral. LCPE occurs since the number of charged particles exiting the sensitive volume (cavity) of the detector - *"out-scattering"* - is equal to the number of charged particles entering the sensitive volume (cavity) of the detector – *"in-scattering"*. Hence, *"out-scattering"* from the region of interest is compensated by the *"in-scattering"* toward the region of interest, which is illustrated in Figure 2.1 - A. However, if the photon beam is too small in its lateral dimension, out-scatter from the beam is not compensated by the in-scatter as shown in Figure 2.1 - B., leading to the violation of CPE.

Loss (or lack) of LCPE occurs when the half width or radius of the beam is equal to or smaller than the lateral range of the secondary electrons in the medium. Since the water collision kerma $K_{col,w}$ is equal to the absorbed dose to water D_w as long as CPE exists, ratio $D_w/K_{col,w}$ can be used as a measure of the degree of CPE. Relationship between $D_w/K_{col,w}$ and different nominal beam energies is presented in Figure 2.2. The minimum half width (radius) of the beam at which $K_{col,w} = D_w$ still holds is defined as the *lateral charge particle equilibrium range* $r_{LCPE}[cm]$ and is given in the TRS-483 by

$$r_{LCPE}[cm] = 8.369 \cdot TPR_{20,10}(10) - 4.382 \quad (2.1)$$

$TPR_{20,10}(10)$ is tissue-phantom ratio in water at depths of 20 and 10 g/cm^2, for a field size of 10×10 cm^2 and source-to-chamber distane of 100 cm used as the beam quality index.

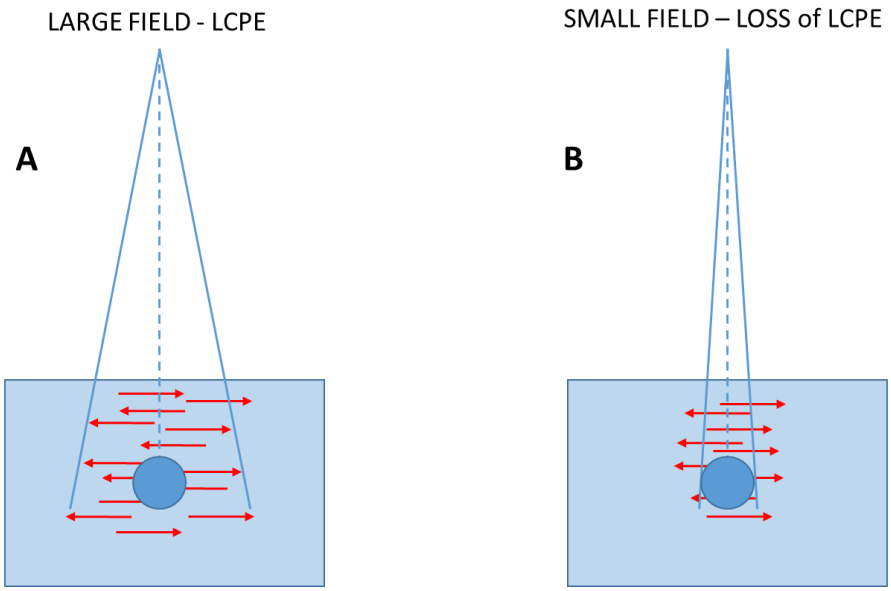

Figure 2.1. Drawing A: situation in large field where lateral charge particle equilibrium exists; drawing B: situation in small field, where loss (lack) of lateral charge particle equilibrium sets in. Lengths of arrows illustrate lateral range of charged particles r_{LCPE}.

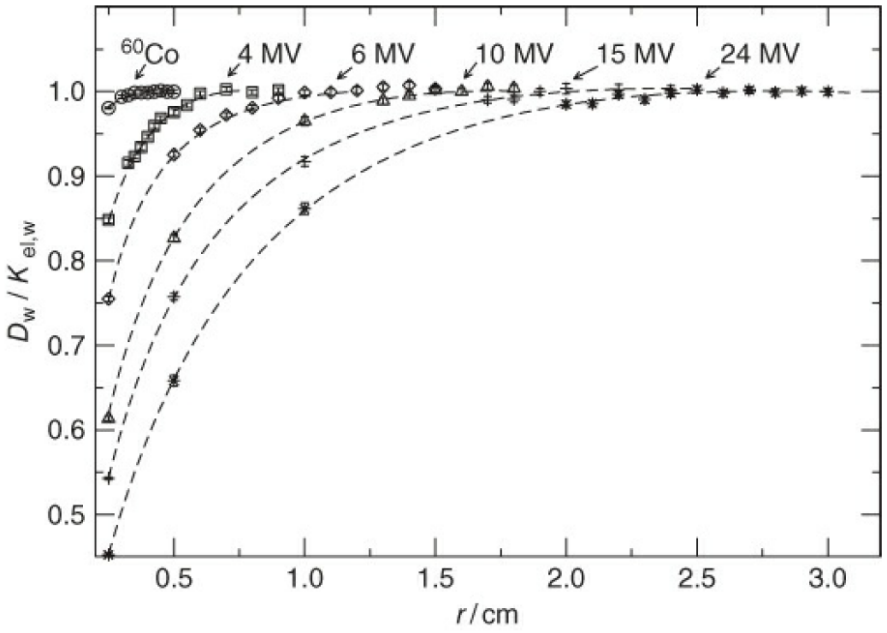

Figure 2.2. Ratios of dose-to-water to water-electronic kerma $D_w/K_{el,w}$ for various nominal beam energies and beam radii..[10] Arrows show the point where $D_w/K_{el,w}$ becomes lower than unity for particular energy and indicate the lateral charged particle equilibrium r_{LCPE} for that energy. Figure from P Andreo et al. Fundamentals of ionizing radiation dosimetry (2017).

It can be seen from Eq. (2.1) and Figure 2.2 that the loss of LCPE is more pronounced for beams having higher energies, meaning that the loss of LCPE occurs at larger field sizes for higher energies (in that case the electron ranges increase). An example: for 6 and 10 MV beams, which were used in our study, $TPR_{20,10}(10)$ values are 0.67 and 0.76 respectively, thus the corresponding values for r_{LCPE} are approximately 1.2 cm and 2.0 cm. We can conclude that in 6 MV beam small field, loss of LCPE exists for fields with diameter (width/length in the case of square fields) smaller than 2.4 cm, while in 10 MV beam the limiting field size (diameter) is around 4 cm. 6 and 10 MV beams were also used throughout the experimental part of the study.

2.1.2 Partial source occlusion

Partial source occlusion is related to the finite size of the primary photon source, denoted also as focal spot, which is created by a narrow electron beam coming from the flight tube of linear accelerator and impinging the target. In the target itself, photons are produced by the bremsstrahlung interactions. Since the effective size of the photon source is finite, it may become partially obscured by the field collimating system, viewed from the point of measurement in the phantom as shown in Figure 2.3. However, partial occlusion of the primary photon source becomes important only when the field size is comparable to the size of the focal spot, which is below 5 mm for modern clinical linear accelerators. Thus, partial source occlusion steps in at field sizes smaller than those where the loss of LCPE starts.

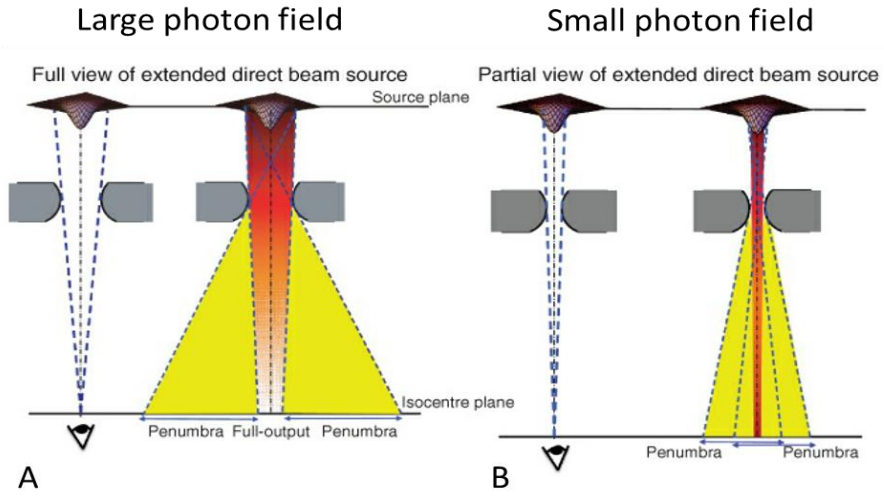

Figure 2.3. Illustration of the partial source occlusion. Left figure A presents the situation in a large photon beam where the source is not obscured by collimators. Figure B on the right shows the case of a small photon beam where the source occlusion exists and results in overlapping penumbrae. Adapted from Aspradakis et al.[7]

Partial source occlusion leads to the overlapping of penumbra resulting in lower beam output (Figure 2.4) In addition, apparent field widening occurs, meaning that there is a mismatch between nominal field size as defined by the collimator settings and true radiation field size defined at the full width half maximum (FWHM) of the lateral beam profile. True radiation field size can be significantly larger than the nominal field size, particularly for square small fields with dimensions below 1.0 × 1.0 cm^2. Both issues can have serious negative impact on radiotherapy treatments if the data required for the treatment planning systems (TPS) are not adequately obtained or have been incorrectly imported in the TPS. Moreover, since the definition of field size has not been unique in the past and was not explicitly reported in some of the research studies conducted in the last decade, published data are to some degree scattered with respect to the definition of the field size.

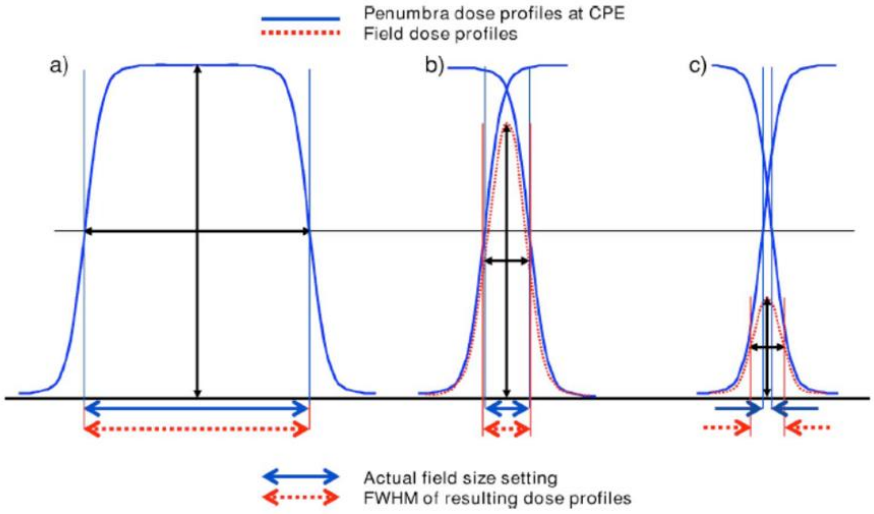

Figure 2.4. Effect of overlapping penumbrae on the true radiation field size (red color) in terms of FWHM and comparison with nominal field size marked with blue color. There is no effect neither on the field size nor on the field output for broad beams (left figure a); as the field becomes smaller, output becomes lower, however still without any significant difference between nominal and true radiation fields (middle figure b); significant decrease in beam output as well as pronounced difference between true and nominal fields is present in very small fields (right figure c). Figure from Das et al.[53]

2.2 Detector related small field conditions

There are two main issues related to the characteristics of the detector which cause incorrect response of the detector in small fields: volume averaging effect and the density of the detector's sensitive volume along with physical properties of extra-cameral components.

2.2.1 Volume averaging

When exposed to radiation, a detector produces a signal which is proportional to the average absorbed dose across its sensitive volume. If the size of the detector is comparable to the dimension of the high dose region of small field, the measured signal will be always lower than the true dose in the center of the field as if it would be measured with an ideal infinitesimally small point detector, which does not exist; the situation is illustrated in Figure 2.5.

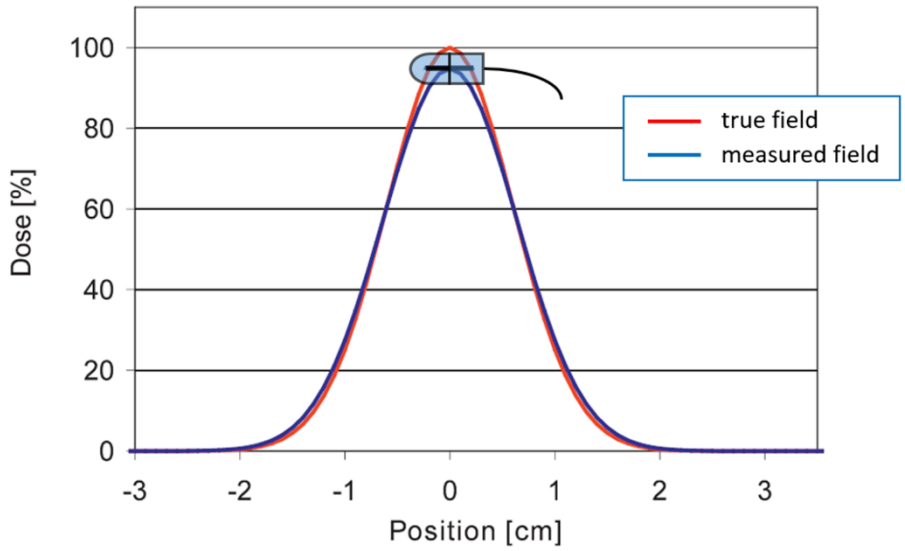

Figure 2.5. Schematic presentation of the volume averaging effect when an ionization chamber is placed in a small beam with comparable dimensions. Ionization chamber will not produce a signal proportional to the maximal dose in the center of the field. Instead, measured signal will be reduced with respect to the true dose due to the volume averaging effect over the portion of the beam that coincides with the sensitive volume of the chamber. Figure adapted from Wuerfel.[54]

The size of the detector leads, in general, to an under-response in small beams below 2.0×2.0 cm^2 due to volume averaging effect, since the size of presently available detectors is comparable the size of such small radiation field. Volume averaging effect can be considered as purely geometrical concept and thus dependent only on the shape and the size of the detector's sensitive volume and the size of small field. Volume averaging consideration will be thoroughly discussed later in the chapter Materials and methods.

2.2.2 Detector perturbation effects

In addition to the volume averaging, there are important issues related to the perturbation effects caused by the detector material and its overall constructional characteristics. Response of the detector depends strongly on the density of the detector's sensitive volume as well as on the

physical properties of the extra-cameral components such as wall, electrodes, stems, etc. Upon the detector's mass and electronic density, it can under or over respond caused by the difference in mass (or electronic) density with respect to water. In the case of high-Z materials, for instance, extra-cameral components can increase the response of the detector, since the number of electrons reaching the cavity (sensitive volume) is relatively higher than it would be in the case if those components would have physical properties same as water. It is especially important for solid-state detectors (silicon diodes and diamonds) which have higher mass density than water. On one hand, higher density of those detectors yields to higher signal to noise ratio, which is an advantage over small ionization chambers having air filled cavities. However, due to higher density of active volume and other components of solid-state detectors, an over response in small fields is usually observed, which requires corrections.

To summarize, volume averaging and perturbation effects can significantly influence the detector's response in small fields. Although the corrections of measured signal may add up to unity in some specific cases, for example, if the under response of the detector due to the volume averaging is equal to the over response due to higher detector's density Also, they strongly depend on the type of the detector used for measurements.

Therefore, volume averaging and perturbation effects are critical in the small field dosimetry and require corrections which can be considerably large as well as uncertain. Although the corrections of measured signal may add up to unity in some specific cases, for example, if the under response of the detector due to the volume averaging is equal to the over response due to higher detector's density, we need to understand basic physics of small fields and execute measurements with great care.

To minimize or eliminate correction factors related to the volume of the detector and its material we would need to use a detector having very small sensitive volume with density equal or close to that of water. Unfortunately, there is no such detector presently available on the market.

Another approach to by-pass the introduction of unacceptably large correction factors is to avoid small field conditions described. In that case, the size of the square field defined by FWHM has to fulfil the condition

$$FWHM \geq 2 \cdot r_{LCPE} + d \tag{2.2}$$

where r_{LCPE} is lateral charge particle equilibrium range as defined earlier, whilst d is the largest dimension of the detector's (ionization chamber) outer boundary as schematically shown in

Figure 2.6. Note, that in general, largest dimensions in longitudinal and radial directions are not necessarily equal. Since r_{LCPE} is rather large already for 6 MV beams - around 1.2 cm as shown earlier – small field condition from Eq. (2.2) is fulfilled only for field sizes larger than around 2.5×2.5 cm^2 even for the smallest ionization chambers presently available. Because there is a necessity to determine output factors for field sizes well below those that satisfy relation in Eq. (2.2), we are unavoidably confronted with small field dosimetry problems connected to the loss of LCPE and to the determination of accurate correction factors of measured signals using different detector types, which was one of the pivotal aims of our study.

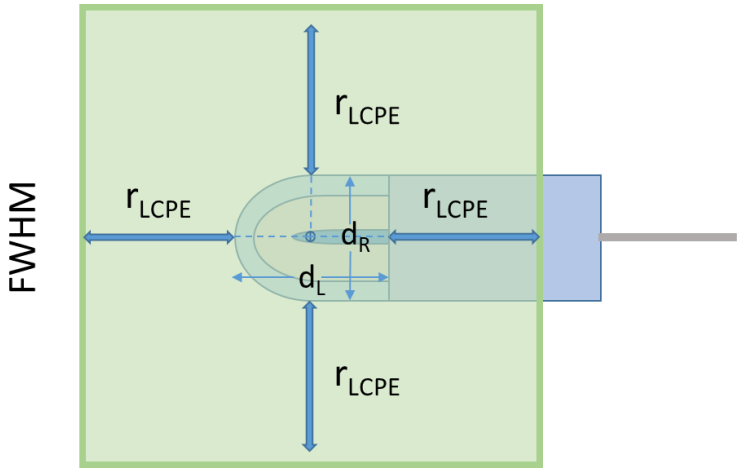

Figure 2.6. Schematic drawing (beam's eye view) of small field condition with respect to the lateral charged particle equilibrium (LCPE) and dimensions of the ionization chamber in this specific example. Small field conditions exist when the radiation field defined by full width half maximum (FWHM) extends at least a distance r_{LCPE} beyond the outer boundaries of the ionization chamber. Note, that in the above case longitudinal dimension d_L of the ionization chamber is larger than the radial dimension d_R, hence we need to consider d_R for the calculation of r_{LCPE}.

3 IAEA TRS-483 CoP FORMALISM FOR REFERENCE AND RELATIVE DOSIMETRY

The IAEA TRS-483 CoP provides guidelines for reference and relative dosimetry in small static fields used in radiotherapy. In addition to the recommendation on the characteristics of detectors suitable for reference and relative dosimetry, as well as on required measurement conditions, TRS-483 presents a dosimetry formalism based on the work of Alfonso et al.,[8] some aspects are presented in the following sections in particular the guidance for the determination of field output factors and detector specific output correction factors in small fields which were two key elements in our work.

3.1 Reference dosimetry of small fields

The formalism for reference dosimetry in the TRS-483 is the same to that recommended by Alfonso et al.[8] with some minor modifications. Several important definitions for field sizes were introduced in the new formalism:

f_{ref} – conventional reference field 10 cm × 10 cm used for calibrations at the standard laboratory and for clinical reference dosimetry for radiotherapy machines where such field can be established in reference conditions i.e., SAD = 100 cm and 10 cm depth

f_{msr} – machine specific reference field for radiotherapy treatment units where conventional reference field 10 cm × 10 cm cannot be established e.g., GammaKnife®, Tomotherapy®, and CyberKnife®. The *msr* field is usually the largest achievable field as close as possible to the size of the conventional reference field

f_{clin} – clinical small radiation field at which we need to determine the absorbed dose to water

The formalism is based on the use of an ionization chamber and allows three different approaches depending on the type of calibration coefficient provided by the standard laboratory for the ionization chamber and beam quality for which a calibration coefficient is available.

3.1.1 Chamber calibrated specifically for the f_{msr}

If the user has a calibration coefficient of an ionization chamber measured for the f_{msr}, the absorbed dose to water at the reference depth z_{ref} in water in the absence of the ionization chamber is given by:

$$D_{w,Q_{msr}}^{f_{msr}} = M_{Q_{msr}}^{f_{msr}} \cdot N_{D,w,Q_{msr}}^{f_{msr}} \tag{3.1}$$

where $M_{Q_{msr}}^{f_{msr}}$ is the reading of the ionization chamber in the user's beam under the reference conditions corrected for environmental and other influencing quantities, while $N_{D,w,Q_{msr}}^{f_{msr}}$ is the calibration coefficient in terms of absorbed dose to water obtained at the machine specific reference beam quality Q_{msr} and machine specific reference field size f_{msr}. This is the preferred approach, however, only few standard laboratories provide calibrations of ionization chambers in the user's reference field f_{msr} and beam quality Q_{msr}.

3.1.2 Chamber calibrated for a conventional reference field, with generic beam quality correction factor available

Usually, the standard laboratories measure calibration coefficient of an ionization chamber in a reference beam quality (in most cases ^{60}Co) and a conventional reference field 10 cm × 10 cm. In that case, the absorbed dose to water in the absence of the ionization chamber is given by:

$$D_{w,Q_{msr}}^{f_{msr}} = M_{Q_{msr}}^{f_{msr}} \cdot N_{D,w,Q_0}^{f_{ref}} \cdot k_{Q_{msr},Q_0}^{f_{msr},f_{ref}} \tag{3.2}$$

where $M_{Q_{msr}}^{f_{msr}}$ is the reading of the ionization chamber in the user's beam under the reference conditions corrected for environmental and other influencing quantities, while $k_{Q_{msr},Q_0}^{f_{msr},f_{ref}}$ is the beam quality correction factor to correct for the difference between the response of ionization chamber in a conventional reference calibration field f_{ref} and beam quality Q_0 used in the standard laboratory and the response in the machine specific reference field f_{msr} and user's beam quality Q_{msr}.

3.1.3 Chamber calibrated for a conventional reference field, without generic beam quality correction factor available

In this case, a third approach has to be followed and the absorbed dose to water for the f_{msr} and Q_{msr} is given by

$$D_{w,Q_{msr}}^{f_{msr}} = M_{Q_{msr}}^{f_{msr}} \cdot N_{D,w,Q_0}^{f_{ref}} \cdot k_{Q,Q_0}^{f_{ref}} \cdot k_{Q_{msr},Q}^{f_{msr},f_{ref}} \tag{3.3}$$

Most of the radiotherapy treatment units that cannot realize 10 cm × 10 cm reference field can realize the f_{msr} substantially above the limits which define conditions for small fields as defined in Eq. (2.2). Therefore, $k_{Q_{msr},Q}^{f_{msr},f_{ref}}$ correction factors are close to unity with the exception of GammaKnife® machine which can presently generate only beams up to 18 mm in diameter.

3.1.4 Conventional linear accelerators

In our study, we have investigated properties of small fields on conventional linear accelerators which can form reference field 10 cm × 10 cm. In this case, the machine specific reference field is equal to the conventional reference field, $f_{msr} = f_{ref}$. Substituting all indices *msr* with indices *ref*, Eq. (3.2) reduces to the formalism from TRS-398,

$$D_{w,Q_{ref}}^{f_{ref}} = M_{Q_{ref}}^{f_{ref}} \cdot N_{D,w,Q_0}^{f_{ref}} \cdot k_{Q_{ref},Q_0}^{f_{ref},f_{ref}} \tag{3.4}$$

Further omission of the redundant indices f_{ref} and ref, yields to

$$D_{w,Q} = M_Q \cdot N_{D,w,Q_0} \cdot k_{Q,Q_0} \tag{3.5}$$

which is the same equation for the determination of absorbed dose to water under the reference conditions as it is used in the TRS-398 dosimetry protocol.[1]

3.2 Relative dosimetry of small fields

IAEA TRS-483 provides general recommendations regarding the detectors suitable for relative dosimetry of small fields emphasizing that there is no ideal detector for measurements in small fields. Also, recommendations on suitable phantoms and set-up are provided in details. Particular attention is given to the orientation of various point detectors with respect to the central beam axis. For example, for measurements of lateral beam profiles, a general rule is that detector is oriented with its smallest dimension of active volume perpendicular to the scanning direction, which is not always possible. For ionization chambers, it is advised to orient chamber with its stem parallel to the central beam axis to minimize stem effect. Recommendations on possible orientations of an ionization chamber and a solid-state detector with respect to the central beam axis are given in Table 3.1 for measurements of lateral beam profiles and the determination of field output factors. Figures 3.1 - A and B provide a graphical illustration of

suitable orientation for ionization chambers and solid-state detectors (diodes and diamond detector).

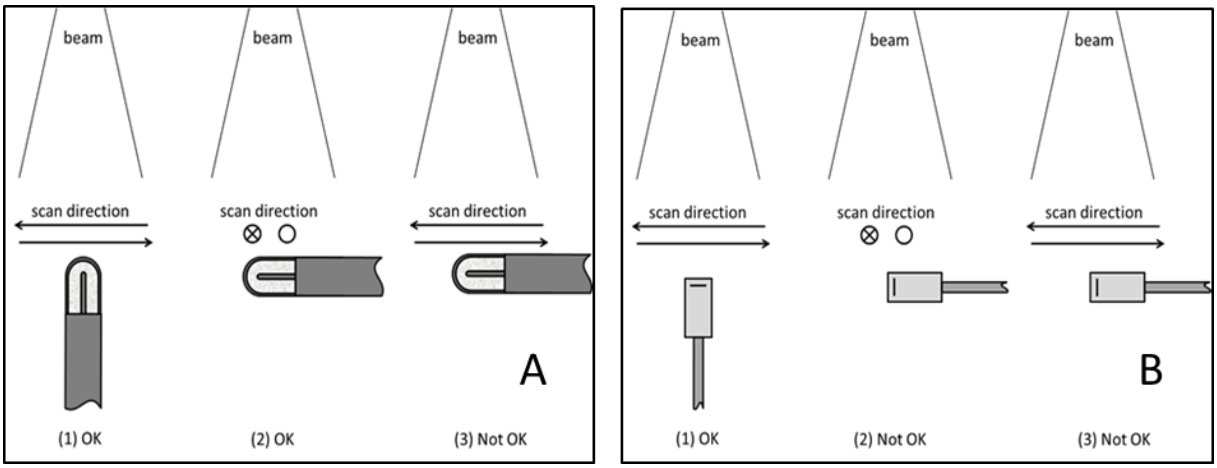

Figure 3.1. Recommended detector orientations for measurements of lateral beam profiles: Left drawing A for ionization chambers and right drawing B for solid-state detectors (diodes and diamond detector). Figure adapted from TRS-483.[10]

Table 3.1 Advised detector orientation, with respect to the central beam axis in small photon fields. Table adapted from TRS-483.[10]

Detector type	Detector's geometrical reference	Lateral beam profiles	Field output factors
Cylindrical micro ionization chamber	Axis	Parallel or Perpendicular	Perpendicular
Silicon shielded diode	Axis	Parallel	Parallel
Silicon unshielded diode	Axis	Parallel	Parallel
Diamond detector	Axis	Parallel	Parallel
Radiochromic film	Axis	Perpendicular	Perpendicular

3.3 Field output factors and detector specific output correction factors

In the relative dosimetry of large fields, the quotient of the absorbed dose in a clinical field f_{clin} and the absorbed dose in a reference field f_{ref} is termed as *total scatter factor ($S_{c,p}$)* or *relative dose factor (RDF),* or sometimes simply as *output factor* (*OF).* It is usually approximated by the ratio of detector readings $M_Q(f_{clin})$ and $M_Q(f_{ref})$ in clinical and reference field respectively as

$$OF(f_{clin}) = \frac{D_{w,Q}(f_{clin})}{D_{w,Q}(f_{ref})} \approx \frac{M_Q(f_{clin})}{M_Q(f_{ref})} \tag{3.6}$$

The approximation is based on the fact that stopping power ratios and perturbation factors are practical constant with field size, for large fields, at a given photon beam energy.

In the case of small fields, this does not hold true anymore, since the perturbation factors and volume averaging effects depends considerably on the field size, on the detector type, size, and its material and on the type of accelerator which was discussed in the previous chapter. Using the notation from TRS-483, it is necessary to apply the exact definition of output factor as a dose ratio in two fields, f_{clin} and f_{msr}

$$\Omega_{Q_{clin},Q_{msr}}^{f_{clin},f_{msr}} = \frac{D_{w,Q_{clin}}^{f_{clin}}}{D_{w,Q_{msr}}^{f_{msr}}} \tag{3.7}$$

The symbol $\Omega_{Q_{clin},Q_{msr}}^{f_{clin},f_{msr}}$ called *field output factor* is introduced at this point, to emphasize that it is not identical to the conventional *OF* (or *RDF* or $S_{c,p}$). As the $\Omega_{Q_{clin},Q_{msr}}^{f_{clin},f_{msr}}$ is not equal to the dose ratio between detector readings $M_{Q_{clin}}^{f_{clin}}$ and $M_{Q_{msr}}^{f_{msr}}$ in clinical and machine specific reference fields, the ratio of readings is multiplied by a proportionality factor called *output correction factor* $k_{Q_{clin},Q_{msr}}^{f_{clin},f_{msr}}$, or more appropriately, *detector specific output correction factor*, leading to the final expression for field output factors in small fields as defined in the TRS-483

$$\Omega_{Q_{clin},Q_{msr}}^{f_{clin},f_{msr}} = \frac{M_{Q_{clin}}^{f_{clin}}}{M_{Q_{msr}}^{f_{msr}}} \cdot k_{Q_{clin},Q_{msr}}^{f_{clin},f_{msr}} \tag{3.8}$$

Combining Eqs. (3.6) and (3.7) we can write down the general equation for detector specific output correction factors $k_{Q_{clin},Q_{msr}}^{f_{clin},f_{msr}}$ as

$$k_{Q_{clin},Q_{msr}}^{f_{clin},f_{msr}} = \frac{D_{w,Q_{clin}}^{f_{clin}} / M_{Q_{clin}}^{f_{clin}}}{D_{w,Q_{msr}}^{f_{msr}} / M_{Q_{msr}}^{f_{msr}}} \tag{3.9}$$

In principle, $k_{Q_{clin},Q_{msr}}^{f_{clin},f_{msr}}$ depends on many factors such as the perturbation of particle fluence and volume averaging effects, in particular, on the field size, detector type, and the design, size, and non-water equivalency of most of the detectors.

Similar as we did in section 3.1, we can modify Eqs. (3.8) and (3.9) in the case of conventional linear accelerators, which can realize reference field 10 cm × 10 cm, by substituting *msr* indices with *ref*, yielding to simplified expressions for field output factor

$$\Omega_{Q_{clin},Q_{ref}}^{f_{clin},f_{ref}} = \frac{M_{Q_{clin}}^{f_{clin}}}{M_{Q_{ref}}^{f_{ref}}} \cdot k_{Q_{clin},Q_{ref}}^{f_{clin},f_{ref}} \tag{3.10}$$

and detector specific output correction factor

$$k_{Q_{clin},Q_{ref}}^{f_{clin},f_{ref}} = \frac{D_{w,Q_{clin}}^{f_{clin}} / M_{Q_{clin}}^{f_{clin}}}{D_{w,Q_{ref}}^{f_{ref}} / M_{Q_{ref}}^{f_{ref}}} \tag{3.11}$$

for this specific case. Since we have conducted our experimental part of the study on conventional linear accelerators, the last two equations are most relevant for our study.

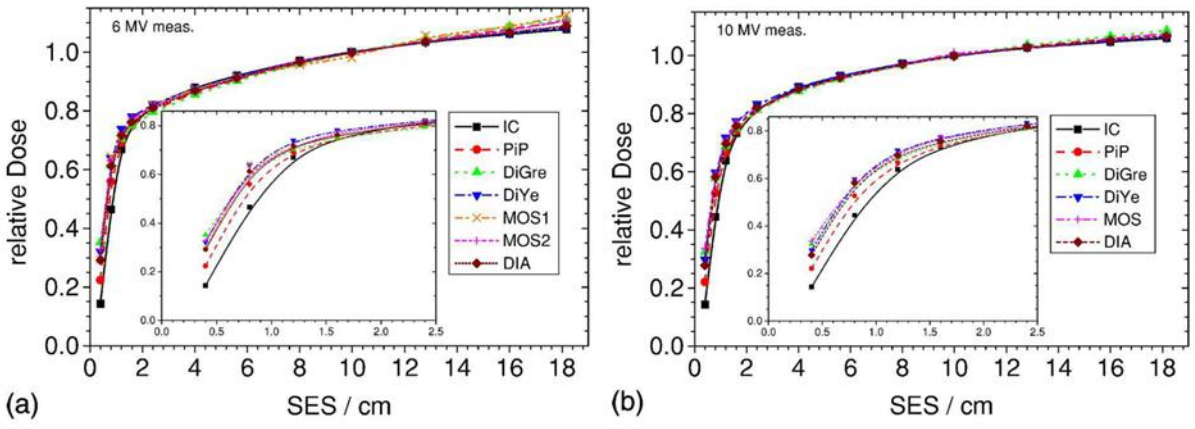

Figure 3.2. Measured uncorrected dose in 6 (a) and 10 MV (b) beams for different detectors normalized to 10 cm × 10 cm reference field, fitted by an analytical function. SES denotes side of equivalent square field. Figure from Sauer and Wilbert.[13]

The fact is, that field output factors decrease rapidly with decreasing field size, most notably for field sizes below 2.0 cm × 2.0 cm, which is shown in Figure 3.2. from one of the

early experimental studies by Sauer and Wilbert.[13] They have experimentally determined output factors for several detectors in 6 and 10 MV beams and fitted the data by an analytical function. Although the study was conducted before new small field dosimetry formalism has been published by Alfonso et el., there are already some similarities to the TRS-483 formalism in the approach by Sauer and Wilbert.

Lastly mentioned study was of particular importance for our work since we have applied the analytical function proposed by Sauer and Wilbert for the determination of field output factors based on the measurements performed with two reference detectors, the approach which will be presented in detail in the fifth chapter Methods and materials.

While there are several known factors that influence the field output factors and detector specific output correction factors discussed earlier in chapter 2, it is also of interest to know whether $\Omega_{Q_{clin},Q_{ref}}^{f_{clin},f_{ref}}$ and $k_{Q_{clin},Q_{ref}}^{f_{clin},f_{ref}}$ depend also on the way the field is collimated on the linear accelerator (e.g., using multileaf collimator - MLC or jaws) and whether $k_{Q_{clin},Q_{ref}}^{f_{clin},f_{ref}}$ significantly depend on the orientation of the ionization chamber in small photon fields. These issues were also investigated in the experimental part of our study and are addressed and discussed in the continuation of the thesis.

4 DETECTORS FOR RELATIVE SMALL FIELD DOSIMETRY

Several detector types have been used in the past for relative small beam dosimetry, including cylindrical ionization chambers, silicon diodes, diamond detectors, plastic or organic scintillators, radiographic and radiochromic films, metal oxide semiconductor field-effect transistor detectors (MOSFET), thermoluminescent dosimeters (TLD), alanine, to mention some of them. Detector choice for small field dosimetry can be made considering three main rules:[10]

(i) The detector has a small active volume to minimize volume averaging effect. In the ideal case, the detector should sample the fluence at a point

(ii) The detector is water equivalent, i.e., it is constructed of materials which minimize perturbation effects

(iii) The detector has a linear response which is energy independent or with clearly known energy dependence

Presently there is no commercially available ideal detector, which would fulfill all key conditions outlined above. In the following sections, the most important characteristics of five different detector types will be shortly presented, since those detectors were used in our study for the determination of field output factors $\Omega_{Q_{clin},Q_{ref}}^{f_{clin},f_{ref}}$ and detector specific output correction factors $k_{Q_{clin},Q_{ref}}^{f_{clin},f_{ref}}$ in small beams as defined in the previous chapter.

4.1 Cylindrical ionization chambers

While in general there are two different types of air-filled ionization chambers, parallel-plate and cylindrical (thimble), we limit our description to the last type only since cylindrical ionization chambers have been proven as most suitable for clinical reference dosimetry.

Cylindrical ionization chambers are the most frequently used type of detector in radiotherapy. They have been a backbone of clinical dosimetry for decades and all present reference dosimetry protocols,[1,2,3] based on the determination of absorbed dose to water, rely on the measurements using ionization chambers.

An ionization chamber is composed by an air-filled cavity surrounded by a conductive outer wall having a central collecting electrode in the middle of the cavity on the chamber's axis as schematically shown in Figure 4.1. The wall usually consists of graphite and polymethylmethacrylate (PMMA), while the central electrode is commonly made of aluminum although some chambers have a graphite or steel electrode. To minimize leakage current, outer electrode (wall) and central electrode are separated by an insulator. Most widely used cylindrical ionization chambers is that of Farmer type having 0.6 cm^3 active volume. While Farmer-type ionization chamber is not suitable for relative dosimetry of small fields due to its large volume, it is still a gold standard in conventional radiotherapy dosimetry, in particular for absolute calibration of megavoltage beams from linear accelerators in terms of dose to water.

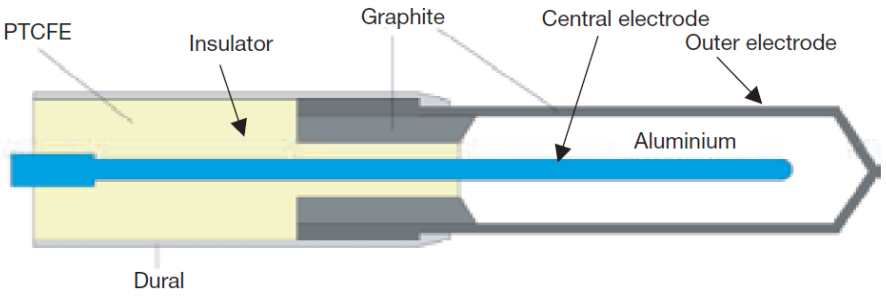

Figure 4.1. Schematic drawing of a cylindrical Farmer-type ionization chamber showing its basic components and materials. Figure from E.B.Podgorsak, Radiation Oncology Physics: A handbook for teachers and students (2005).

Principles of operation are following: when a suitable polarizing voltage is applied to the chamber which is exposed to radiation, air in the chamber's cavity becomes ionized. Positive ions are attracted to the negative electrode (cathode) and the negative electrons to the positive electrode (anode) causing a flow of electrical current which is measured by an electrometer and is proportional to the released charge. Operating voltage range typically from 100 to 800 V depends on the type of the ionization chamber, most frequently from 300 to 400 V. If the applied voltage is to low, some of the electrons and ions may recombine before they reach electrodes. In that case, a collection of ions and electrons is incomplete, and we need to correct the electrometer's reading by the recombination correction factor. A formalism from the IAEA TRS-398 CoP can be applied for the determination of absorbed dose to water after correcting measured charge for environmental and other influencing quantities.

Instead of Farmer-type chambers, several small vented air ionization chambers and microchambers of a volume of 0.01 – 0.3 cm^2 have been designed specifically for dosimetry measurements in small fields. Smaller ionization chambers exhibit smaller volume averaging effect. However, signal to noise ratio might be a limiting factor for clinical use of a chamber having very small active volume. Even if some ionization chambers have extremely small active volume, for example below 0.01 cm^3, we cannot consider them as a point detector; there is always a small field under which a volume averaging would be unacceptable large, leading to a high under response at very small fields.

While small and micro ionization chambers might have a slightly different design compared to the Farmer-type chambers, their basic components and operational characteristics are similar.

4.2 Silicon diodes

Silicon diodes are widely used radiation detectors for clinical dosimetry. The diodes are produced in two types as p-type and n-type diode depending on the lightly doped base silicon substrate. Since n-type diode is more affected by the radiation damage, only p-type diode is suitable for clinical dosimetry. Figure 4.2 shows a schematic drawing of a p-type diode as well as the related x-ray image.

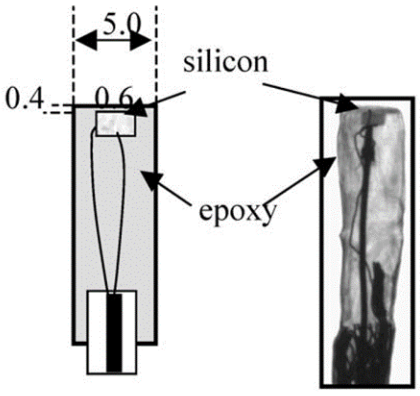

Figure 4.2. Schematic drawing (left) and x-ray image (right) of an IBA SFD unshielded silicon diode. Dimensions shown in the figure are in mm. Figure from McKerracher and Thwaites.[55]

One of the main advantages of diode detector over ionization chamber is its higher sensitivity, i.e., better signal to noise ratio. Considering the energy needed to produce an ion pair in silicon and in the air (3.6 eV for silicon versus 34 eV for air), and the difference in their

densities (2.3 g/cm^3 for silicon versus $1.23 \cdot 10^{-3}$ g/cm^3 for air), silicon diode will produce close to 18000 higher signal than an air-filled ionization chambers of the same volume. That brings us to the second significant advantage of diodes – they can be made very small. Indeed, commercially available diodes have very small active volumes which are at least two or three orders of magnitude smaller than the corresponding volumes (air cavities) in micro and mini ionization chambers (see Tables 5.1 and 5.2 in chapter Methods and materials), which makes them pertinent for relative small field dosimetry.

However, an important disadvantage of diodes is their energy dependence; they over-respond to low energy scattered photons due to high mass energy absorption coefficient ratio $(\mu_{en}/\rho)_{Si,w}$ of silicon ($Z_{Si} = 14$) relative to that of water ($Z_{eff,w} = 7.42$), as shown in Figure 4.3. The absorption coefficient ratio $(\mu_{en}/\rho)_{Si,w}$ increases significantly at low photon energies exhibiting a peak around 20 keV.

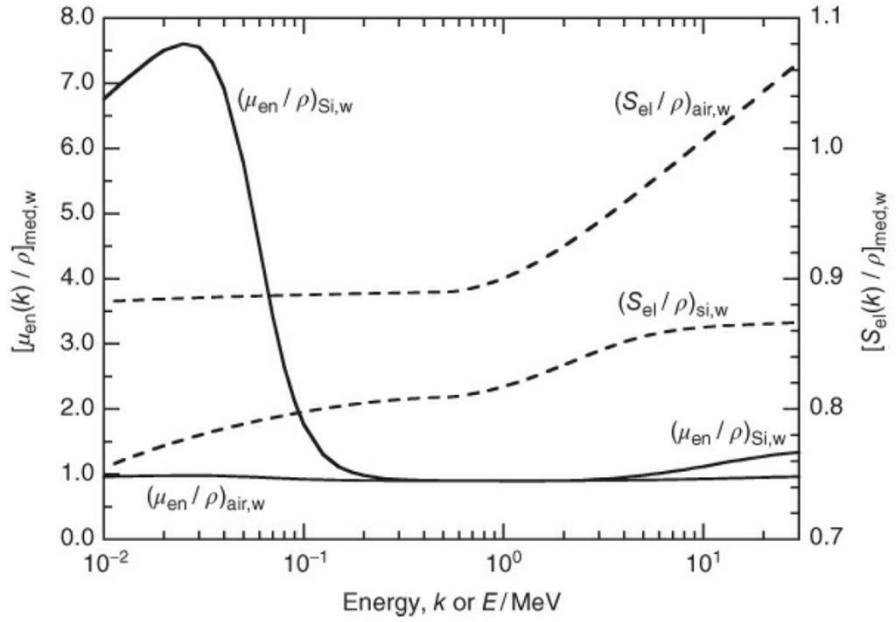

Figure 4.3. Ratios of mass energy absorption coefficients μ_{en}/ρ and electron stopping powers S_{el}/ρ for silicon and air relative to water.

Over-response of diodes is their important characteristic in large fields, while in small fields, where the amount of low energy photons is reduced, over-response becomes less significant. To absorb some of the low energy photons, several silicon diodes are energy compensated, i.e., their sensitive volume is shielded with high-density material. However, such shielded diodes have an unwanted effect in small fields, where the scattered radiation is

reduced, and the amount of low energy photons becomes very low. Namely, the presence of high-density material increases the fluence of secondary electrons in the silicon, resulting in over-response of diodes in small fields. Therefore, for measurements in small fields, unshielded diodes without metallic shielding are recommended.[10]

4.3 Synthetic micro diamond detector

Synthetic micro diamond is one of the newest detectors suitable for small field dosimetry. Presently, the only commercially available synthetic diamond detector is PTW 60019 microDiamond (PTW, Freiburg, Germany) shown in Figure 4.4. Its properties are similar to those of silicon diodes such as high sensitivity (7000 times higher response compared to the air filled ionization chamber of the same size) and small size of the active volume. However, micro diamond detector has one important advantage over silicon diodes: since the mass absorption coefficient ratio of diamond to water $(\mu_{en}/\rho)_{C,w}$ is nearly constant over a wide range of photon energies, micro diamond detector is nearly energy independent and does not suffer from over-response to low energy photons as silicon diodes.

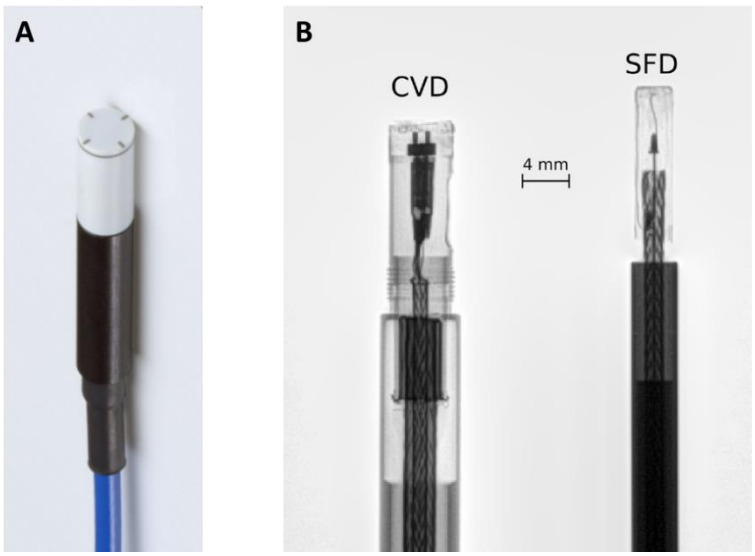

Figure 4.4. Photo of a PTW 60019 microDiamond detector (A) and digital x-ray image of micro diamond and one of the smallest silicon diode presently on the market, IBA SFD (B). Figure B is adapted from Larraga-Gutierrez et al.[56]

The micro diamond detector consists of a single crystal layer of 1 μm thickness and 2.2 mm in diameter, yielding a sensitive volume of around 0.004 mm^3, which is the smallest

active volume among presently available detectors used in small field dosimetry. It is embedded in RW3 solid water (PTW, Freiburg, Germany) housing, filled with epoxy raisins. In principle, the detector operates as a Schottky diode with a zero external bias voltage, similar as in the case of silicon diodes.

Despite small dimensions of sensitive layer, volume averaging effect can play an important role in a very small fields below 1.0 × 1.0 cm^2, since the diameter of sensitive volume becomes comparable to the field dimensions, which may require non-negligible correction of measured signals.

Excellent physical characteristics of micro diamond detector have attracted several research groups to investigate its behavior in small megavoltage beams.[35,44,48,56–58,59,60] While there is a large number of publications on this subject, there is no definite consensus on the behavior and response of micro diamond detector in a very small fields below 1.0 × 1.0 cm^2. Presently it is still an interesting topic and a matter of debate.[44,24] Micro diamond detector and its response in small fields is discussed in detail also in the present thesis.

4.4 Radiochromic film

Radiochromic film is a two-dimensional radiation detector. Presently, the most widely used type of radiochromic film is Gafchromic EBT3 film, schematically shown in Figure 4.5. It consists of an active layer with nominal thickness of 28 μm sandwiched between two matte polyester sheets with a thickness of 125 μm each. Such film structure makes the film symmetric, with the same response regardless of the utilized orientation. The composition of EBT3 film is shown in Table 4.1 by elemental composition.

Figure 4.5. Schematic drawing of Gafchromic EBT3 film components.

Table 4.1 Elemental composition and effective atomic number Z_{eff} of Gafchromic EBT3 film

Composition of EBT3 Gafchromic film [%]					
H	Li	C	O	Al	Z_{eff}*
38.4	0.1	43.7	17.7	0.2	6.71

Radiochromic films have three important strengths which make them suitable for dose measurements in radiation fields with steep dose gradients, and in particular for dosimetry in small fields of megavoltage photon beams where we have lack (loss) of lateral charged particle equilibrium:

i. They have very weak energy dependence in clinical megavoltage photon beams.[61,62]
ii. Their composition is near water (tissue) equivalent.[63]
iii. They have very high spatial resolution, resolving details of at least 25 μm or even smaller

Also, radiochromic film does not require physical, chemical or thermal post-irradiation processing which is an advantage compared to the conventional radiographic films. It develops by itself, due to polymerization of the active layer of the film. As a result of polymerization induced by radiation, the film changes color and can be analyzed using the software after being scanned by a flatbed scanner. However, since the color changes due to polymerization is a slow process, it takes time to complete development – typically 24 hours.

Radiochromic films are less sensitive than radiographic films. However their wide dynamic range from 0.2 to 10 Gy (for EBT3 type), makes them suitable for many applications in clinical dosimetry. They are almost insensitive to visible light and can be immersed in water. Since they exhibit some sensitivity to UV light and temperature, they need to be appropriately stored in boxes in a room with stable and controlled temperature, although no temperature corrections are needed.

Unlike many other radiotherapy dosimeters, radiochromic film has non-linear dose-response which should be corrected for. Therefore a calibration procedure is required before measurements. For the calibration purpose, a set of films is irradiated with known doses to obtain a calibration or sensitometric curve for the subsequent determination of doses for particular clinical dosimetry measurements.

4.5 Plastic scintillator

Plastic scintillators are relatively new detectors used in clinical radiotherapy, although scintillation dosimetry has been known for a long time. First commercially available plastic scintillator is Exradin W1 plastic scintillating detector (W1 PSD) manufactured by Standard Imaging (Standard Imaging, Middleton, WI, USA).

The W1 PSD is made of scintillating polystyrene fiber enclosed by an acrylic scintillator housing as shown in Figure 4.6. The physical density of plastic scintillating fiber is 1.05 g/cm^3, with a sensitive volume of 1 mm in diameter and 3 mm in length. When exposed to radiation, atoms in the scintillating fiber excite. The scintillation light produced in the active volume of the detector is guided through a 3 m long optical fiber to a photodetector (photodiode).

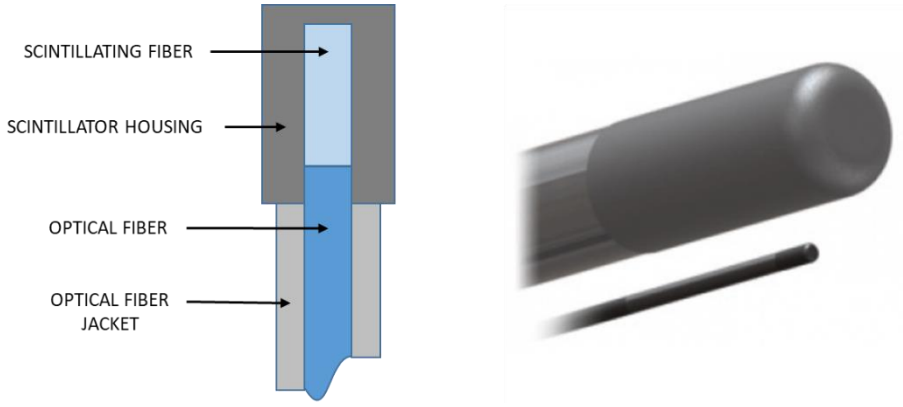

Figure 4.6. Schematic drawing (left) and a photo (right) of a plastic scintillator detector Exradin W1.

Photodetector splits up the light (photons in the visible part of the spectrum) into two components: green which is mainly scintillating light, and blue, mainly produced by Čerenkov radiation. Optical output is converted into electrical signal which can be measured with suitable electrometer as collected charge in two separate channels. For the elimination of unwanted Čerenkov part of the signal, two channel electrometer is commonly used. Such configuration allows automatic correction for the Čerenkov part of the signal. Alternative approach is to use two electrometers, each for one of the output channels; in that case, contribution of Čerenkov radiation has to be calculated manually, providing that preliminary calibration has been performed.[64]

5 MATERIALS AND METHODS

5.1 Experimental set-up

Dosimetry measurements were performed at two hospitals on two different state of the art linear accelerators, Elekta Versa HD™ (Elekta AB, Stockholm, Sweden) and Varian TrueBeam™ (Varian Medical Systems, Palo Alto, CA), using high-energy photon beams of 6 and 10 MV. Beams with flattening filters (WFF) as well as flattening filter free (FFF) beams, denoted hereafter as 6 MV WFF, 6 MV FFF, 10 MV WFF, and 10 MV FFF, were used for all measurements. The measurement geometry consisted of an isocentric set-up with a source-to-surface (SSD) distance of 90 cm, a depth of 10 cm and gantry at 0°. For each point measurement, 100 MU were delivered, for nine square fields with nominal side lengths of 0.5, 0.8, 1.0, 1.5, 2.0, 3.0, 4.0, 5.0 and 10.0 cm. The 10 × 10 cm^2 field size was used as the reference field size for the calculation of field output factors and detector specific output correction factors. At least three measurements were taken for each specific set-up unless otherwise specified. For all point measurements in water, a reference class PTW Unidos^{webline} (PTW, Freiburg, Germany) electrometer was used throughout the study.

In this study, the dose response of 16 types of detectors was investigated. These consisted of a plastic scintillator Exradin W1 (Standard Imaging, Middleton, WI, USA), radiochromic film EBT3 (Ashland Inc., Wayne, NJ, USA), seven solid-state detectors, i.e., six diodes and a synthetic micro diamond detector, and seven ionization chambers, i.e., detectors which are commercially available, in regular clinical use and recommended in the TRS-483 CoP as suitable for small field dosimetry. For the solid-state detectors and ionization chambers, the same detectors with the same serial numbers were used for measurements on both linacs; EBT3 films from two different lots were used for measurements in the two linacs. The Exradin W1 plastic scintillator detector (W1 PSD) and the EBT3 film detectors were considered as the reference detectors and were used for the determination of an analytical function for field output factors. Based on this analytical function, detector specific output correction factors for the seven solid-state detectors and seven ionization chambers were obtained in the form of an analytical function and as discrete values.

A 3D water phantom (Blue Phantom 2, IBA Dosimetry, Schwarzenbruck, Germany) was used for the measurements in the first center on an Elekta Versa HD linac for all detectors

except for the EBT3 films, for which RW3 Solid Water phantom (PTW Freiburg, Freiburg, Germany) in the form of 30 × 30 cm^2 slabs were used. Radiation fields were shaped with MLC in cross-line (x) direction and with jaws in the in-line (y) direction.

For all detectors, except for EBT3 films, an MP3-M water phantom (PTW, Freiburg, Germany) was used for measurements in the second center equipped with a Varian TrueBeam linac. For EBT3 films, 30 × 30 cm^2 slabs of Virtual Water (Standard Imaging, Middleton, WI, USA) were used. To match the nominal field sizes on Varian TrueBeam with those on the Elekta Versa HD, radiation fields on Varian TrueBeam were collimated using the linac jaws in both axes, x and y.

5.2 Radiochromic films EBT3

Weak energy dependence,[61,62] near water-equivalence,[63] and high spatial resolution are the most important properties of radiochromic films, that justify their use as a reference detector for relative dosimetry in small fields in MV photon beams. However, since uncertainties in data obtained using films can become significant from mishandling of films, careful handling of films is crucial to obtain meaningful and accurate results. A strict protocol for film dosimetry was therefore followed throughout this study, from film cutting to final scanning considering various corrections related to radiochromic film dosimetry.[65,66]

5.2.1 Film preparation and irradiation

Gafchromic EBT3 films from lot 04071601 were used for measurements on Elekta Versa HD linac and from lot 06291702 on Varian TrueBeam linac. From each lot, two films were employed for calibration. Each calibration film was cut into seven strips with dimensions 20.32 × 3.5 cm^2. One strip was left unexposed; the other six were irradiated with a 6 MV WFF beam. Calibration strips cut from both films were irradiated with 50, 100, 150, 200, 250, 300, 350, 400, 450, 500 (two pieces) and 600 MU on Elekta Versa HD, and with 60, 120, 180, 240, 300, 360, 420, 480, 540, 600 (two pieces) and 720 MU on Varian TrueBeam. Field sizes of 25 × 25 cm^2 were used to expose them with homogenous doses.

Field output factors were measured with three pieces of films for each combination of field size and photon beam. In total, 108 pieces of films (i.e., four photon beams times nine fields times three measurements) were irradiated on each linac. To reduce film uncertainties,[67] central doses were kept to about 2 Gy or higher than that for all fields. On Elekta Versa HD, films were

irradiated with 500 MU for field output factor measurements, while on Varian TrueBeam linac they were irradiated with 600 MU. The difference in MU reflects the fact that Elekta linac was calibrated isocentrically (1 cGy/MU at source-to-surface distance SSD = 90 cm, and depth 10 cm), while Varian linac was calibrated at the depth of maximum ionization (1 cGy/MU at SSD = 100 cm, depth d_{max}). Latter also explains the selection of MU for calibration films. Five unexposed films were also scanned to apply lateral corrections. The orientation of all films (i.e., calibration strips, films employed for field output factor measurements and unexposed films) were marked to ensure consistency in scanning.

5.2.2 Scanning

To reduce uncertainties, all films were scanned prior to and following irradiation. An Epson Expression 10000XL (Seiko Epson Corporation, Nagano, Japan) flatbed scanner was used for measurements made on the Elekta linac, while an Epson Expression 11000XL was used for measurements made on the Varian linac. Scanners were warmed up for at least 30 minutes before readings. A frame, cut out from a transparency sheet was employed to place films in a reproducible and centered position on the scanner. Whenever there was a gap between the frame and the film pieces along the axis parallel to the lamp, it was closed with idle film pieces to minimize the cross-talk effect.[68] Before acquisitions and after long pauses, five empty scans were taken to stabilize the lamp. Each reading was repeated five times, and the first scan was discarded. Scans were made in reflection mode and portrait orientation. Images were acquired with Epson Scan v3.49a software in 48-bit RGB mode (16 bit per channel) with processing tools turned off, and saved as TIFF files. Resulting images were obtained as the average of repeated scans. To correct for inter-scan variations, every film was scanned together with an unexposed calibration strip. Calibration films and field output factor film pieces were scanned with 50 dpi and 150 dpi resolution, respectively. Lateral corrections were derived from the unexposed films and the calibration strips.

5.2.3 Dose calculation and field dimensions

Doses were computed using the Multigaussian model[69] for radiochromic film dosimetry implemented in Radiochromic.com v3.0,[70] after applying lateral and inter-scan corrections. Data analysis was carried out with the R statistical computing environment.[71]

For each film, field dimensions along x and y directions were determined from measurements of the full width at half maximum (FWHM), and central doses as the mean of

the dose values in a circular region of interest (ROI) drawn in the central part of the irradiated field with a diameter of 0.5 mm. The center of the irradiated field was defined as the center of the dose profiles in both directions. Since central doses and field dimensions were calculated from measurements made on three different film pieces for each field, the final results were taken as the average of these three measurements.

5.3 Equivalent square small field size S_{clin}

Nominal field sizes were converted to the equivalent square small field sizes S_{clin} for each field following the approach originally suggested by Cranmer-Sargison et al.,[72] used by other authors[37] and adopted by TRS-483 according to

$$S_{clin} = \sqrt{A \cdot B} \tag{5.1}$$

where A corresponds to the radiation field width (FWHM) in the in-line direction y and B (FWHM) for the cross-line direction x perpendicular to the former. S_{clin} has the same meaning as FS_{eff} in the original work by Cranmer-Sargison et al. Radiation field widths A and B were determined from EBT3 film measurements as described earlier, and have been applied for all detectors used in the study. In the present study, A and B correspond to the field widths defined by the FWHM at the measurement depth of 10 cm.

Applicability of the expression for equivalent square small field size S_{clin} is conditional,[10] meaning that A and B have to fall within the limits as follows

$$0.7 < \frac{A}{B} < 1.4 \tag{5.2}$$

Since in general, measured field sizes defined by FWHM could be rectangular even if they are nominally square as it was the case in our study, especially for smallest fields. Fulfillment of this condition was checked for all investigated field sizes.

5.4. Exradin W1 plastic scintillator

W1 PSD has radiological properties similar to EBT3 films with densities close to the values of water and belongs to the group of reference detectors, which are perturbation free except for volume averaging.[10] Near water equivalency and small dimensions makes W1 PSD suitable for relative dosimetry in small fields and thus was used as the second reference detector for the present study in combination with EBT3 films.[25,64,73,74,75]

The scintillator signal is contaminated with Čerenkov radiation, produced in the active volume of the scintillator and in the optical fiber, which needs to be corrected for. The most practical and widely used method for correcting the Čerenkov signal is spectral discrimination technique which is considered as an accurate and adequate method for removing Čerenkov signal/light.[76,77] This method was also adopted in the present study.

In the present study, W1 PSD axis was always oriented parallel to the beam axis. The Čerenkov calibration procedure recommended by the manufacturer, Standard Imaging, for small-field measurements, based on the method described by Morin et al.[78] and adopted by others, [25,35,79,80] was followed in the present study.

Čerenkov light ratio (CLR) coefficient, needed for correction of the scintillator signal, was calculated as

$$CLR = \frac{M_{max,10}^{Ch1} - M_{min,10}^{Ch1}}{M_{max,10}^{Ch2} - M_{min,10}^{Ch2}} \tag{5.3}$$

where superscripts *Ch1* and *Ch2* stand for measured charge *M* with first and second channel respectively. With PTW Unidos^{webline} electrometer we measured scintillation signal (green light) in *Ch1*, while for *Ch2* we used standard PTW Unidos electrometer for measurement of charge mainly produced by Čerenkov radiation (blue light). Subscripts max and min correspond to maximum (~30 cm) and minimum (~10 cm) fiber length which is in the radiation field, and subscripts 10 stand for the nominal radiation field 10 × 10 cm^2 applied during the Čerenkov calibration procedure. The Čerenkov-corrected signal (collected charge) $M_{f_{clin}}$ for a particular small clinical field f_{clin} was then obtained from two readings in both channels as

$$M_{f_{clin}} = M_{f_{clin}}^{Ch1} - CLR \cdot M_{f_{clin}}^{Ch2} \tag{5.4}$$

CLR coefficient was determined for all four photon beams on both linacs, Elekta Versa HD and Varian TrueBeam. For each photon beam, the energy-specific values of CLR were obtained from three sets of measurements, and the average value was used as the final value for particular CLR. Note, that $M_{f_{clin}}$ in Eq. (5.4) has the same meaning as $M_{Q_{clin}}^{f_{clin}}$ in Eq. (3.10).

5.5 Solid-state detectors

Six diodes and a micro diamond detector were selected among variety of solid-state detectors for the determination of their specific output correction factors: IBA SFD diode and IBA Razor

diode (IBA Dosimetry, Schwarzenbruck, Germany), PTW 60008 Diode P, PTW 60012 Diode E, PTW 60018 Diode SRS, PTW 60019 microDiamond (PTW, Freiburg, Germany) and SN EDGE detector (Sun Nuclear, Melbourne, FL, USA). The selection was based on their physical dimensions, characteristics, and availability for clinical use. Figure 5.1 shows all solid-state detectors used in the present study while Table 5.1 lists their basic physical properties and dimensions.

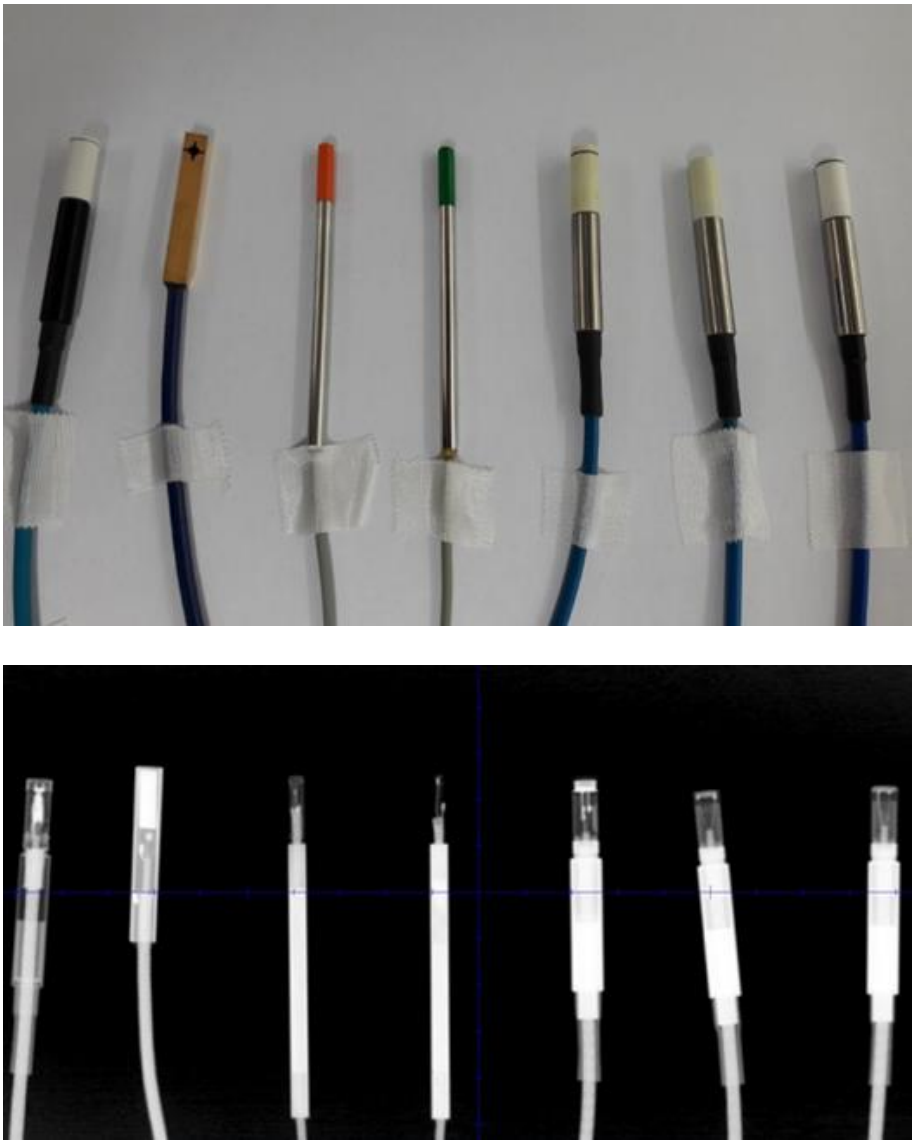

Figure 5.1. The photo on top of the figure and x-ray image at the bottom of seven solid-state detectors, six diodes and micro diamond detector used in the present study. From left to right: PTW 60019 mD, SN EDGE Detector, IBA Razor diode, IBA SFD diode, PTW 60008 Diode P, PTW 60012 Diode E and PTW 60018 Diode SRS.

It is worth mentioning that PTW 60008 P and PTW 60012 E diodes were superseded by newer models, PTW 60016 P and PTW 60017 E diodes respectively. However, the physical construction of the newer models is basically identical to their predecessors.[16] The equivalency between the PTW 60008 P and 60016 P diodes and 60012 E and 60017 E diodes has also been demonstrated in the MC study by Francescon et al,[81] where the output correction factors were found to be the same.

Table 5.1. Summary of basic characteristics and properties of the seven solid-state detectors included in the study.

Detector type	Active volume dimensions [mm]	Sensitive material	Material density [g/cm^3]	Z_{eff}	Reference depth [mm]
IBA SFD diode	Disc, Ø 0.6 thickness 0.06	Silicone	2.33	14	0.8
IBA Razor diode	Disc, Ø 0.6 thickness 0.02	Silicone	2.33	14	0.8
PTW 60008 Diode P	Disc, Ø 1.2 thickness 0.03	Silicone	2.33	14	2.0
PTW 60012 Diode E	Disc, Ø 1.2 thickness 0.03	Silicone	2.33	14	1.3
PTW 60018 Diode SRS	Disc, Ø 1.2 thickness 0.25	Silicone	2.33	14	1.3
SN EDGE detector	Square 0.8 x 0.8 thickness 0.03	Silicone	2.33	14	0.3
PTW 60019 mD	Disc, Ø 2.2 thickness 0.001	Synthetic diamond	3.53	6	1.0

Before measurements, which were performed with the PTW Unidos^{webline} electrometer for all solid-state detectors, each detector was positioned with its effective point of measurement (physical depth) at the reference depth of 10 cm, and with its stem parallel to the beam axis. The only exception was the SN EDGE detector, which was positioned with its stem orthogonally to the beam axis, due to its different design (see Figure 5.1).

Lateral alignment of detectors along the central beam axis was made in three consecutive steps for each detector separately after the initial CAX alignment has been performed:

a) initial set up using room lasers;

b) repositioning (centering) of the detector after acquiring lateral beam profiles along cross-line and in-line directions;

c) finally, each detector was moved in manual mode in 0.2 mm (0.1 mm if necessary) steps along both x and y directions and irradiated with 100 MU to find the position where the collected charge was maximal.

The position where the collected charge reached the highest value was assumed as the central beam axis, i.e., the center of the field, and the final position for each detector. The above procedure for lateral alignment of detectors was done separately for each photon beam. Similar alignment procedure is also recommended in the ICRU Report 91.[9]

For each radiation field, three consecutive measurements of 100 MU each were taken. $M_{Q_{clin}}^{f_{clin}}$ in Eq. (3.8) represents the average value of the three measured values. To limit the influence of environmental conditions, $M_{Q_{ref}}^{f_{ref}}$ for 10 x 10 cm^2 reference field was always measured prior to the smallest clinical field and at the end of each measurement session for the selected beam energy. For reference field, the average value of six measurements was considered as the final value for $M_{Q_{ref}}^{f_{ref}}$.

5.6 Ionization chambers

Seven mini and micro ionization chambers were selected for the determination of their specific output correction factors: IBA CC04 and IBA Razor (IBA Dosimetry, Schwarzenbruck, Germany), PTW 31016 3D PinPoint, PTW 31021 3D Semiflex, PTW 31022 3D PinPoint, PTW 31023 PinPoint (PTW, Freiburg, Germany) and SI Exradin A16 (Standard Imaging, Middleton, WI, USA). The selection was based on their physical dimensions, characteristics, and suitability for clinical use, following the recommendations from the TRS-483. Two ionization chambers, IBA Razor and SI Exradin A16, included in the study, are classified as micro ionization chambers having the active volume V ≤ 0.01 cm^3, while the rest of the chambers belonging to the group of small, sometimes denoted as mini ionization chambers with active volumes 0.01 cm^3 < V < 0.3 cm^3. Table 5.2 lists their basic physical properties and dimensions.

It is worth noting that PTW 31022 3D PinPoint and PTW 31023 PinPoint chambers superseded previous models PTW 31016 3D PinPoint and PTW 31014/31015 PinPoint, respectively. Newer models are mostly the same as their predecessors without notable constructional or geometrical differences. However, there is a difference in the nominal

chamber voltage as specified by the manufacturer: for PTW 31023 PinPoint chamber the nominal voltage is 200 V, while for older models PTW 31014/31015 PinPoint the nominal voltage is 400 V. Throughout the study manufacture's specification regarding the nominal voltage were followed without exception.

Similarly, IBA Razor ionization chamber superseded previous model IBA CC01. However, in this case, there are constructional differences. Unlike the old model having a steel electrode, a newer model has been designed with a graphite one. The rest of the characteristics, i.e., cavity dimensions, wall material, and wall thickness, remained unmodified.

Table 5.2. Summary of basic properties of seven ionization chamber used in this study.

Detector type	Cavity volume [cm^3]	Cavity length/radius [mm]	Wall material	Wall thickness [g/cm^2]	Central electrode
IBA CC04	0.04	3.6/2.0	C552	0.070	C-552
IBA Razor	0.01	3.6/1.0	C552	0.088	Graphite
PTW 31016 PinPoint 3D	0.016	2.9/1.45	PMMA + Graphite	0.085	Aluminium
PTW 31021 Semiflex 3D	0.07	4.8/2.4	PMMA + Graphite	0.084	Aluminium
PTW 31022 PinPoint 3D	0.016	2.9/1.45	PMMA + Graphite	0.084	Aluminium
PTW 31023 PinPoint	0.015	5.0/1.0	PMMA + Graphite	0.085	Aluminium
SI Exradin A16	0.007	2.4/1.2	C552	0.088	Steel[a]

[a] Silver plated and cooper clad steel wire

For the determination of field output factors in small photon fields, the recommended orientation for ionization chamber, with respect to the central beam axis, is perpendicular i.e. chamber's axis (stem) is perpendicular to the central beam axis.[10] TRS-483 CoP does not recommend parallel orientation since at the time of publishing, there were only limited data available for the orientation with the chamber stem parallel to the central axis of the beam. Such an approach was additionally explained in the recent publication by the authors of the TRS-483

CoP in their response to the *"Comments on the TRS-483 protocol on small field dosimetry"* and can be considered as appropriate.[12,82]

However, some air-filled ionization chambers show noticeable stem effect, which can be minimized if the chamber is oriented with its stem parallel to the beam axis. Further, many air-filled ionization chambers are designed in a way that they have relatively large cavity lengths in the direction of the chamber axis. Later can significantly increase volume averaging effect if a chamber is placed with its stem perpendicular to the beam axis. Both concerns, as well as lack of data for parallel orientation in the present literature, brought as to the conclusion to perform measurements in both orientations as shown in Figure 5.2., and present data which might be valuable supplement to the present data sets in the literature and can possibly lead to the alternative recommendation regarding the orientation of ionization chamber in small photon beams.

The execution of measurements was in principle the same as in the case of solid-state detectors and is described in section 5.5, with one exception. For lateral alignment of the ionization chambers with central beam axis, lateral beam profiles along cross-line and in-line directions were acquired in the same orientation of the ionization chamber as it was used for point measurements subsequently. That means that for the perpendicular orientation of the chamber we had to perform beam profile measurements in the orientation which is not recommended in the TRS-483 CoP. On the contrary, for the parallel orientation of the ionization chamber we performed profile scans in the advised orientation, and from apparent reason, we kept the same orientation for point measurements, the orientation which is not recommended in the TRS-483 CoP. In brief, measurements with solid-state detectors were always performed in advised orientation (for profile scans and point measurements), while it was not the case with ionization chambers since it was not possible following our measurement protocol; an ambiguity, connected to our experimental approach, which we tried to resolve in our work.

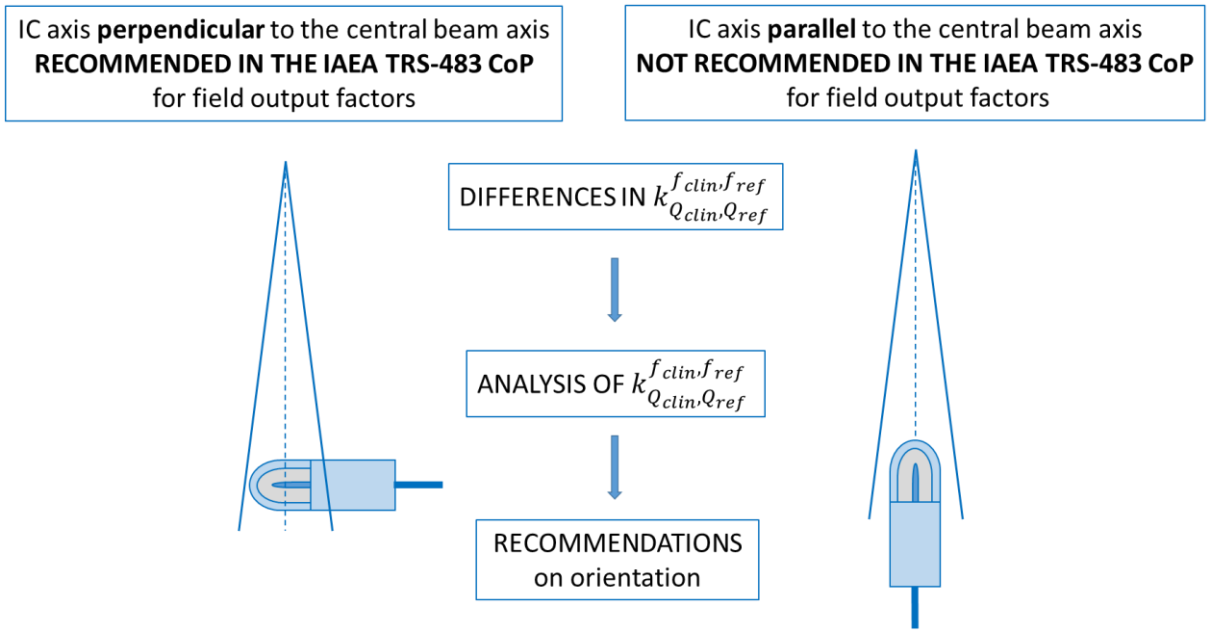

Figure 5.2. Two experimental set-ups with respect to the orientation of ionization chambers; perpendicular, as advised in the TRS-483 CoP (left) and parallel, which is not recommended.

Observed differences in $k_{Q_{clin},Q_{ref}}^{f_{clin},f_{ref}}$ values between perpendicular and parallel orientation were thoroughly analyzed and are discussed later in the thesis for all seven ionization chambers. Based on our findings, recommendation regarding the orientation of ionization chambers in small photon beams was given.

5.7 Volume averaging correction

Since EBT3 films and W1 PSD detector are almost water equivalent and have weak energy dependence, it is assumed in the present study that they have no perturbation correction factors.[10] However, their signals still need to be corrected for volume averaging effects for the determination of field output factors. It is evident for scintillator as it has a finite size. However, it might not be so evident for radiochromic films. Radiochromic film is considered as a detector with almost infinite resolution. Inherently it might be the case. However, there are two limitations which need to be considered in clinical dosimetry - scanning resolution, which the user decides upon and the selected size of the film detector. Both need to be defined, i.e., one needs to define a specific finite area (ROI) of the film which will be used as a detector area of the EBT3 film for data analysis as well as scanning resolution which will be used for subsequent evaluation. As mentioned earlier, in the present study, the ROI was chosen to have a diameter

of 0.5 mm, and the scanning resolution was chosen to have a value of 150 dpi for field output factor measurements.

According to IAEA TRS-483 CoP, $k_{Q_{clin},Q_{ref}}^{f_{clin},f_{ref}}$ for these two detectors can be simplified as follows

$$k_{Q_{clin},Q_{ref}}^{f_{clin},f_{ref}} = k_{vol} \tag{5.5}$$

where k_{vol} is the volume averaging correction factor due to the detector's finite size and represents the only correction factor that was considered for the two reference detectors in the present study and has a purely geometrical concept.

Combining Eqs. (3.10) and (5.5), average signal readings $M_{Q_{clin}}^{f_{clin}}$ of EBT3 films and W1 PSD can be corrected for volume averaging k_{vol} to determine discrete field output factors for small clinical fields as

$$\Omega_{Q_{clin},Q_{ref}}^{f_{clin},f_{ref}} = \frac{M_{Q_{clin}}^{f_{clin}}}{M_{Q_{ref}}^{f_{ref}}} k_{vol} \tag{5.6}$$

Doses measured from EBT3 films were employed to calculate k_{vol} factors. For each small field S_{clin} and beam energy E, film doses in a region of interest with dimensions 3 mm x 3 mm (i.e., from -1.5 mm to +1.5 mm in cross-plane direction x and in-plane direction y) centered on the beam axes were fitted to a bivariate Gaussian function

$$f(x, y, S_{clin}, E) = a \cdot e^{-\frac{1}{2}\left(\left(\frac{x}{b}\right)^2 + \left(\frac{y}{c}\right)^2\right)} \tag{5.7}$$

using fit parameters, a, b and c. The volume averaging correction factors k_{vol} were calculated as

$$k_{vol} = (a \cdot \pi r^2)\left(a \cdot \iint_A f(x, y, S_{clin}, E)\, dx\, dy\right)^{-1} \tag{5.8}$$

This approach is similar to the previously published studies by Morin et al.[78] and Papaconstadopoulos et al.[25,48] r in Eq. (5.8) is the radius of the detector's sensitive volume in a plane orthogonal to the beam axis. The detector's radius r was replaced with the size of the equivalent square field side length d (note that this "equivalent square field size length d" is defined here for performing the integration of Eq. (5.8); this is different from the "equivalent square small field size S_{clin}" defined in Eq. (5.1)), applying the expression $\pi r^2 = d^2$ yields the result

$$k_{vol} = \frac{d^2}{2\pi bc \cdot erf\left(\frac{d/2}{\sqrt{2}\cdot b}\right) erf\left(\frac{d/2}{\sqrt{2}\cdot c}\right)} \tag{5.9}$$

Therefore, given the field size S_{clin} and beam energy E, the parameters d, b and c are necessary to calculate the k_{vol} factor of a specific detector; note that parameter a cancels out already in the Eq. (5.8) The first parameter d was obtained from the detector specifications, with the exception of EBT3 films, where the diameter of the detector (i.e. central ROI for the EBT3 films) was chosen as 0.5 mm. For W1 PSD we used the value r = 0.5 mm following vendor specifications. The other two parameters were derived from film dose fit. k_{vol} were calculated for all solid-state detectors including the EBT3 and W1 PSD using the expression given in Eq. (5.9).

To check whether 150 dpi scanning resolution was adequate and sufficient for the determination of k_{vol}, several sets of films were scanned for the smallest field sizes using the 1200 dpi resolution and the values of k_{vol} thus obtained were compared with those obtained using the 150 dpi scanning resolution. No detectable differences in k_{vol} were observed between both approaches; therefore 150 dpi scanning resolution was used for film scanning throughout the present study.

5.8. Field output factors

For the determination of field output factors, EBT3 films and W1 PSD were used equivalently, without any preference.

Signals $M_{Q_{clin}}^{f_{clin}}(EBT3)$ measured with EBT3 films were corrected for volume averaging as

$$M_{Q_{clin}}^{f_{clin}}(EBT3)_{corr} = M_{Q_{clin}}^{f_{clin}}(EBT3) \cdot k_{vol}^{f_{clin}}(EBT3) \tag{5.10}$$

where $k_{vol}^{f_{clin}}$ denotes volume averaging correction factor for specific clinical field f_{clin} (in the present study $f_{clin} \equiv S_{clin}$). In addition to volume averaging correction, signals for the W1 PSD detector, $M_{Q_{clin}}^{f_{clin}}(W1\ PSD)$, were further normalized as

$$M_{Q_{clin}}^{f_{clin}}(W1\ PSD)_{N,corr} = \frac{M_{Q_{clin}}^{f_{clin}}(W1\ PSD) \cdot k_{vol}^{f_{clin}}(W1\ PSD)}{\bar{\epsilon}} \tag{5.11}$$

Where $\bar{\epsilon}$ is the average value of ratios of measured signals between W1 PSD and EBT3 films for each particular photon beam of the specific linac, calculated as

$$\bar{\epsilon} = \frac{1}{9} \sum_{f_{clin}} \frac{M_{Q_{clin}}^{f_{clin}}(W1\ PSD) \cdot k_{vol}^{f_{clin}}(W1\ PSD)}{M_{Q_{clin}}^{f_{clin}}(EBT3) \cdot k_{vol}^{f_{clin}}(EBT3)} \tag{5.12}$$

where summation goes over all nine clinical small fields selected in this study.

$M_{Q_{clin}}^{f_{clin}}(EBT3)_{corr}$ values obtained from Eq. (5.10) determined by EBT3 films and $M_{Q_{clin}}^{f_{clin}}(W1\ PSD)_{N,corr}$ values from Eq. (5.11) determined by W1 PSD, were fitted together by the analytical function proposed by Sauer and Wilbert,[13]

$$\Omega(S_{clin}) = P_{\infty} \frac{S_{clin}^{n}}{l^{n} + S_{clin}^{n}} + S_{\infty}\left(1 - e^{-b \cdot S_{clin}}\right) \tag{5.13}$$

which was normalized to $\Omega(S_{clin} = 10\ cm) = 1$. P_{∞}, S_{∞}, l, n and b are the fitting parameters, adjusted according to a routine, which optimizes the maximum likelihood estimation (MLE). For brevity and to avoid potential ambiguity, subscripts and superscripts were omitted from $\Omega(S_{clin})$, which is in the form of an analytical function, unlike the $\Omega_{Q_{clin},Q_{ref}}^{f_{clin},f_{ref}}$ which is used for discrete values of field output factors. Furthermore, S_{clin} was kept in the same form as in Eq. (5.1) to emphasize that it stands for the equivalent square small field sizes rather than the nominal field sizes; it has the same meaning as symbol *s*, used by Sauer and Wilbert in their original work. The use of analytical function, instead of the discrete values for field output factors, reduces uncertainties in W1 PSD and EBT3 film measurements. In addition, the functional form of field output factors $\Omega(S_{clin})$ allows one to calculate discrete values for field output factors for any equivalent square small field size within the range of small field sizes used in this study.

5.9. Output correction factors

For every solid-state detector and seven ionization chambers discrete values of detector specific output correction factors $k_{Q_{clin},Q_{ref}}^{f_{clin},f_{ref}}(S_{clin})$ were calculated for each measured equivalent square small field size S_{clin} as

$$k_{Q_{clin},Q_{ref}}^{f_{clin},f_{ref}}(S_{clin}) = \frac{\Omega_{Q_{clin},Q_{ref}}^{f_{clin},f_{ref}}}{M_{Q_{clin}}^{f_{clin}} / M_{Q_{ref}}^{f_{ref}}} \tag{5.14}$$

Discrete values of field output factors $\Omega_{Q_{clin},Q_{ref}}^{f_{clin},f_{ref}}$ were obtained from the analytical function $\Omega(S_{clin})$ in Eq. (5.13). $k_{Q_{clin},Q_{ref}}^{f_{clin},f_{ref}}(S_{clin})$ values were fitted by the analytical function published in TRS-483 [10]

$$k(S_{clin}) = \frac{1 + d \cdot e^{-\frac{10-a}{b}}}{1 + d \cdot e^{-\frac{S_{clin}-a}{b}}} + c \cdot (S_{clin} - 10) \tag{5.15}$$

with fitting coefficients, a, b, c and d. Instead of symbol S, which is used in TRS-483 CoP, in the analytical function in Eq. (5.15), symbol S_{clin} was used instead to emphasize that in the present study equivalent square field sizes were used without exception. As in the case for field output factors, subscripts and superscripts are omitted in the notations for output correction factors in Eq. (5.15) to indicate that in this case, output correction factors have functional form.

Also, the discrete values of $k_{Q_{clin},Q_{ref}}^{f_{clin},f_{ref}}(S_{clin})$ were calculated and reported for all detectors, photon beams and small fields, applying Eq. (5.14).

6 RESULTS

6.1 Equivalent square small field size S_{clin}

For each nominal field size, corresponding equivalent square field sizes S_{clin} (clinical field) were calculated based on EBT3 film measurements and applying Eq. (5.1). Data for nominal and equivalent square small field sizes are presented in Table 6.1. Throughout this thesis field sizes will be indicated with nominal values, however, they will represent, without exception, the corresponding S_{clin} values. For brevity, square field sizes will be denoted as nominal square field side lengths, e.g., instead of 0.5 × 0.5 cm^2, notation 0.5 cm will be used henceforth.

Table 6.1 Nominal field sizes and corresponding equivalent square small field sizes S_{clin} on Elekta Versa HD and Varian TrueBeam linacs measured with EBT3 radiochromic films and applying Eq. (5.1).

Nominal square field side length [cm]	$S_{clin}[cm]$ - Elekta Versa HD				$S_{clin}[cm]$ - Varian TrueBeam			
	6 MV WFF	6 MV FFF	10 MV WFF	10 MV FFF	6 MV WFF	6 MV FFF	10 MV WFF	10 MV FFF
0.5	0.60	0.59	0.62	0.58	0.56	0.54	0.57	0.55
0.8	0.87	0.85	0.87	0.86	0.81	0.82	0.84	0.81
1.0	1.03	1.03	1.06	1.04	1.01	0.99	1.03	1.02
1.5	1.51	1.52	1.55	1.52	1.50	1.49	1.52	1.51
2.0	2.04	2.03	2.05	2.04	2.00	1.99	2.01	1.99
3.0	3.06	3.04	3.08	3.02	3.03	3.00	3.00	2.98
4.0	4.04	4.03	4.06	4.01	4.03	3.99	4.02	3.98
5.0	5.04	5.01	5.05	4.99	5.02	5.00	5.01	4.96
10.0	10.04	9.94	10.05	9.90	10.03	9.96	10.02	9.87

While equivalent square small field sizes S_{clin} are nearly identical to the nominal field sizes for field sizes ≥ 1 cm, they differ rather significantly for the two smallest fields, 0.5 and 0.8 cm, regardless of the photon beam or collimation (linac) being used.

The uncertainty of field size dimensions was determined from EBT3 films and was found to be < 0.1 mm. The same level of uncertainty of field set-up reproducibility was determined with repeated measurements of lateral beam profiles with several diodes at FWHM for smallest field sizes.

6.2 Field output factors

Figure 6.1 shows graphs for field output factors determined from measurements made on Elekta Versa HD linac with EBT3 films and W1 PSD detector. The red circles and blue triangles represent field output factors for the EBT3 film and W1 PSD detectors respectively. Measured signals were corrected for volume averaging using Eqs. (5.8) and (5.9) when k_{vol} exceeded 0.1%. For the Elekta linac, these values are given in Table 6.4 for all photon beams. The uncertainties for each data point correspond to 1 SD. The solid lines in Figure 6.1 represent fits to both sets of data using the analytical function given in Eq. (5.13). Relative uncertainties (1 SD) of the fits were largest for the smallest field size of 0.5 cm and were found to be 1.0%, 1.3%, 1.2% and 1.4% for photon beams 6 MV WFF, 6 MV FFF, 10 MV WFF and 10 MV FFF respectively. In addition to the curves in Fig. 6.1, discrete values of field output factors $\Omega_{Q_{clin},Q_{ref}}^{f_{clin},f_{ref}}$ were calculated using Eq. (15) and are given in Table 6.2 for all selected small fields and energies for the Elekta Versa HD linac.

Table 6.2 Discrete values of field output factors for nine selected field sizes calculated from the analytical function in Eq. (5.13) for all investigated photon beams on Elekta VersaHD linac. Uncertainties (1 SD) are shown in brackets and represent absolute uncertainties in the last digit.

Field size[a] [cm]	Elekta Versa HD			
	6 MV WFF	6 MV FFF	10 MV WFF	10 MV FFF
0.5	0.454 (5)	0.478 (6)	0.438 (5)	0.481 (7)
0.8	0.620 (5)	0.640 (6)	0.584 (5)	0.626 (6)
1.0	0.678 (5)	0.703 (6)	0.650 (5)	0.688 (6)
1.5	0.763 (5)	0.786 (6)	0.750 (5)	0.780 (6)
2.0	0.804 (5)	0.825 (6)	0.801 (6)	0.835 (6)
3.0	0.849 (5)	0.870 (6)	0.858 (6)	0.890 (6)
4.0	0.880 (5)	0.900 (7)	0.891 (6)	0.923 (7)
5.0	0.907 (5)	0.924 (7)	0.918 (6)	0.945 (7)
10.0	1.001 (0)	0.999 (0)	1.001 (0)	0.999 (0)

[a] Field size is indicated as nominal square field side length. The relationship between the nominal field size and the corresponding equivalent square small field sizes S_{clin} is provided in Table 6.1 for all photon beams and field sizes. Note that because S_{clin} are not exactly equal to 10.0 cm for reference field size (Table 6.1), corresponding field output factors slightly differ from value 1.000 for that field.

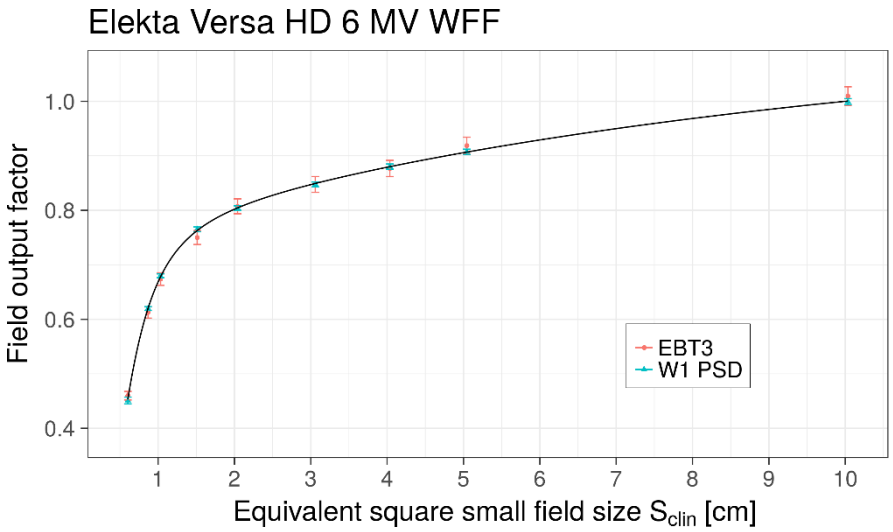
Elekta Versa HD 6 MV WFF
Field output factor
1.0
0.8
0.6
0.4
1
2
3
4
5
6
7
8
9
10
Equivalent square small field size S_{clin} [cm]
EBT3
W1 PSD

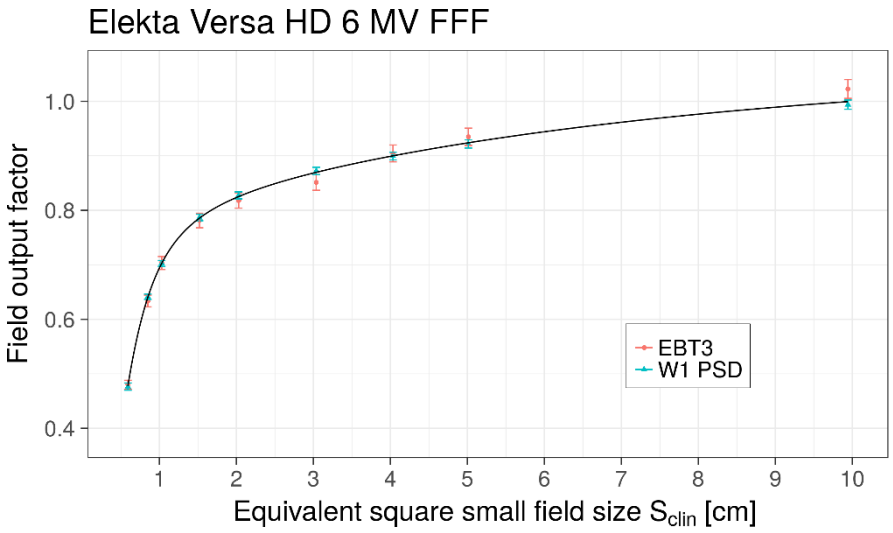
Elekta Versa HD 6 MV FFF
Field output factor
1.0
0.8
0.6
0.4
1
2
3
4
5
6
7
8
9
10
Equivalent square small field size S_{clin} [cm]
EBT3
W1 PSD

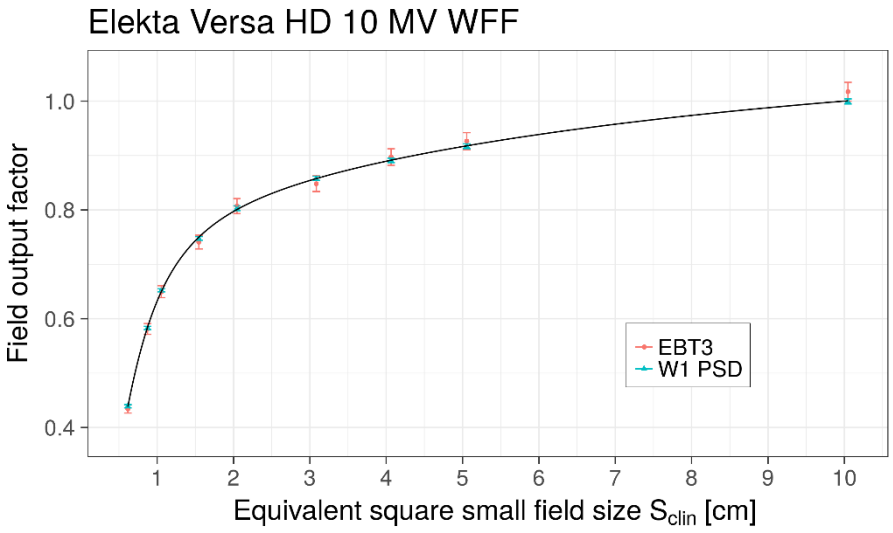
Elekta Versa HD 10 MV WFF
Field output factor
1.0
0.8
0.6
0.4
1
2
3
4
5
6
7
8
9
10
Equivalent square small field size S_{clin} [cm]
EBT3
W1 PSD

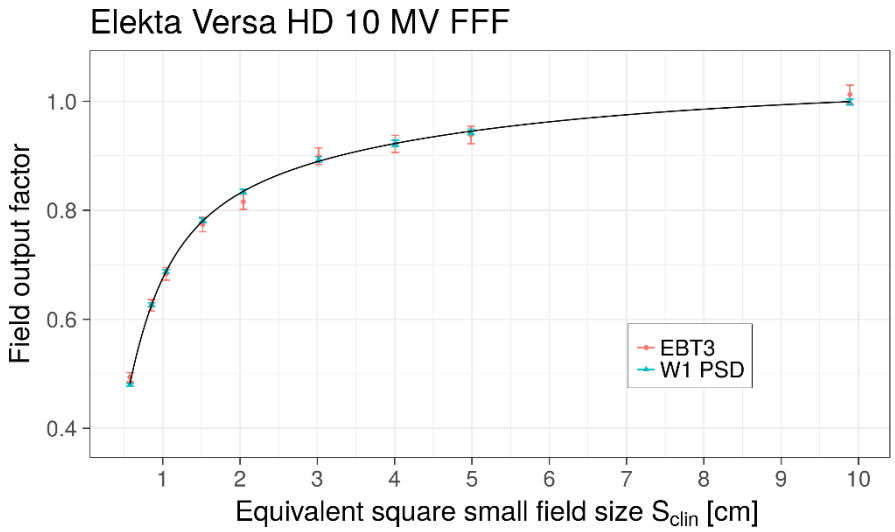

Figure 6.1. Field output factors vs. S_{clin} on Elekta Versa HD linac for four investigated photon beams. The red circles and blue triangles represent field measured field output factors along with their respective uncertainties (1 SD) determined using EBT3 film and W1 PSD detectors respectively. The solid lines represent fits to both sets of data using the analytic function given in Eq. (5.13).

Field output factors determined from measurements made on the Varian TrueBeam linac with EBT3 films and W1 PSD detector are shown in Figure 6.2. The red circles and blue triangles represent field output factors for the EBT3 film and W1 PSD detectors respectively. Similar to the Elekta linac, measured signals were corrected for volume averaging using Eqs. (5.8) and (5.9) when k_{vol} exceeded 0.1%; for the Varian linac values of k_{vol} are given in Table 6.4 for all photon beams. The solid lines in Figure 6.2 represent fits to both sets of data using the analytical function given by Eq. (5.13). Largest relative uncertainties (1 SD) of the fits were again found for the smallest field size of 0.5 cm and were found to be 2.0%, 2.2%, 2.5% and 1.6% for photon beams 6 MV WFF, 6 MV FFF, 10 MV WFF and 10 MV FFF respectively. Discrete values of field output factors for all selected small fields and energies for the Varian TrueBeam are given in Table 6.3. These values were calculated using the fitting function given by Eq. (5.13).

Table 6.3 Discrete values of field output factors for nine selected field sizes calculated from the analytical function in Eq. (5.13) for all investigated photon beams on Varian TrueBeam linac. Uncertainties (1 SD) are shown in brackets and represent absolute uncertainties in the last one or two digits.

Field size[a] [cm]	Varian TrueBeam			
	6 MV WFF	6 MV FFF	10 MV WFF	10 MV FFF
0.5	0.482 (9)	0.513 (11)	0.412 (10)	0.468 (7)
0.8	0.632 (8)	0.654 (10)	0.556 (8)	0.615 (7)
1.0	0.694 (8)	0.701 (10)	0.625 (9)	0.687 (7)
1.5	0.761 (9)	0.772 (11)	0.730 (9)	0.780 (8)
2.0	0.793 (9)	0.806 (11)	0.785 (10)	0.828 (8)
3.0	0.834 (9)	0.844 (11)	0.844 (10)	0.881 (8)
4.0	0.866 (9)	0.871 (11)	0.880 (10)	0.914 (9)
5.0	0.893 (9)	0.895 (10)	0.907 (10)	0.937 (9)
10.0	1.001 (0)	0.999 (0)	1.000 (0)	0.999 (0)

[a] Field size is indicated as nominal square field side length. The relationship between the nominal field size and the corresponding equivalent square small field sizes S_{clin} is provided in Table 6.1 for all photon beams and field sizes. Note that because S_{clin} are not exactly equal to 10.0 cm for reference field size (Table 6.1), corresponding field output factors slightly differ from value 1.000 for that field.

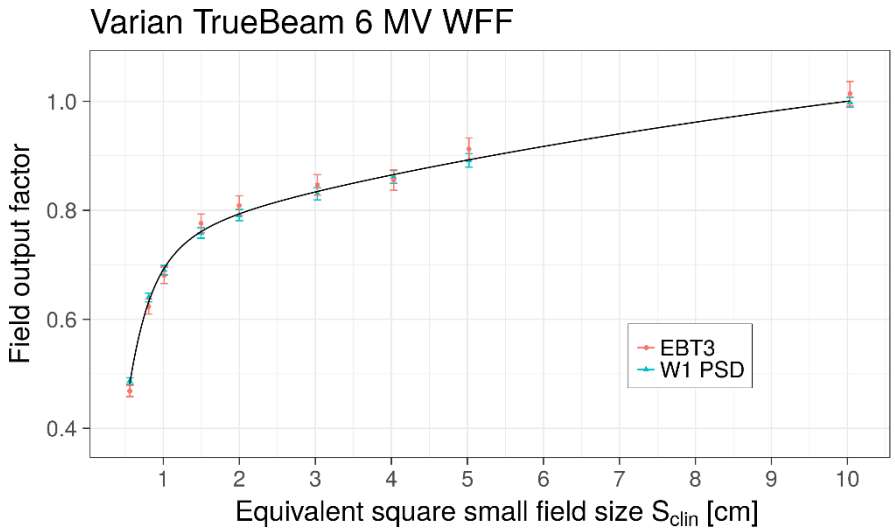

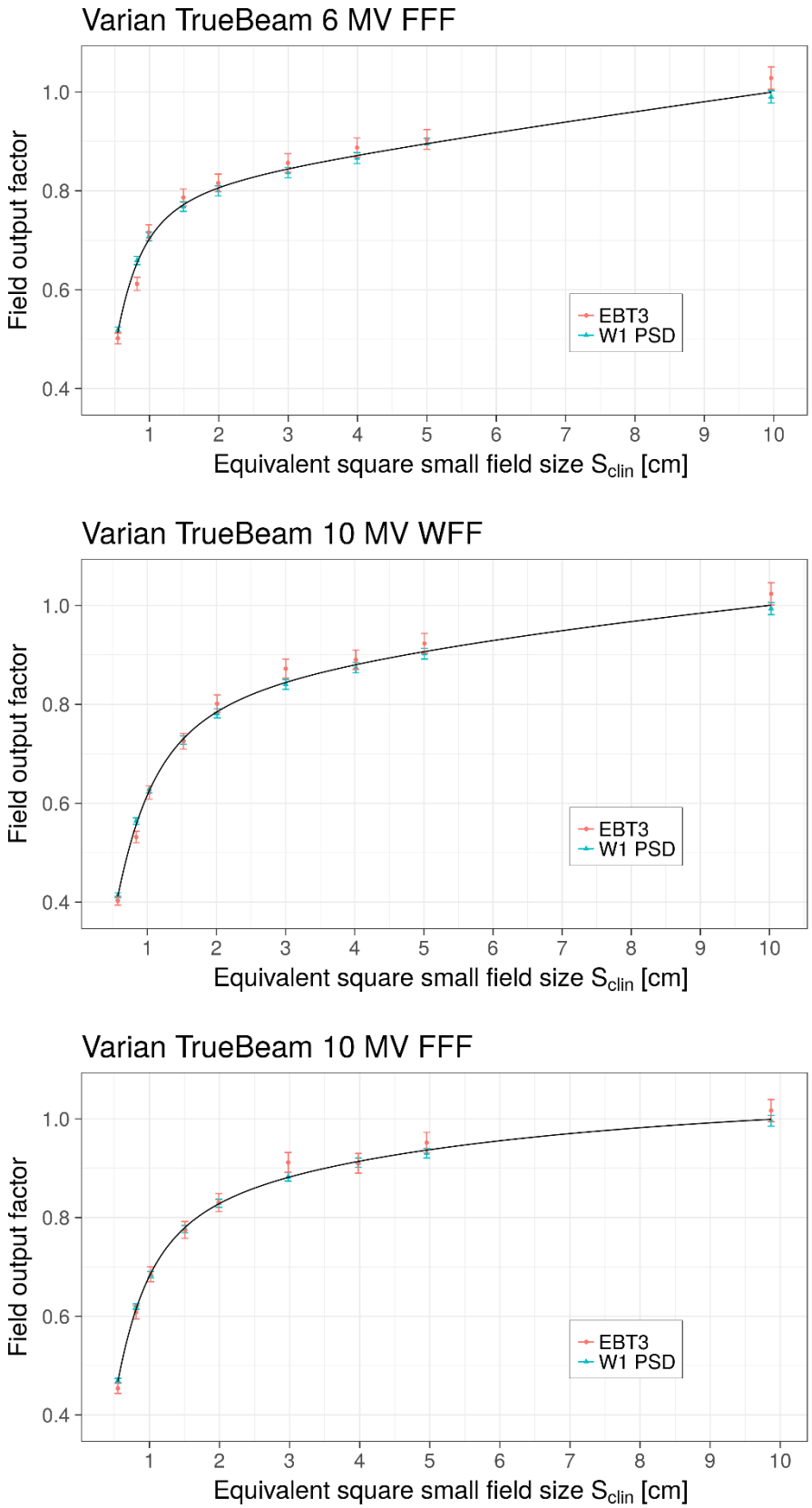

Figure 6.2. Field output factors vs S_{clin} on Varian TrueBeam linac for four investigated photon beams. The red circles and blue triangles represent field output factors along with their respective uncertainties (1 SD) determined using EBT3 film and W1 PSD detector respectively. The solid lines represent fits to both sets of data using the analytic function given in Eq. (5.13).

Table 6.4 Calculated volume averaging correction factors k_{vol} for EBT3 films and W1 PSD for the three smallest field sizes on Elekta VersaHD and Varian TrueBeam linacs; these values were taken into account for the determination of field output factors.

Elekta Versa HD

Field size[a] [cm]	EBT3	W1 PSD	EBT3	W1 PSD
	6 MV WFF		6 MV FFF	
0.5	1.002	1.008	1.002	1.008
0.8	1.000	1.002	1.000	1.002
1.0	1.000	1.001	1.000	1.001
	10 MV WFF		10 MV FFF	
0.5	1.002	1.007	1.002	1.007
0.8	1.000	1.002	1.000	1.002
1.0	1.000	1.001	1.000	1.001

Varian TrueBeam

Field size[a] [cm]	EBT3	W1 PSD	EBT3	W1 PSD
	6 MV WFF		6 MV FFF	
0.5	1.002	1.009	1.002	1.009
0.8	1.000	1.004	1.000	1.002
1.0	1.000	1.001	1.000	1.000
	10 MV WFF		10 MV FFF	
0.5	1.002	1.008	1.002	1.008
0.8	1.001	1.004	1.000	1.003
1.0	1.000	1.001	1.000	1.001

[a] Field size is indicated as a nominal square small field side length. The relationship between the nominal field size and the corresponding equivalent square small field sizes S_{clin} is provided in Table 6.1 for all photon beams and field sizes.

The five fitting coefficients of the analytical function from Eq. (5.13) are given Table 6.5 for all investigated photon beams on both linacs.

Table 6.5 Values of fitting parameters for the analytical function given in Eq. (5.13). This function was used to fit the field output factor datasets obtained using the EBT3 films and W1 PSD detectors on the two linacs for four photon beams.

E	P_∞	n	l	S_∞	b
	Elekta Versa HD				
6 MV WFF	0.751	2.701	0.542	0.384	0.105
6 MV FFF	0.767	2.614	0.514	0.299	0.151
10 MV WFF	0.774	2.183	0.578	0.313	0.130
10 MV FFF	0.829	1.791	0.511	0.198	0.214
	Varian TrueBeam				
6 MV WFF	0.741	2.646	0.461	0.508	0.072
6 MV FFF	0.790	2.097	0.419	1.424	0.016
10 MV WFF	0.816	1.844	0.588	0.478	0.050
10 MV FFF	0.816	1.904	0.497	0.227	0.173

To quantify the statistical significance of differences between field output factors given in Tables 6.2 and 6.3 for WFF and FFF beams for particular photon beam and linac, one-tailed Student's t-test was performed. These results are shown in Table 6.6.

Table 6.6 Statistical significance (p-values) of differences of field output factors between WFF and FFF beams on Elekta Versa HD and Varian TrueBeam linacs for 6 and 10 MV beams. For the determination of p-values one-tailed Student's t-test was performed.

p-values				
Field size[a] [cm]	Elekta Versa HD		Varian TrueBeam	
	6 MV WFF/FFF	10 MV WFF/FFF	6 MV WFF/FFF	10 MV WFF/FFF
0.5	0.023	0.010	0.049	0.012
0.8	0.034	0.009	0.069	0.008
1.0	0.023	0.010	0.263	0.009
1.5	0.026	0.015	0.189	0.014
2.0	0.034	0.014	0.166	0.022
3.0	0.033	0.016	0.213	0.030
4.0	0.039	0.019	0.333	0.035
5.0	0.058	0.028	0.427	0.043
10.0	0.006	0.015	0.001	0.038

[a] Field size is indicated as nominal square field side length. The relationship between the nominal field size and the corresponding equivalent square small field sizes S_{clin} is provided in Table 6.1 for all photon beams and field sizes.

6.3 Detector specific output correction factors

6.3.1 Solid-state detectors

Figures 6.3 and 6.4 shows in four separate graphs detector specific output correction factors $k_{Q_{clin},Q_{ref}}^{f_{clin},f_{ref}}(S_{clin})$ as a function of equivalent square small field sizes S_{clin} for seven solid-state detectors and four photon beams; these were determined using Eq. (5.14) on Elekta Versa HD linac. The solid curves in these figures represent fits to the data points using the analytic function $k(S_{clin})$ given by Eq. (5.15). For brevity $k_{Q_{clin},Q_{ref}}^{f_{clin},f_{ref}}(S_{clin})$ will be denoted as $k_{Q_{clin},Q_{ref}}^{f_{clin},f_{ref}}$ henceforth. The data points obtained from Eq. (5.14) were fitted down to the field size of

0.8 cm to ensure acceptable fit of the selected fitting function – values of output correction factors for field size 0.5 cm were omitted from the fit.

For comparison and further analysis, individual discrete values for $k_{Q_{clin},Q_{ref}}^{f_{clin},f_{ref}}$, obtained for the Elekta Versa HD linac using Eq. (5.14), are provided in Table 6.7 for all photon beams and selected field sizes. It should be noted that the $k_{Q_{clin},Q_{ref}}^{f_{clin},f_{ref}}$ correction factor thus determined represents the "total" correction factor for a particular detector and includes contributions for both volume averaging correction factor as well as perturbations correction factors. The $k_{Q_{clin},Q_{ref}}^{f_{clin},f_{ref}}$ factors thus determined can then be compared directly with those reported in TRS-483 for the corresponding detectors.

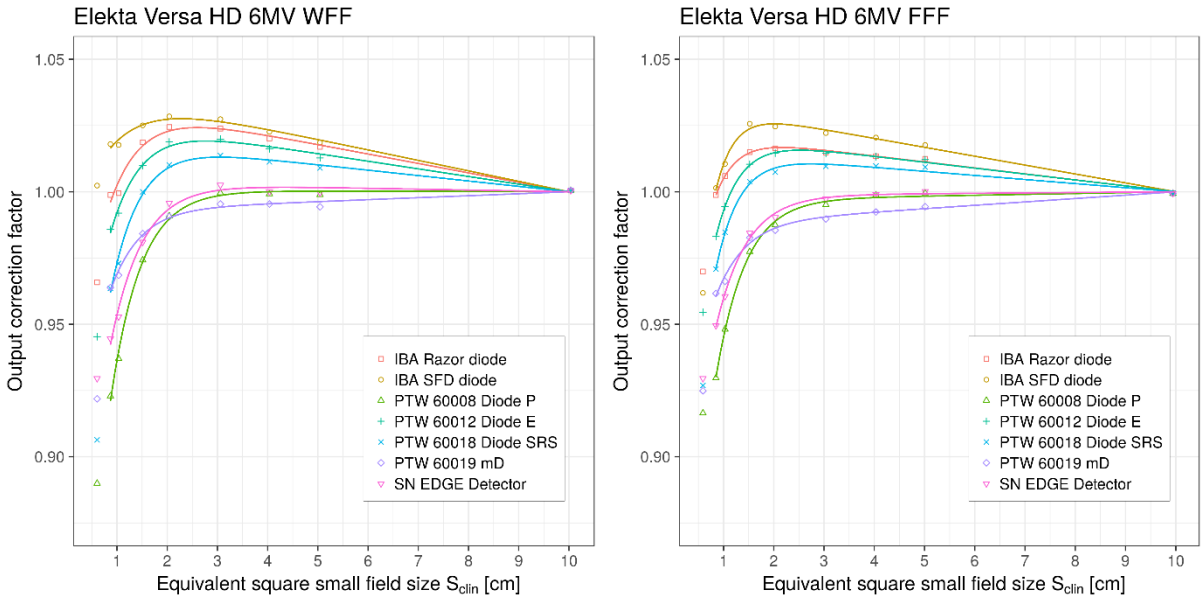

Figure 6.3. Detector specific output correction factors $k_{Q_{clin},Q_{ref}}^{f_{clin},f_{ref}}$ for seven solid-state detectors for 6 MV WFF and FFF on Elekta Versa HD linac. Output correction factors are presented as individual values/points and as analytical function applying Eqs. (5.14) and (5.15) respectively. Measured data represent "total" correction factors and include contributions from both, volume averaging effect as well as perturbation correction factors. 0.5 cm field was not considered for fitting.

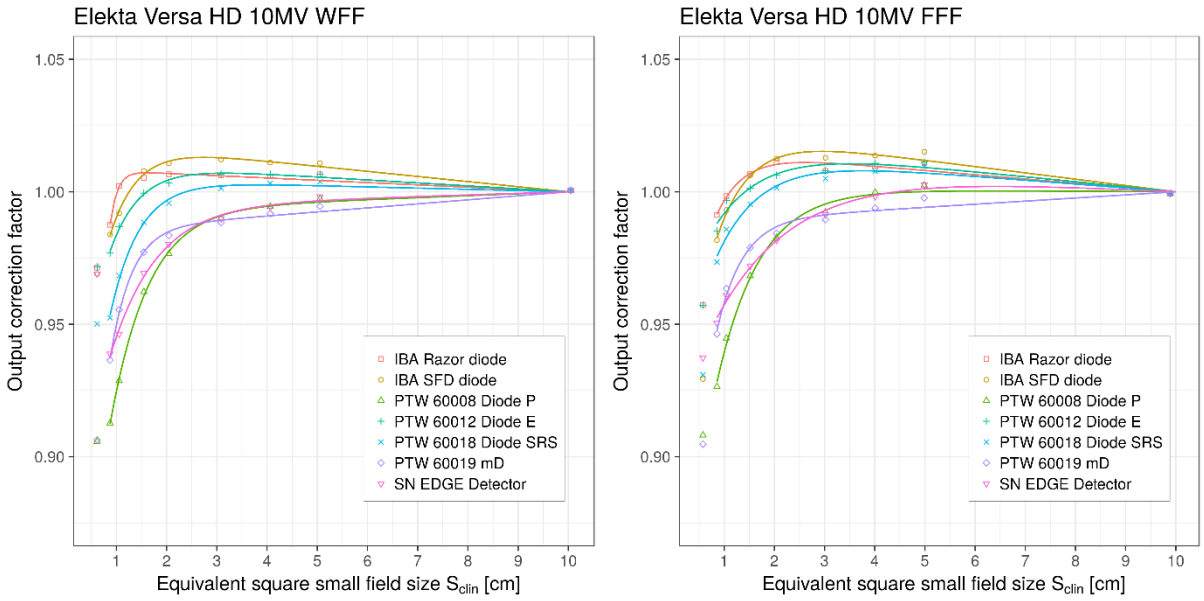

Figure 6.4 Detector specific output correction factors $k_{Q_{clin},Q_{ref}}^{f_{clin},f_{ref}}$ for seven solid-state detectors for 10 MV WFF and FFF beams on Elekta Versa HD linac. Output correction factors are presented as individual values/points and as analytical function applying Eqs. (5.14) and (5.15) respectively. Measured data represent "total" correction factors and include contributions from both, volume averaging effect as well as perturbation correction factors. 0.5 cm field was not considered for fitting.

Table 6.7 Detector specific output correction factors $k_{Q_{clin},Q_{ref}}^{f_{clin},f_{ref}}$ obtained on Elekta Versa HD linac for six diodes and a microDiamond detector and four investigated photon beams. These values were obtained by using Eq. (5.14). Values in brackets show absolute uncertainties (1 SD) in the last one or two digits. Measured data represent "total" correction factors and include contributions from both, volume averaging effect as well as perturbation correction factors.

E	Field size[a] (cm)	IBA SFD diode	IBA Razor diode	PTW 60008 Diode P	PTW 60012 Diode E	PTW 60018 Diode SRS	SN EDGE Detector	PTW 60019 mD
6 MV WFF	0.5	1.002 (10)	0.966 (10)	0.890 (9)	0.945 (10)	0.906 (9)	0.930 (10)	0.922 (10)
	0.8	1.018 (8)	0.999 (8)	0.923 (7)	0.986 (7)	0.964 (7)	0.945 (7)	0.964 (8)
	1.0	1.018 (7)	0.999 (7)	0.937 (6)	0.992 (7)	0.973 (7)	0.953 (7)	0.968 (7)
	1.5	1.025 (6)	1.019 (7)	0.974 (6)	1.010 (6)	1.000 (6)	0.981 (6)	0.984 (7)
	2.0	1.028 (7)	1.024 (7)	0.991 (6)	1.019 (7)	1.010 (6)	0.996 (7)	0.991 (7)
	3.0	1.027 (6)	1.024 (6)	1.000 (6)	1.020 (6)	1.014 (6)	1.003 (6)	0.995 (6)
	4.0	1.023 (6)	1.020 (6)	0.999 (6)	1.016 (6)	1.011 (6)	1.000 (6)	0.995 (6)
	5.0	1.019 (6)	1.017 (6)	0.999 (6)	1.013 (6)	1.009 (6)	1.000 (6)	0.994 (6)
	10.0	1.001 (0)	1.001 (2)	1.001 (1)	1.001 (0)	1.001 (0)	1.001 (2)	1.001 (3)
6 MV FFF	0.5	0.962 (12)	0.970 (12)	0.916 (12)	0.955 (12)	0.927 (12)	0.930 (12)	0.925 (12)
	0.8	1.001 (9)	0.999 (9)	0.930 (9)	0.983 (9)	0.971 (9)	0.949 (9)	0.962 (9)
	1.0	1.011 (9)	1.006 (9)	0.948 (8)	0.994 (8)	0.985 (8)	0.961 (8)	0.966 (8)
	1.5	1.026 (8)	1.015 (8)	0.977 (7)	1.010 (8)	1.004 (8)	0.984 (8)	0.983 (8)
	2.0	1.025 (8)	1.016 (8)	0.987 (8)	1.015 (8)	1.007 (8)	0.990 (8)	0.985 (8)
	3.0	1.022 (7)	1.015 (7)	0.995 (7)	1.014 (7)	1.010 (7)	0.997 (7)	0.990 (7)
	4.0	1.020 (8)	1.013 (7)	0.999 (7)	1.013 (7)	1.010 (7)	0.999 (7)	0.992 (7)
	5.0	1.018 (8)	1.012 (8)	1.000 (8)	1.012 (8)	1.009 (8)	1.000 (8)	0.994 (8)
	10.0	0.999 (0)	0.999 (0)	0.999 (1)	0.999 (1)	0.999 (0)	0.999 (1)	0.999 (0)

Table 6.7 (continued) Detector specific output correction factors $k_{Q_{clin},Q_{ref}}^{f_{clin},f_{ref}}$ obtained on Elekta Versa HD linac for six diodes and a microDiamond detector and four investigated photon beams. These values were obtained by using Eq. (5.14). Values in brackets show absolute uncertainties (1 SD) in the last one or two digits. Measured data represent "total" correction factors and include contributions from both, volume averaging effect as well as perturbation correction factors

E	Field size[a] (cm)	IBA SFD diode	IBA Razor diode	PTW 60008 Diode P	PTW 60012 Diode E	PTW 60018 Diode SRS	SN EDGE Detector	PTW 60019 mD
10 MV WFF	0.5	0.969 (12)	0.971 (12)	0.906 (11)	0.972 (12)	0.950 (12)	0.969 (12)	0.906 (11)
	0.8	0.984 (8)	0.988 (8)	0.913 (8)	0.977 (8)	0.952 (8)	0.939 (8)	0.936 (8)
	1.0	0.992 (8)	1.002 (8)	0.929 (7)	0.987 (8)	0.968 (8)	0.946 (7)	0.955 (8)
	1.5	1.008 (7)	1.005 (7)	0.962 (7)	0.999 (7)	0.989 (7)	0.969 (7)	0.977 (7)
	2.0	1.011 (7)	1.007 (7)	0.977 (7)	1.003 (7)	0.996 (7)	0.980 (7)	0.984 (7)
	3.0	1.012 (7)	1.006 (7)	0.990 (6)	1.007 (6)	1.001 (7)	0.990 (7)	0.988 (7)
	4.0	1.011 (7)	1.006 (7)	0.995 (6)	1.007 (6)	1.003 (7)	0.994 (6)	0.992 (7)
	5.0	1.011 (7)	1.007 (7)	0.997 (7)	1.007 (7)	1.004 (7)	0.998 (7)	0.995 (7)
	10.0	1.001 (0)	1.001 (2)	1.001 (1)	1.001 (1)	1.001 (2)	1.001 (1)	1.001 (3)
10 MV FFF	0.5	0.929 (13)	0.957 (13)	0.908 (13)	0.957 (13)	0.931 (13)	0.937 (13)	0.905 (13)
	0.8	0.982 (10)	0.991 (10)	0.926 (9)	0.985 (10)	0.973 (10)	0.951 (9)	0.946 (9)
	1.0	0.993 (9)	0.998 (9)	0.945 (8)	0.997 (9)	0.986 (9)	0.961 (9)	0.963 (9)
	1.5	1.006 (8)	1.007 (8)	0.968 (7)	1.001 (8)	0.995 (8)	0.972 (7)	0.979 (7)
	2.0	1.012 (8)	1.011 (8)	0.983 (7)	1.006 (8)	1.001 (8)	0.982 (8)	0.984 (8)
	3.0	1.013 (7)	1.008 (7)	0.992 (7)	1.008 (7)	1.005 (7)	0.991 (7)	0.990 (7)
	4.0	1.014 (8)	1.010 (8)	1.000 (7)	1.011 (8)	1.008 (8)	0.998 (7)	0.994 (7)
	5.0	1.015 (8)	1.011 (8)	1.002 (8)	1.011 (8)	1.010 (8)	1.003 (8)	0.998 (8)
	10.0	0.999 (1)	0.999 (1)	0.999 (0)	0.999 (2)	0.999 (2)	0.999 (1)	0.999 (1)

[a]Field size is indicated as nominal square field side length. The relationship between the nominal size and the corresponding equivalent square small field sizes S_{clin} is provided in Table 6.1 for all photon beams and field sizes.

Figures 6.5 and 6.6 shows detector specific output correction factors $k_{Q_{clin},Q_{ref}}^{f_{clin},f_{ref}}$ for seven solid-state detectors for four photon beams on Varian TrueBeam linac. Output correction factors are presented as individual values/points and as analytical function applying Eqs. (5.14) and (5.15) respectively. The data obtained from Eq. (5.14) were fitted down to the field size of 0.8 cm to ensure acceptable fit of the selected fitting function – points for field size 0.5 cm were omitted from the fit.

For comparison and further analysis, individual discrete values for $k_{Q_{clin},Q_{ref}}^{f_{clin},f_{ref}}$ are provided in Table 6.8 for all photon beams and field sizes. $k_{Q_{clin},Q_{ref}}^{f_{clin},f_{ref}}$ represent "total" output correction factors for a particular detector and include contributions from both volume averaging effect as well as perturbation correction factors.

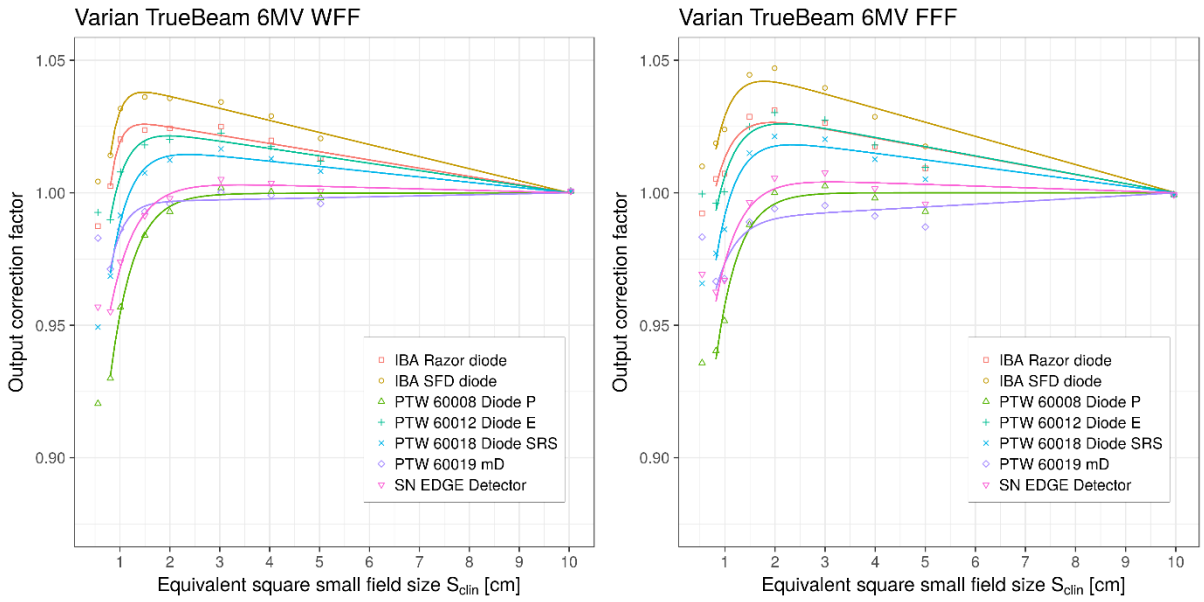

Figure 6.5. Detector specific output correction factors $k_{Q_{clin},Q_{ref}}^{f_{clin},f_{ref}}$ for seven solid-state detectors for 6 MV WFF and FFF beams on Varian TrueBeam linac. Output correction factors are presented as individual values/points and as analytical function applying Eqs. (5.14) and (5.15) respectively. Measured data represent "total" correction factors and include contributions from both, volume averaging effect as well as perturbation correction factors. 0.5 cm field was not considered for fitting.

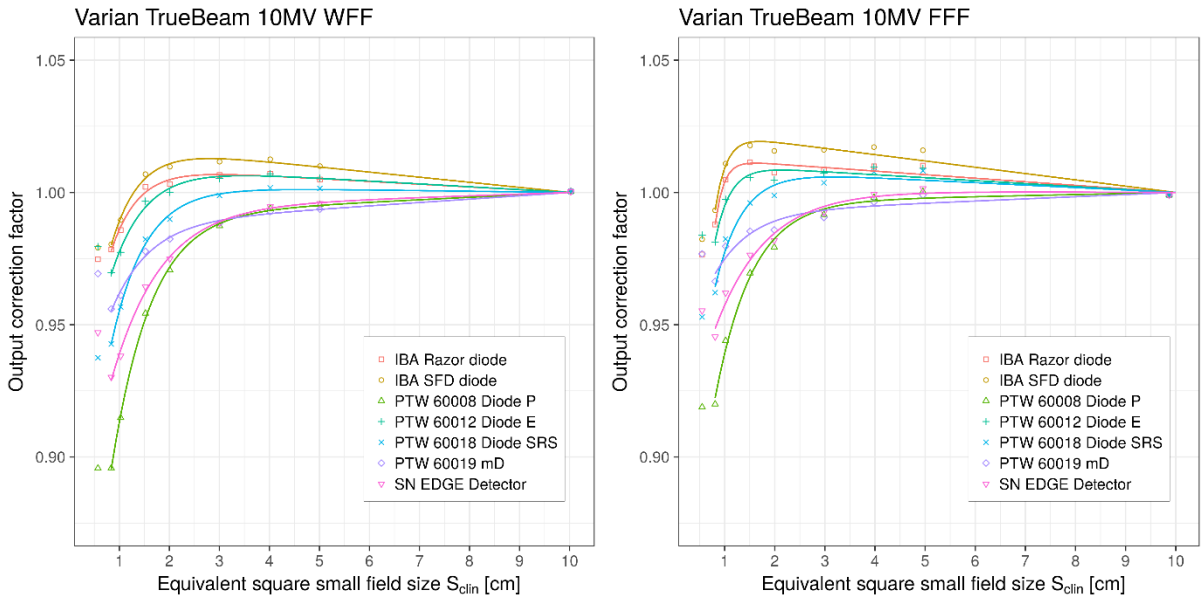

Figure 6.6. Detector specific output correction factors $k_{Q_{clin},Q_{ref}}^{f_{clin},f_{ref}}$ for seven solid-state detectors for 10 MV WFF and FFF beams on Varian TrueBeam linac. Output correction factors are presented as individual values/points and as analytical function applying Eqs. (5.14) and (5.15) respectively. Measured data represent "total" correction factors and include contributions from both, volume averaging effect as well as perturbation correction factors. 0.5 cm field was not considered for fitting.

Table 6.8 Detector specific output correction factors $k_{Q_{clin},Q_{ref}}^{f_{clin},f_{ref}}$ obtained on Varian TrueBeam linac for six diodes and a microDiamond detector and four investigated photon beams. These values were obtained by using Eq. (5.14). Values in brackets show absolute uncertainties (1 SD) in the last one or two digits. Measured data represent "total" correction factors and include contributions from both, volume averaging effect as well as perturbation correction factors.

E	Field size[a] (cm)	IBA SFD diode	IBA Razor diode	PTW 60008 Diode P	PTW 60012 Diode E	PTW 60018 Diode SRS	SN EDGE Detector	PTW 60019 mD
6 MV WFF	0.5	1.004 (20)	0.987 (19)	0.920 (18)	0.993 (20)	0.949 (19)	0.957 (19)	0.983 (19)
	0.8	1.014 (13)	1.002 (13)	0.930 (12)	0.990 (13)	0.969 (13)	0.955 (13)	0.971 (13)
	1.0	1.032 (12)	1.020 (12)	0.957 (11)	1.008 (12)	0.991 (12)	0.974 (12)	0.986 (12)
	1.5	1.036 (12)	1.024 (11)	0.984 (11)	1.018 (11)	1.007 (11)	0.991 (11)	0.993 (11)
	2.0	1.036 (12)	1.024 (12)	0.993 (11)	1.020 (12)	1.012 (12)	0.998 (11)	0.996 (11)
	3.0	1.034 (11)	1.025 (11)	1.002 (11)	1.023 (11)	1.017 (11)	1.005 (11)	1.000 (11)
	4.0	1.029 (11)	1.020 (11)	1.000 (11)	1.017 (11)	1.013 (11)	1.004 (11)	0.999 (11)
	5.0	1.021 (11)	1.013 (11)	0.998 (10)	1.012 (11)	1.008 (10)	1.001 (10)	0.996 (10)
	10.0	1.001 (1)	1.001 (0)	1.001 (1)	1.001 (1)	1.001 (1)	1.001 (1)	1.001 (0)
6 MV FFF	0.5	1.010 (23)	0.992 (22)	0.936 (21)	1.000 (22)	0.966 (22)	0.969 (22)	0.983 (22)
	0.8	1.019 (16)	1.005 (15)	0.940 (14)	0.996 (15)	0.977 (15)	0.963 (15)	0.967 (15)
	1.0	1.024 (15)	1.007 (15)	0.952 (14)	1.000 (14)	0.986 (14)	0.967 (14)	0.968 (14)
	1.5	1.045 (15)	1.029 (14)	0.988 (14)	1.025 (14)	1.015 (14)	0.996 (14)	0.989 (14)
	2.0	1.047 (14)	1.031 (14)	1.000 (14)	1.030 (14)	1.021 (14)	1.006 (14)	0.994 (14)
	3.0	1.040 (13)	1.026 (13)	1.003 (13)	1.027 (13)	1.020 (13)	1.008 (13)	0.995 (13)
	4.0	1.029 (12)	1.017 (12)	0.998 (12)	1.018 (12)	1.013 (12)	1.002 (12)	0.991 (12)
	5.0	1.018 (11)	1.009 (11)	0.993 (11)	1.010 (11)	1.005 (11)	0.996 (11)	0.987 (11)
	10.0	0.999 (1)	0.999 (0)	0.999 (0)	0.999 (1)	0.999 (1)	0.999 (1)	0.999 (0)

Table 6.8 (continued) Detector specific output correction factors $k_{Q_{clin},Q_{ref}}^{f_{clin},f_{ref}}$ obtained on Varian TrueBeam linac for six diodes and a microDiamond detector and four investigated photon beams. These values were obtained by using Eq. (5.14). Values in brackets show absolute uncertainties (1 SD) in the last one or two digits. Measured data represent "total" correction factors and include contributions from both, volume averaging effect as well as perturbation correction factors.

E	Field size[a] (cm)	IBA SFD diode	IBA Razor diode	PTW 60008 Diode P	PTW 60012 Diode E	PTW 60018 Diode SRS	SN EDGE Detector	PTW 60019 mD
10 MV WFF	0.5	0.979 (25)	0.975 (25)	0.896 (23)	0.979 (25)	0.938 (24)	0.947 (24)	0.969 (24)
	0.8	0.980 (14)	0.978 (14)	0.896 (13)	0.970 (14)	0.943 (14)	0.930 (14)	0.956 (14)
	1.0	0.990 (14)	0.986 (14)	0.915 (13)	0.977 (13)	0.957 (13)	0.938 (13)	0.961 (13)
	1.5	1.007 (13)	1.002 (13)	0.954 (12)	0.997 (13)	0.982 (12)	0.964 (12)	0.978 (12)
	2.0	1.010 (13)	1.003 (13)	0.971 (12)	1.000 (13)	0.990 (13)	0.975 (12)	0.982 (12)
	3.0	1.012 (12)	1.007 (12)	0.987 (12)	1.005 (12)	0.999 (12)	0.989 (12)	0.988 (12)
	4.0	1.013 (12)	1.007 (12)	0.994 (12)	1.007 (12)	1.002 (12)	0.995 (12)	0.993 (12)
	5.0	1.010 (11)	1.005 (11)	0.995 (11)	1.005 (11)	1.002 (11)	0.996 (11)	0.994 (11)
	10.0	1.000 (1)	1.000 (1)	1.000 (1)	1.000 (0)	1.000 (1)	1.000 (1)	1.000 (0)
10 MV FFF	0.5	0.982 (17)	0.977 (16)	0.919 (15)	0.984 (17)	0.953 (16)	0.955 (16)	0.977 (16)
	0.8	0.993 (12)	0.988 (12)	0.920 (11)	0.981 (12)	0.962 (12)	0.945 (12)	0.966 (12)
	1.0	1.011 (11)	1.005 (11)	0.944 (10)	0.997 (11)	0.982 (11)	0.962 (11)	0.980 (11)
	1.5	1.018 (10)	1.011 (10)	0.970 (9)	1.006 (10)	0.996 (9)	0.976 (9)	0.985 (9)
	2.0	1.016 (10)	1.008 (10)	0.979 (9)	1.005 (10)	0.999 (10)	0.982 (9)	0.986 (9)
	3.0	1.016 (9)	1.009 (9)	0.992 (9)	1.007 (9)	1.004 (9)	0.992 (9)	0.991 (9)
	4.0	1.017 (9)	1.010 (9)	0.998 (9)	1.010 (9)	1.008 (9)	0.999 (9)	0.996 (9)
	5.0	1.016 (9)	1.010 (9)	1.000 (9)	1.009 (9)	1.008 (9)	1.002 (9)	0.999 (9)
	10.0	0.999 (1)	0.999 (1)	0.999 (0)	0.999 (0)	0.999 (1)	0.999 (1)	0.999 (1)

[a]Field size is indicated as nominal square field side length. The relationship between the nominal size and the corresponding equivalent square small field sizes S_{clin} is provided in Table 6.1 for all photon beams and field sizes.

6.3.2 Ionization chambers

Figures 6.7 and 6.8 show detector specific output correction factors $k_{Q_{clin},Q_{ref}}^{f_{clin},f_{ref}}$ for seven ionization chambers included in the study, for four photon beams on Elekta Versa HD linac.

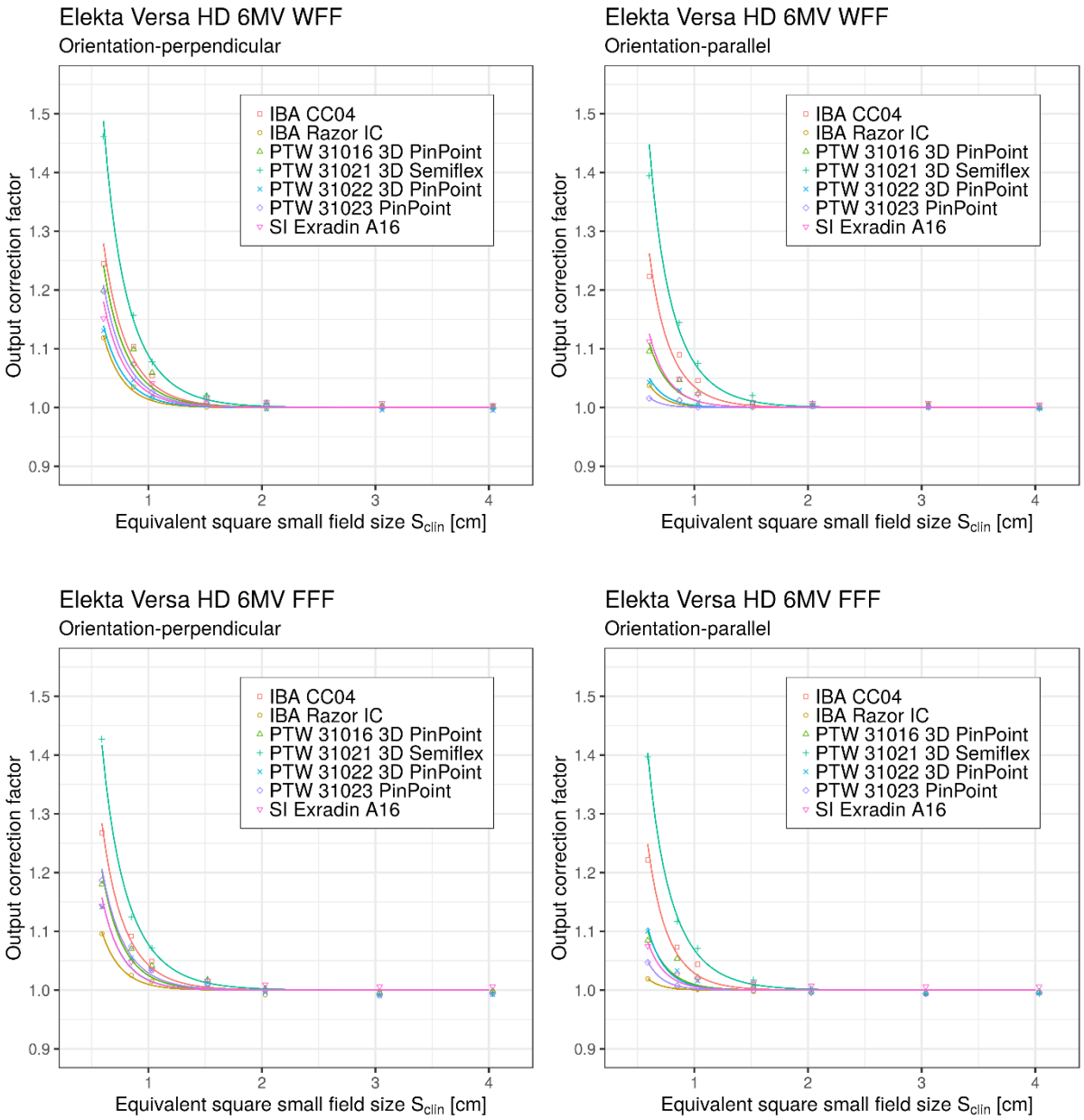

Figure 6.7. Detector specific output correction factors $k_{Q_{clin},Q_{ref}}^{f_{clin},f_{ref}}$ for seven ionization chambers for 6 MV beams and two investigated orientations of ionization chambers on Elekta Versa HD linac. Output correction factors are presented as individual values/points and as analytical function applying Eqs. (5.14) and (5.15) respectively. Measured data represent "total" correction factors and include contributions from both, volume averaging effect as well as perturbation correction factors.

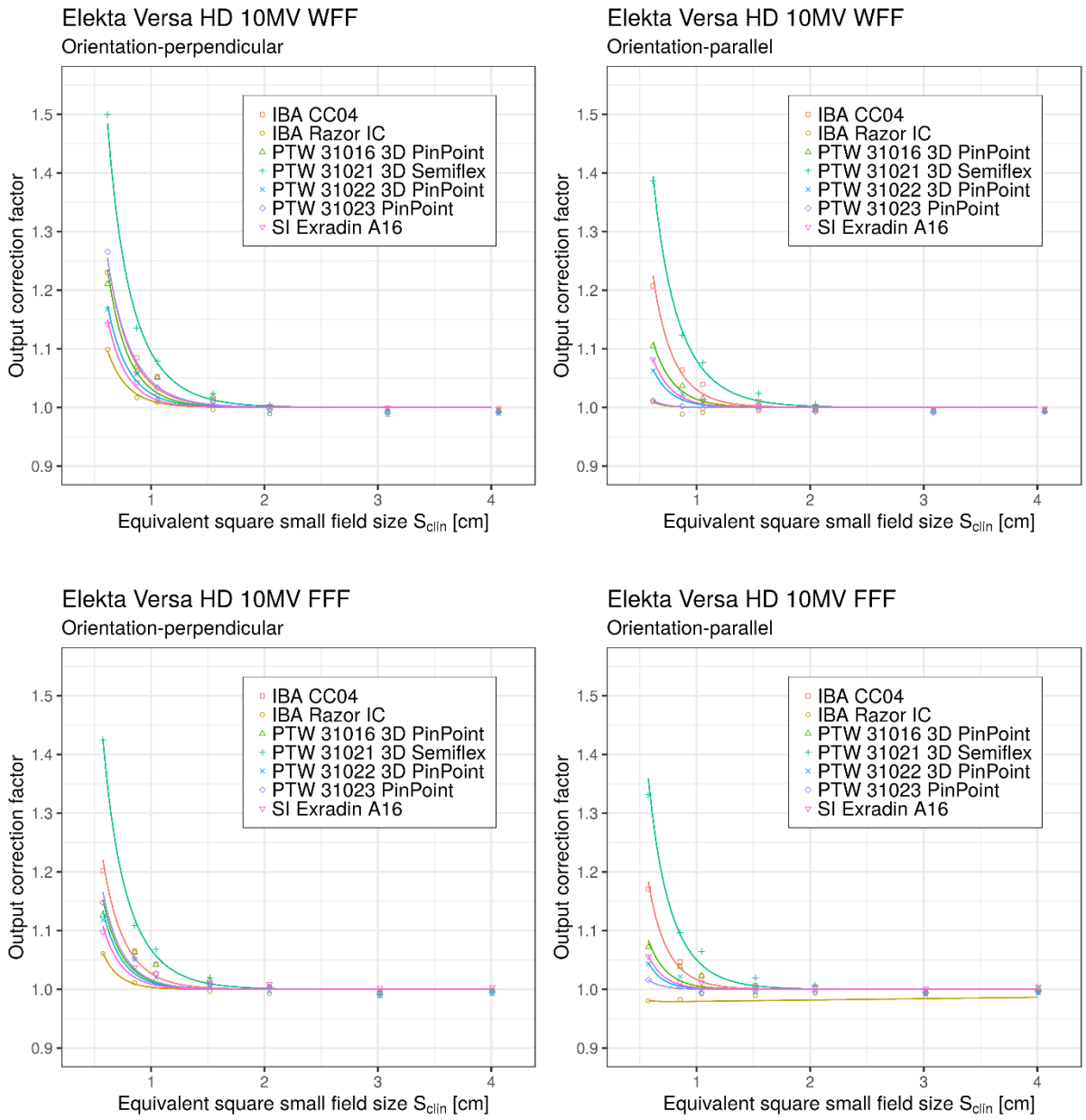

Figure 6.8. Detector specific output correction factors $k_{Q_{clin},Q_{ref}}^{f_{clin},f_{ref}}$ for seven ionization chambers for 10 MV beams and two investigated orientations of ionization chambers on Elekta Versa HD linac. Output correction factors are presented as individual values/points and as analytical function applying Eqs. (5.14) and (5.15) respectively. Measured data represent "total" correction factors and include contributions from both, volume averaging effect as well as perturbation correction factors.

Data are presented separately in eight graphs for two investigated orientations – with chamber's axis perpendicular to the central beam axis and with chamber's axis parallel to the central beam axis as described in chapter 5. For comparison and further analysis, corresponding individual values for $k_{Q_{clin},Q_{ref}}^{f_{clin},f_{ref}}$ are provided in Tables 6.9 and 6.10.

Table 6.9 Output correction factors $k_{Q_{clin},Q_{ref}}^{f_{clin},f_{ref}}$ obtained on Elekta Versa HD linac for seven ionization chambers and four investigated photon beams shown for perpendicular orientation relative to the beam axis. These values were obtained by using Eq. (5.14). Values in brackets show absolute uncertainties (1 SD) in the last one or two digits. Measured data represent "total" correction factors and include contributions from both, volume averaging effect as well as perturbation correction factors.

E	Field size[a] (cm)	IBA CC04	IBA Razor IC	PTW 31016 3D PinPoint	PTW 31021 3D Semiflex	PTW 31022 3D PinPoint	PTW 31023 PinPoint	SI Exradin A16
6 MV WFF	0.5	1.245 (19)	1.119 (17)	1.199 (18)	1.461 (25)	1.131 (18)	1.198 (20)	1.152 (17)
	0.8	1.104 (9)	1.036 (9)	1.099 (9)	1.157 (10)	1.047 (10)	1.074 (9)	1.073 (9)
	1.0	1.054 (7)	1.017 (7)	1.059 (7)	1.077 (8)	1.020 (7)	1.026 (7)	1.042 (7)
	1.5	1.011 (6)	1.001 (6)	1.020 (6)	1.020 (6)	1.005 (6)	1.007 (6)	1.015 (7)
	2.0	1.004 (6)	0.998 (7)	1.008 (6)	1.008 (6)	0.997 (6)	1.004 (6)	1.010 (7)
	3.0	1.002 (6)	1.001 (6)	1.003 (6)	1.001 (6)	0.996 (6)	0.999 (6)	1.007 (6)
	4.0	1.000 (6)	1.002 (6)	1.002 (6)	0.999 (6)	0.995 (6)	0.998 (6)	1.004 (6)
	5.0	1.000 (6)	1.004 (6)	1.004 (6)	1.000 (6)	0.996 (6)	0.998 (6)	1.003 (6)
	10.0	1.001 (0)	1.001 (1)	1.001 (0)	1.001 (0)	1.001 (0)	1.001 (1)	1.001 (2)
6 MV FFF	0.5	1.267 (22)	1.096 (18)	1.180 (20)	1.427 (26)	1.142 (22)	1.187 (21)	1.143 (19)
	0.8	1.092 (11)	1.025 (10)	1.070 (11)	1.124 (12)	1.055 (11)	1.075 (11)	1.048 (11)
	1.0	1.049 (9)	1.015 (9)	1.042 (9)	1.072 (9)	1.034 (9)	1.034 (9)	1.035 (9)
	1.5	1.010 (8)	1.003 (8)	1.017 (8)	1.018 (8)	1.007 (8)	1.010 (8)	1.016 (8)
	2.0	0.998 (8)	0.992 (8)	1.003 (8)	1.001 (8)	0.996 (8)	1.000 (8)	1.009 (8)
	3.0	0.994 (7)	0.995 (7)	0.996 (7)	0.994 (7)	0.991 (7)	0.991 (7)	1.006 (7)
	4.0	0.996 (7)	0.998 (7)	0.999 (7)	0.995 (7)	0.992 (7)	0.994 (7)	1.006 (7)
	5.0	0.997 (8)	0.999 (8)	0.999 (8)	0.996 (8)	0.995 (8)	0.995 (8)	1.006 (8)
	10.0	0.999 (0)	0.999 (0)	0.999 (0)	0.999 (0)	0.999 (0)	0.999 (0)	0.999 (0)

Table 6.9 (cont.) Output correction factors $k_{Q_{clin},Q_{ref}}^{f_{clin},f_{ref}}$ obtained on Elekta Versa HD linac for seven ionization chambers and four investigated photon beams shown for perpendicular orientation relative to the beam axis. These values were obtained by using Eq. (5.14). Values in brackets show absolute uncertainties (1 SD) in the last one or two digits. Measured data represent "total" correction factors and include contributions from both, volume averaging effect as well as perturbation correction factors.

E	Field size[a] (cm)	IBA CC04	IBA Razor IC	PTW 31016 3D PinPoint	PTW 31021 3D Semiflex	PTW 31022 3D PinPoint	PTW 31023 PinPoint	SI Exradin A16
10 MV WFF	0.5	1.230 (19)	1.099 (17)	1.211 (19)	1.499 (26)	1.167 (21)	1.265 (21)	1.143 (18)
	0.8	1.085 (10)	1.017 (9)	1.070 (10)	1.135 (11)	1.057 (11)	1.061 (10)	1.042 (11)
	1.0	1.053 (9)	1.009 (8)	1.051 (9)	1.079 (9)	1.011 (9)	1.034 (8)	1.020 (8)
	1.5	1.012 (7)	0.996 (7)	1.020 (7)	1.024 (7)	1.005 (8)	1.011 (7)	1.008 (7)
	2.0	0.998 (7)	0.989 (7)	1.000 (7)	1.004 (7)	0.993 (7)	0.997 (7)	1.002 (7)
	3.0	0.994 (6)	0.992 (6)	0.993 (6)	0.994 (6)	0.988 (6)	0.989 (6)	0.999 (6)
	4.0	0.994 (6)	0.995 (6)	0.995 (6)	0.993 (6)	0.990 (6)	0.992 (6)	0.999 (6)
	5.0	0.996 (7)	0.998 (7)	0.997 (7)	0.995 (7)	0.993 (7)	0.995 (7)	1.000 (7)
	10.0	1.001 (1)	1.001 (0)	1.001 (0)	1.001 (1)	1.001 (1)	1.001 (0)	1.001 (1)
10 MV FFF	0.5	1.202 (20)	1.061 (17)	1.126 (18)	1.425 (24)	1.118 (18)	1.148 (19)	1.098 (17)
	0.8	1.065 (11)	1.011 (11)	1.063 (11)	1.109 (12)	1.051 (11)	1.053 (11)	1.038 (11)
	1.0	1.042 (10)	1.009 (9)	1.042 (10)	1.068 (10)	1.020 (10)	1.027 (11)	1.027 (9)
	1.5	1.009 (8)	0.997 (8)	1.016 (8)	1.020 (8)	1.002 (8)	1.009 (8)	1.011 (8)
	2.0	1.004 (8)	0.993 (8)	1.003 (8)	1.005 (8)	0.996 (8)	1.002 (8)	1.009 (8)
	3.0	0.995 (7)	0.993 (7)	0.994 (7)	0.996 (7)	0.989 (7)	0.990 (7)	1.002 (7)
	4.0	0.998 (7)	0.998 (7)	0.997 (7)	0.998 (7)	0.992 (7)	0.994 (7)	1.003 (7)
	5.0	1.001 (8)	1.001 (8)	0.999 (8)	1.000 (8)	0.997 (8)	0.997 (8)	1.005 (8)
	10.0	0.999 (1)	0.999 (0)	0.999 (0)	0.999 (1)	0.999 (1)	0.999 (0)	0.999 (0)

[a] Field size is indicated as nominal square field side length. The relationship between the nominal field size and the corresponding equivalent square small field sizes S_{clin} is provided in Table 6.1 for all photon beams and field sizes.

Table 6.10 Output correction factors $k_{Q_{clin},Q_{ref}}^{f_{clin},f_{ref}}$ obtained on Elekta Versa HD linac for seven ionization chambers and four investigated photon beams shown for parallel orientation relative to the beam axis. These values were obtained by using Eq. (5.14). Values in brackets show absolute uncertainties (1 SD) in the last one or two digits. Measured data represent "total" correction factors and include contributions from both, volume averaging effect as well as perturbation correction factors.

E	Field size[a] (cm)	IBA CC04	IBA Razor IC	PTW 31016 3D PinPoint	PTW 31021 3D Semiflex	PTW 31022 3D PinPoint	PTW 31023 PinPoint	SI Exradin A16
6 MV WFF	0.5	1.223 (19)	1.037 (15)	1.096 (16)	1.394 (23)	1.043 (15)	1.016 (14)	1.112 (16)
	0.8	1.090 (9)	1.012 (9)	1.047 (9)	1.145 (10)	1.029 (9)	1.012 (8)	1.049 (9)
	1.0	1.046 (7)	1.003 (7)	1.024 (7)	1.075 (8)	1.009 (7)	1.000 (8)	1.022 (7)
	1.5	1.009 (6)	1.001 (6)	1.007 (6)	1.021 (6)	1.002 (6)	1.001 (6)	1.009 (6)
	2.0	1.003 (6)	1.005 (7)	1.004 (6)	1.007 (6)	1.002 (6)	1.003 (6)	1.008 (7)
	3.0	1.002 (6)	1.005 (6)	1.003 (6)	1.000 (6)	1.000 (6)	1.001 (6)	1.007 (6)
	4.0	0.999 (6)	1.004 (6)	1.000 (6)	0.998 (6)	0.998 (6)	1.000 (6)	1.005 (6)
	5.0	1.000 (6)	1.005 (6)	1.000 (6)	0.999 (6)	0.998 (6)	0.999 (6)	1.004 (6)
	10.0	1.001 (0)	1.001 (2)	1.001 (0)	1.001 (1)	1.001 (0)	1.001 (0)	1.001 (2)
6 MV FFF	0.5	1.222 (21)	1.019 (16)	1.085 (18)	1.397 (25)	1.100 (18)	1.047 (17)	1.075 (18)
	0.8	1.073 (11)	1.005 (10)	1.054 (11)	1.117 (11)	1.033 (10)	1.008 (10)	1.026 (10)
	1.0	1.044 (9)	1.001 (9)	1.022 (9)	1.071 (9)	1.016 (9)	1.002 (9)	1.019 (9)
	1.5	1.009 (8)	0.998 (8)	1.005 (8)	1.017 (8)	1.002 (8)	1.000 (8)	1.012 (8)
	2.0	0.999 (8)	0.996 (8)	0.998 (8)	1.003 (8)	0.997 (8)	0.996 (8)	1.007 (8)
	3.0	0.994 (7)	0.995 (7)	0.996 (7)	0.995 (7)	0.994 (7)	0.994 (7)	1.006 (7)
	4.0	0.995 (7)	0.997 (7)	0.997 (7)	0.994 (7)	0.995 (7)	0.996 (7)	1.006 (7)
	5.0	0.996 (8)	0.998 (8)	0.998 (8)	0.996 (8)	0.996 (8)	0.995 (8)	1.007 (8)
	10.0	0.999 (0)	0.999 (0)	0.999 (0)	0.999 (1)	0.999 (0)	0.999 (0)	0.999 (1)

Table 6.10 (cont.) Output correction factors $k_{Q_{clin},Q_{ref}}^{f_{clin},f_{ref}}$ obtained on Elekta Versa HD linac for seven ionization chambers and four investigated photon beams, shown for parallel orientation relative to the beam axis. These values were obtained by using Eq. (5.14). Values in brackets show absolute uncertainties (1 SD) in the last one or two digits. Measured data represent "total" correction factors and include contributions from both, volume averaging effect as well as perturbation correction factors.

E	Field size[a] (cm)	IBA CC04	IBA Razor IC	PTW 31016 3D PinPoint	PTW 31021 3D Semiflex	PTW 31022 3D PinPoint	PTW 31023 PinPoint	SI Exradin A16
10 MV WFF	0.5	1.207 (19)	1.010 (15)	1.104 (17)	1.386 (23)	1.063 (16)	1.012 (15)	1.082 (17)
	0.8	1.064 (10)	0.989 (9)	1.037 (9)	1.123 (10)	1.023 (10)	1.002 (11)	1.017 (9)
	1.0	1.039 (8)	0.991 (8)	1.015 (8)	1.076 (9)	1.008 (8)	0.999 (8)	1.012 (8)
	1.5	1.011 (7)	0.994 (7)	1.004 (7)	1.024 (7)	1.001 (7)	0.998 (7)	1.003 (7)
	2.0	1.000 (7)	0.995 (7)	0.997 (7)	1.005 (7)	0.995 (7)	0.993 (7)	0.996 (7)
	3.0	0.994 (6)	0.995 (6)	0.994 (6)	0.994 (6)	0.993 (6)	0.991 (6)	0.998 (6)
	4.0	0.994 (6)	0.996 (6)	0.994 (6)	0.993 (6)	0.993 (6)	0.993 (6)	0.998 (6)
	5.0	0.996 (7)	0.996 (7)	0.996 (7)	0.995 (7)	0.995 (7)	0.995 (7)	1.000 (7)
	10.0	1.001 (1)	1.001 (1)	1.001 (1)	1.001 (0)	1.001 (0)	1.001 (0)	1.001 (1)
10 MV FFF	0.5	1.171 (19)	0.981 (15)	1.072 (17)	1.331 (22)	1.043 (17)	1.016 (16)	1.056 (17)
	0.8	1.047 (11)	0.983 (10)	1.038 (11)	1.097 (12)	1.022 (11)	1.005 (11)	1.011 (11)
	1.0	1.022 (9)	0.992 (9)	1.023 (10)	1.064 (10)	0.997 (9)	0.995 (10)	1.011 (9)
	1.5	1.006 (8)	0.989 (8)	1.005 (8)	1.019 (8)	0.996 (8)	0.997 (8)	1.002 (8)
	2.0	1.002 (8)	0.993 (8)	1.003 (8)	1.007 (8)	0.997 (8)	0.996 (8)	1.002 (8)
	3.0	0.995 (7)	0.992 (7)	0.997 (7)	0.995 (7)	0.991 (7)	0.993 (7)	1.000 (7)
	4.0	0.998 (7)	0.995 (7)	1.001 (8)	0.997 (7)	0.994 (7)	0.995 (7)	1.004 (7)
	5.0	1.001 (8)	1.000 (8)	1.002 (8)	0.999 (8)	0.998 (8)	0.999 (8)	1.007 (8)
	10.0	0.999 (1)	0.999 (0)	0.999 (2)	0.999 (0)	0.999 (0)	0.999 (0)	0.999 (0)

[a] Field size is indicated as nominal square field side length. The relationship between the nominal field size and the corresponding equivalent square small field sizes S_{clin} is provided in Table 6.1 for all photon beams and field sizes.

Figures 6.9 and 6.10 show detector specific output correction factors $k_{Q_{clin},Q_{ref}}^{f_{clin},f_{ref}}$ for seven ionization chambers included in the study, for four photon beams on Varian TrueBeam linac.

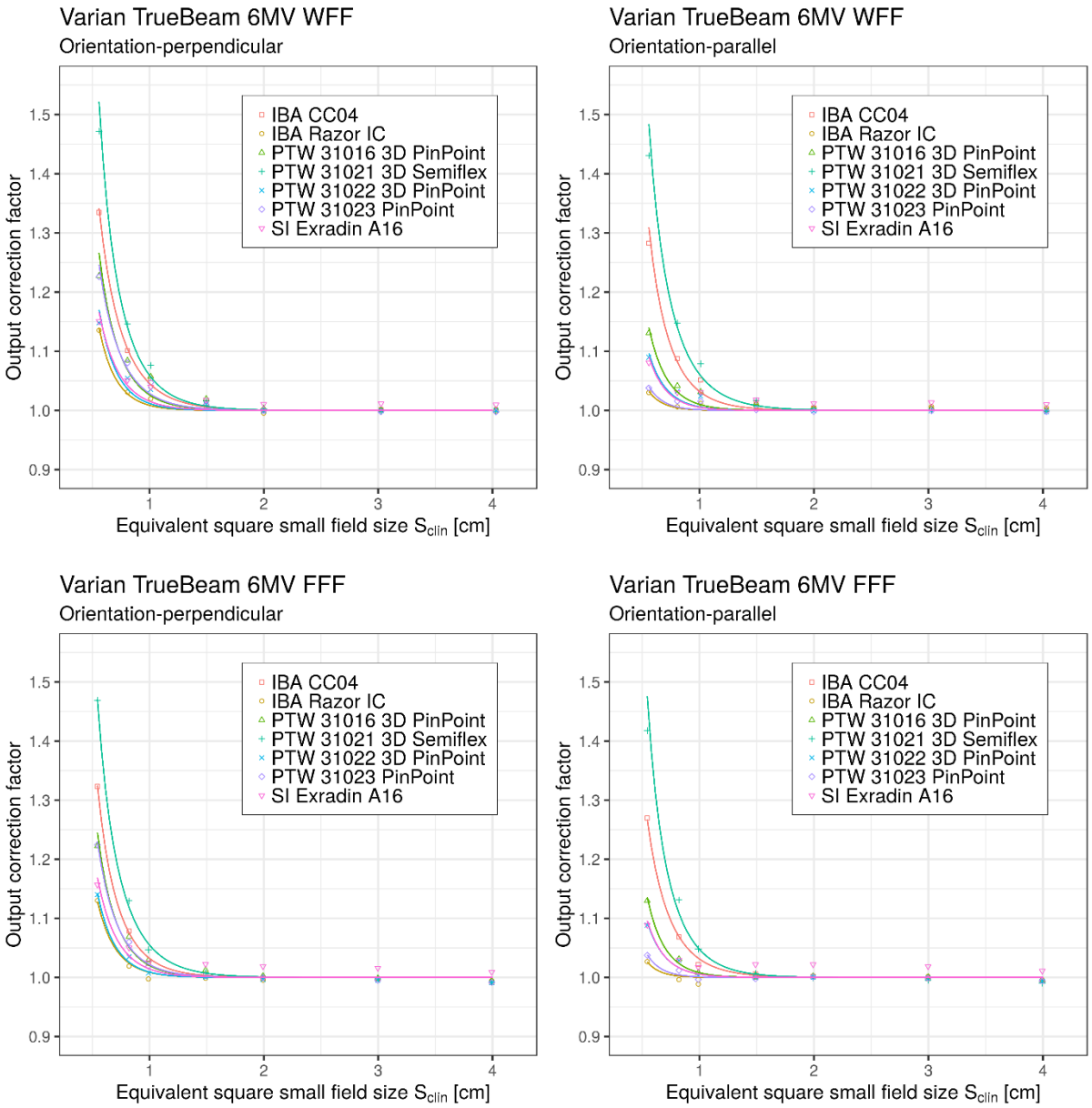

Figure 6.9 Detector specific output correction factors $k_{Q_{clin},Q_{ref}}^{f_{clin},f_{ref}}$ for seven ionization chambers for 6 MV beams and two investigated orientations of ionization chambers on Varian TrueBeam linac. Output correction factors are presented as individual values/points and as analytical function applying Eqs. (5.14) and (5.15) respectively. Measured data represent "total" correction factors and include contributions from both, volume averaging effect as well as perturbation correction factors.

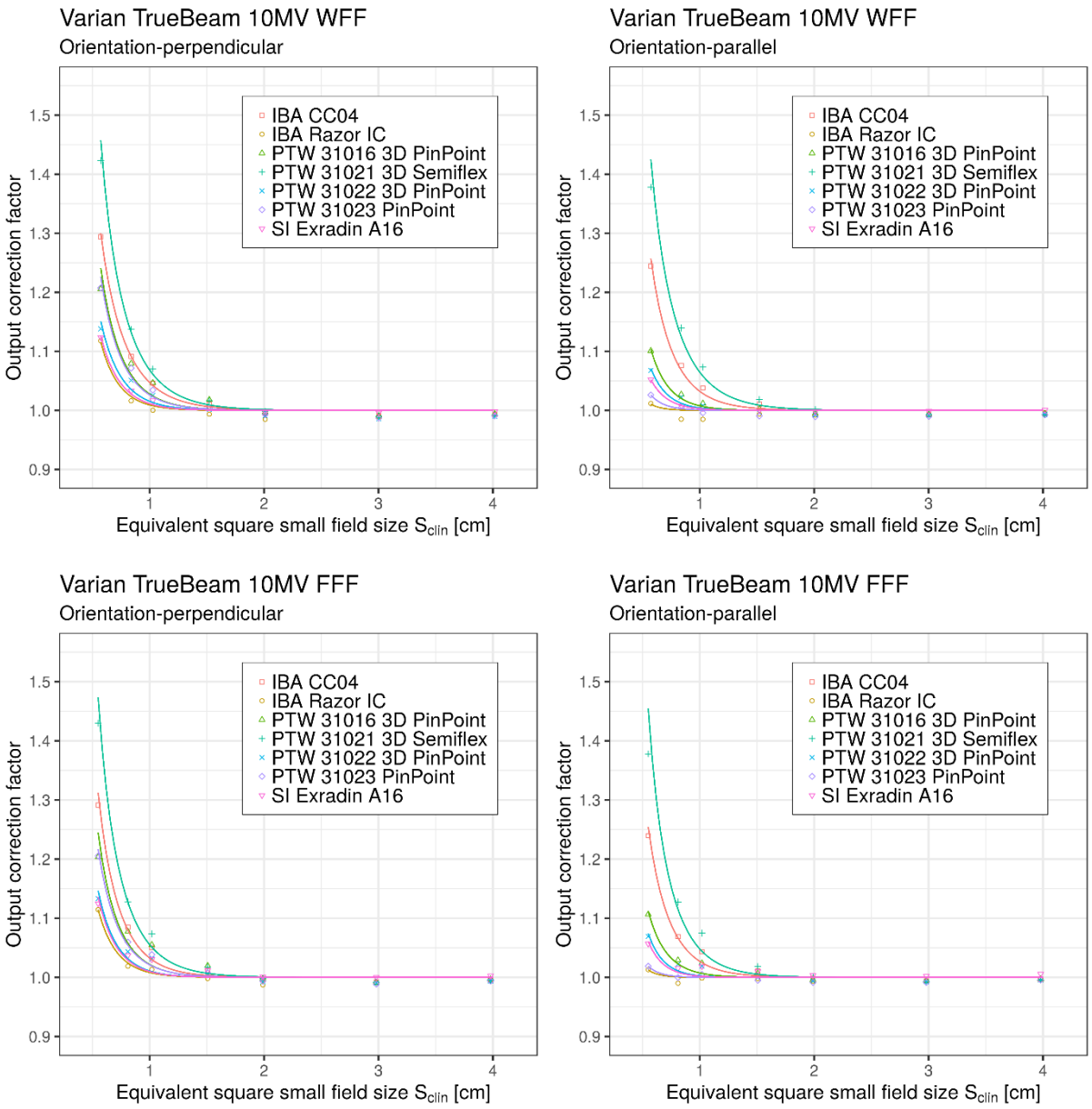

Figure 6.10 Detector specific output correction factors $k_{Q_{clin},Q_{ref}}^{f_{clin},f_{ref}}$ for seven ionization chambers for 10 MV beams and two investigated orientations of ionization chambers on Varian TrueBeam linac. Output correction factors are presented as individual values/points and as analytical function applying Eqs. (5.14) and (5.15) respectively. Measured data represent "total" correction factors and include contributions from both, volume averaging effect as well as perturbation correction factors.

Data are presented separately in eight graphs for two investigated orientations – with chamber's axis perpendicular to the central beam axis and with chamber's axis parallel to the central beam axis as described in chapter 5. For comparison and analysis, corresponding individual values for $k_{Q_{clin},Q_{ref}}^{f_{clin},f_{ref}}$ are provided in Tables 6.11 and 6.12.

Table 6.11 Output correction factors $k_{Q_{clin},Q_{ref}}^{f_{clin},f_{ref}}$ obtained on Varian TrueBeam linac for seven ionization chambers and four investigated photon beams, shown for perpendicular orientation relative to the beam axis. These values were obtained by using Eq. (5.14). Values in brackets show absolute uncertainties (1 SD) in the last one or two digits. Measured data represent "total" correction factors and include contributions from both, volume averaging effect as well as perturbation correction factors.

E	Field size[a] (cm)	IBA CC04	IBA Razor IC	PTW 31016 3D PinPoint	PTW 31021 3D Semiflex	PTW 31022 3D PinPoint	PTW 31023 PinPoint	SI Exradin A16
6 MV WFF	0.5	1.335 (31)	1.135 (25)	1.228 (28)	1.472 (35)	1.148 (25)	1.226 (28)	1.151 (26)
	0.8	1.101 (15)	1.031 (14)	1.084 (15)	1.146 (16)	1.054 (14)	1.080 (15)	1.051 (14)
	1.0	1.054 (13)	1.020 (12)	1.057 (13)	1.076 (13)	1.035 (12)	1.047 (13)	1.040 (12)
	1.5	1.012 (11)	1.003 (11)	1.020 (11)	1.016 (11)	1.010 (11)	1.010 (11)	1.018 (11)
	2.0	1.000 (11)	0.995 (11)	1.003 (12)	1.002 (12)	0.999 (11)	1.000 (11)	1.011 (12)
	3.0	1.001 (11)	1.001 (11)	1.001 (11)	0.999 (11)	0.999 (11)	0.998 (11)	1.012 (11)
	4.0	1.000 (11)	1.002 (11)	1.001 (11)	0.998 (11)	1.000 (11)	0.997 (11)	1.010 (11)
	5.0	0.997 (10)	0.999 (10)	0.998 (10)	0.996 (10)	0.998 (10)	0.995 (10)	1.005 (10)
	10.0	1.001 (1)	1.001 (0)	1.001 (1)	1.001 (0)	1.001 (1)	1.001 (0)	1.001 (0)
6 MV FFF	0.5	1.323 (33)	1.130 (27)	1.222 (30)	1.469 (38)	1.140 (28)	1.224 (30)	1.157 (28)
	0.8	1.079 (17)	1.019 (16)	1.069 (17)	1.130 (18)	1.035 (16)	1.060 (17)	1.050 (16)
	1.0	1.024 (15)	0.997 (14)	1.029 (15)	1.047 (15)	1.007 (15)	1.019 (15)	1.025 (15)
	1.5	1.004 (14)	0.999 (14)	1.012 (14)	1.008 (14)	1.000 (14)	1.003 (14)	1.022 (14)
	2.0	0.999 (14)	0.996 (14)	1.003 (14)	1.000 (14)	0.996 (14)	1.000 (14)	1.019 (14)
	3.0	0.997 (13)	0.998 (13)	0.999 (13)	0.998 (13)	0.995 (13)	0.995 (13)	1.016 (13)
	4.0	0.993 (12)	0.995 (12)	0.995 (12)	0.991 (12)	0.991 (12)	0.991 (12)	1.009 (12)
	5.0	0.989 (11)	0.990 (11)	0.991 (11)	0.988 (11)	0.988 (11)	0.988 (11)	1.003 (11)
	10.0	0.999 (0)	0.999 (1)	0.999 (0)	0.999 (0)	0.999 (0)	0.999 (0)	0.999 (1)

Table 6.11 (cont.) Output correction factors $k_{Q_{clin},Q_{ref}}^{f_{clin},f_{ref}}$ obtained on Varian TrueBeam linac for seven ionization chambers and four investigated photon beams, shown for perpendicular orientation relative to the beam axis. These values were obtained by using Eq. (5.14). Values in brackets show absolute uncertainties (1 SD) in the last one or two digits. Measured data represent "total" correction factors and include contributions from both, volume averaging effect as well as perturbation correction factors.

E	Field size[a] (cm)	IBA CC04	IBA Razor IC	PTW 31016 3D PinPoint	PTW 31021 3D Semiflex	PTW 31022 3D PinPoint	PTW 31023 PinPoint	SI Exradin A16
10 MV WFF	0.5	1.294 (36)	1.099 (17)	1.206 (33)	1.423 (40)	1.138 (31)	1.207 (33)	1.124 (30)
	0.8	1.091 (17)	1.017 (9)	1.079 (16)	1.137 (17)	1.051 (16)	1.072 (16)	1.033 (16)
	1.0	1.046 (15)	1.009 (8)	1.047 (15)	1.070 (15)	1.025 (14)	1.034 (14)	1.017 (14)
	1.5	1.010 (13)	0.996 (7)	1.018 (13)	1.016 (13)	1.001 (13)	1.004 (13)	1.006 (13)
	2.0	0.995 (13)	0.989 (7)	0.997 (13)	0.998 (13)	0.991 (13)	0.993 (13)	0.998 (13)
	3.0	0.991 (12)	0.992 (6)	0.991 (12)	0.991 (12)	0.986 (12)	0.987 (12)	0.996 (12)
	4.0	0.993 (12)	0.995 (6)	0.994 (12)	0.992 (12)	0.990 (12)	0.991 (12)	0.998 (12)
	5.0	0.994 (11)	0.998 (7)	0.994 (11)	0.993 (11)	0.991 (11)	0.992 (11)	0.998 (11)
	10.0	1.000 (0)	1.001 (0)	1.000 (0)	1.000 (0)	1.000 (0)	1.000 (0)	1.000 (0)
10 MV FFF	0.5	1.291 (25)	1.118 (30)	1.204 (23)	1.430 (28)	1.133 (21)	1.205 (23)	1.125 (21)
	0.8	1.085 (14)	1.016 (15)	1.077 (14)	1.128 (14)	1.044 (13)	1.060 (13)	1.037 (13)
	1.0	1.050 (12)	1.000 (14)	1.055 (12)	1.074 (12)	1.031 (12)	1.039 (12)	1.030 (12)
	1.5	1.012 (10)	0.993 (13)	1.020 (10)	1.017 (10)	1.006 (10)	1.008 (10)	1.012 (10)
	2.0	0.996 (10)	0.985 (12)	0.998 (10)	0.998 (10)	0.993 (10)	0.994 (10)	1.001 (10)
	3.0	0.992 (9)	0.989 (12)	0.992 (9)	0.992 (9)	0.990 (9)	0.988 (9)	1.000 (9)
	4.0	0.996 (9)	0.994 (12)	0.997 (9)	0.995 (9)	0.994 (9)	0.994 (9)	1.003 (9)
	5.0	0.998 (9)	0.995 (11)	0.999 (9)	0.998 (9)	0.997 (9)	0.995 (9)	1.005 (9)
	10.0	0.999 (0)	1.000 (1)	0.999 (0)	0.999 (0)	0.999 (0)	0.999 (0)	0.999 (1)

[a] Field size is indicated as nominal square field side length. The relationship between the nominal field size and the corresponding equivalent square small field sizes S_{clin} is provided in Table 6.1 for all photon beams and field sizes.

Table 6.12 Output correction factors $k_{Q_{clin},Q_{ref}}^{f_{clin},f_{ref}}$ obtained on Varian TrueBeam linac for seven ionization chambers and four investigated photon beams, shown for parallel orientation relative to the beam axis. These values were obtained by using Eq. (5.14). Values in brackets show absolute uncertainties (1 SD) in the last one or two digits. Measured data represent "total" correction factors and include contributions from both, volume averaging effect as well as perturbation correction factors.

E	Field size[a] (cm)	IBA CC04	IBA Razor IC	PTW 31016 3D PinPoint	PTW 31021 3D Semiflex	PTW 31022 3D PinPoint	PTW 31023 PinPoint	SI Exradin A16
6 MV WFF	0.5	1.283 (29)	1.030 (22)	1.131 (25)	1.430 (34)	1.090 (24)	1.038 (23)	1.081 (24)
	0.8	1.088 (15)	1.006 (14)	1.042 (14)	1.148 (16)	1.032 (14)	1.016 (14)	1.031 (14)
	1.0	1.052 (12)	1.012 (12)	1.031 (12)	1.079 (13)	1.024 (12)	1.016 (12)	1.031 (12)
	1.5	1.014 (11)	1.007 (11)	1.011 (11)	1.017 (11)	1.003 (11)	1.001 (11)	1.018 (11)
	2.0	1.004 (12)	1.004 (12)	1.003 (12)	1.003 (12)	0.999 (11)	0.998 (11)	1.012 (12)
	3.0	1.003 (11)	1.007 (11)	1.003 (11)	1.000 (11)	1.000 (11)	1.000 (11)	1.014 (11)
	4.0	1.001 (11)	1.005 (11)	1.001 (11)	0.999 (11)	0.998 (11)	0.998 (11)	1.010 (11)
	5.0	0.998 (10)	1.001 (10)	0.998 (10)	0.996 (10)	0.996 (10)	0.996 (10)	1.007 (10)
	10.0	1.001 (0)	1.001 (0)	1.001 (0)	1.001 (0)	1.001 (0)	1.001 (1)	1.001 (0)
6 MV FFF	0.5	1.270 (31)	1.027 (25)	1.130 (27)	1.418 (35)	1.088 (26)	1.037 (25)	1.089 (26)
	0.8	1.068 (17)	0.996 (16)	1.031 (16)	1.131 (18)	1.029 (16)	1.012 (16)	1.029 (16)
	1.0	1.022 (15)	0.989 (14)	1.008 (15)	1.048 (15)	1.003 (15)	0.996 (14)	1.017 (15)
	1.5	1.006 (14)	1.000 (14)	1.004 (14)	1.006 (14)	0.999 (14)	0.998 (14)	1.022 (14)
	2.0	1.002 (14)	1.003 (14)	1.002 (14)	1.000 (14)	1.000 (14)	1.001 (14)	1.022 (14)
	3.0	0.998 (13)	1.002 (13)	1.000 (13)	0.995 (13)	0.999 (13)	0.999 (13)	1.019 (13)
	4.0	0.993 (12)	0.996 (12)	0.995 (12)	0.991 (12)	0.994 (12)	0.994 (12)	1.011 (12)
	5.0	0.990 (11)	0.992 (11)	0.991 (11)	0.986 (11)	0.990 (11)	0.991 (11)	1.004 (11)
	10.0	0.999 (0)	0.999 (1)	0.999 (0)	0.999 (0)	0.999 (0)	0.999 (1)	0.999 (0)

Table 6.12 (cont.) Output correction factors $k_{Q_{clin},Q_{ref}}^{f_{clin},f_{ref}}$ obtained on Varian TrueBeam linac for seven ionization chambers and four investigated photon beams shown for parallel orientation relative to the beam axis. These values were obtained by using Eq. (5.14). Values in brackets show absolute uncertainties (1 SD) in the last one or two digits. Measured data represent "total" correction factors and include contributions from both, volume averaging effect as well as perturbation correction factors.

E	Field size[a] (cm)	IBA CC04	IBA Razor IC	PTW 31016 3D PinPoint	PTW 31021 3D Semiflex	PTW 31022 3D PinPoint	PTW 31023 PinPoint	SI Exradin A16
10 MV WFF	0.5	1.244 (34)	1.012 (27)	1.101 (29)	1.378 (38)	1.068 (28)	1.026 (27)	1.052 (28)
	0.8	1.076 (16)	0.985 (15)	1.027 (16)	1.140 (17)	1.022 (15)	1.004 (15)	1.008 (15)
	1.0	1.038 (15)	0.985 (14)	1.012 (14)	1.073 (15)	1.008 (14)	0.996 (14)	1.003 (14)
	1.5	1.010 (13)	0.994 (13)	1.003 (13)	1.018 (13)	0.996 (13)	0.990 (13)	1.001 (13)
	2.0	0.998 (13)	0.992 (13)	0.995 (13)	1.002 (13)	0.992 (13)	0.989 (13)	0.999 (13)
	3.0	0.993 (12)	0.994 (12)	0.993 (12)	0.993 (12)	0.991 (12)	0.990 (12)	0.999 (12)
	4.0	0.994 (12)	0.996 (12)	0.994 (12)	0.993 (12)	0.993 (12)	0.992 (12)	1.000 (12)
	5.0	0.994 (11)	0.996 (11)	0.994 (11)	0.993 (11)	0.993 (11)	0.993 (11)	1.000 (11)
	10.0	1.000 (0)	1.000 (1)	1.000 (0)	1.000 (0)	1.000 (0)	1.000 (0)	1.000 (0)
10 MV FFF	0.5	1.240 (24)	1.013 (19)	1.107 (21)	1.378 (28)	1.069 (20)	1.019 (19)	1.057 (20)
	0.8	1.069 (14)	0.990 (12)	1.029 (13)	1.127 (14)	1.022 (13)	1.000 (13)	1.015 (13)
	1.0	1.043 (12)	0.999 (11)	1.024 (11)	1.075 (12)	1.019 (11)	1.005 (11)	1.019 (11)
	1.5	1.011 (10)	0.998 (10)	1.007 (10)	1.018 (10)	1.000 (10)	0.995 (9)	1.010 (10)
	2.0	0.998 (10)	0.993 (10)	0.996 (10)	1.001 (10)	0.994 (10)	0.991 (10)	1.004 (10)
	3.0	0.994 (9)	0.995 (9)	0.994 (9)	0.993 (9)	0.992 (9)	0.991 (9)	1.002 (9)
	4.0	0.997 (9)	0.998 (9)	0.997 (9)	0.996 (9)	0.996 (9)	0.996 (9)	1.006 (9)
	5.0	0.998 (9)	1.000 (9)	0.999 (9)	0.997 (9)	0.998 (9)	0.996 (9)	1.007 (9)
	10.0	0.999 (0)	0.999 (0)	0.999 (1)	0.999 (1)	0.999 (1)	0.999 (0)	0.999 (0)

[a] Field size is indicated as nominal square field side length. The relationship between the nominal field size and the corresponding equivalent square small field sizes S_{clin} is provided in Table 6.1 for all photon beams and field sizes.

7 DISCUSSION

7.1 Field output factors

In the present study field output factors for small fields were determined with two reference detectors, radiochromic EBT3 films, and Exradin W1 plastic scintillator, which are considered as perturbation free except for volume averaging. The study was conducted on two different linacs, Elekta Versa HD and Varian TrueBeam, for four photon beams: 6 MV WFF, 6 MV FFF, 10 MV WFF, and 10 MV FFF. On Elekta Versa HD linac, small static fields were shaped with MLC and jaws, while on Varian TrueBeam only jaws were used for field shaping. Measured data were corrected for volume averaging effect obtained from film measurements, and fitted by the analytical function proposed by Sauer and Wilbert. Volume averaging correction factors k_{vol} are found to be almost negligible for EBT3 films (maximum values around 0.2% for the smallest field size) while for W1 PSD they reach almost 1% for the smallest nominal field size of 0.5 cm (see Table 6.4). The data for W1 PSD indicate that volume averaging has to be considered in the determination of field output factors for this detector and other detectors of similar size. The present novel approach for calculating k_{vol} from 2D dose matrices obtained with EBT3 films and fitted to bivariate Gaussian function is a viable option for correcting measured signals for volume averaging effect, not only for two selected reference detectors, but for any small detector with known dimensions of its sensitive volume.

The analytical function from Eq. (5.13) yielded excellent fits to the measured data: uncertainties of the fit ranged from 1.0 to1.4% (1 SD) for the smallest field size of 0.5 cm when measurements were performed on the Elekta Versa HD linac for the photon beams investigated. Results of measurements on Varian TrueBeam exhibited higher uncertainties than on Elekta Versa HD, ranging from 1.6 to 2.5% (1 SD) for the smallest field size of 0.5 cm. Higher uncertainties are possibly due to the higher inhomogeneity of the EBT3 films in the lot that was used on the Varian TrueBeam linac.

As expected, a rapid decrease of field output factors was observed for field sizes below 2.0 cm, regardless of the photon beam or linac used. This decrease is primarily due to the loss of lateral charged-particle equilibrium and partial occlusion of the primary radiation source by different collimating devices used in the study, which is thoroughly described in the literature.[10,51,53,83]

It can be seen from Tables 6.2 and 6.3 that the field output factors for FFF beams of given beam energy are always larger than the field output factors for the corresponding (same energy and linac) WFF beams for all investigated fields. The results of one-tailed Student's t-test given in Table 6.6 show that for 6 and 10 MV beams on Elekta Versa HD and 10 MV beams on Varian TrueBeam, statistically significant differences ($p < 0.05$) are observed for field output factors between the FFF and the corresponding WFF beams for all investigated fields. The only exception is 5.0 cm field for 6 MV beams on Elekta Versa HD where no statistical significance was observed. For 6 MV beams on Varian TrueBeam, similar differences of the same level were found only for the smallest field of 0.5 cm. The present results suggest that in general, for a given linac, small field output factors have to be determined individually for every combination of beam energy and filtration (WFF or FFF) and field size as the differences (see Table 6.6) from each other are/can be statistically significant. Thus, the data presented in this study can potentially be used as a reference data set for field output factors for the two linacs investigated.

While the present novel method for the determination of field output factors was proven as appropriate, it requires significant expertise and high experimental skills in handling W1 PSD detectors and EBT3 films; moreover, it is very time-consuming and demanding.

7.2. Detector specific output correction factors for solid-state detectors

Figures 6.3 to 6.6 show plots of the output correction factors vs. equivalent square small field size S_{clin} for all six diodes and the microDiamond detector. An analysis of the graphs for $k(S_{clin})$ displayed in those four figures show that the curves for all diodes follow a general pattern for all investigated photon beams. As can be seen, for a given value of S_{clin}, the curves for the output correction factors are at the top of the graphs for the IBA SFD diode, followed by IBA Razor diode, PTW 60012 Diode E, PTW 60018 Diode SRS, SN EDGE detector and PTW 60008 Diode P. PTW 60019 microDiamond detector exhibits somewhat different behavior although its curves are very similar to the curves of the PTW 60018 Diode SRS, SN EDGE detector and PTW 60008 Diode P.

In the following two sections, results for investigated solid-state detectors are analyzed, and comparison with the data from IAEA TRS-483 CoP is presented. However, a separate section is devoted to the discussion on the results obtained with the PTW microDiamond detector, which was extensively studied by several research groups.

At this point, we underline that the upcoming analysis and comparisons were strictly done for equivalent square field size S_{clin} as defined in the chapter 5 of the thesis.

7.2.1. Comparison with data given in TRS-483

TRS-483 has recently recommended values of output correction factors $k_{Q_{clin},Q_{ref}}^{f_{clin},f_{ref}}$ for many detectors for 6 and 10 MV WFF and FFF beams for performing accurate relative dosimetry (i.e., measurements of field output factors) in high energy photon beams. Values of $k_{Q_{clin},Q_{ref}}^{f_{clin},f_{ref}}$ for different detectors are given as a function of photon beam (i.e., 6 MV and 10 MV) as well as equivalent square small field size S_{clin}. The data given in TRS-483 for $k_{Q_{clin},Q_{ref}}^{f_{clin},f_{ref}}$ does not distinguish between linacs, filtration of beams (i.e., does not distinguish between WFF and FFF beams), and the types of collimation used, i.e., output correction factors do not depend on whether the collimation is performed using MLC, jaws or SRS cones.

Comparisons were performed between the $k_{Q_{clin},Q_{ref}}^{f_{clin},f_{ref}}$ values obtained in the present study and those recommended in the IAEA TRS-483 CoP for six solid-state detectors for both the filtered (WFF) and unfiltered (FFF) 6 MV and 10 MV photon beams. TRS-483 did not provide any data for the IBA Razor diode, therefore, comparisons could not be performed for this detector.

For every photon beam energy, detector and S_{clin} combination used in the present work, the values of $k_{Q_{clin},Q_{ref}}^{f_{clin},f_{ref}}$ from TRS-483 were obtained by linear interpolation of the corresponding data given in TRS-483. A two-tailed Student's t-test was performed to evaluate the statistical significance of differences between the data for $k_{Q_{clin},Q_{ref}}^{f_{clin},f_{ref}}$ given in TRS-483 and the corresponding data in the present study. Unless stated otherwise, only statistically significant differences will be pointed out in the rest of the discussion.

For IBA SFD diode statistically significant differences ($p < 0.05$) were found only for the smallest field of 0.5 cm on Elekta linac for 6 MV FFF and 10 MV FFF beams.

For PTW 60012 Diode P statistically significant differences ($p < 0.05$) were found on both linacs for 10 MV WFF beams for small fields 1.5 and 2.0 cm. The comparison was not made for fields below 1.5 cm as the data for these fields are not provided in the TRS-483.

For PTW 60012 Diode E statistically significant difference ($p < 0.05$) was found only for one beam, 6 MV WFF on Elekta linac for the smallest field 0.5 cm.

In the case of PTW 60018 Diode SRS, statistically significant differences ($p < 0.05$) were found on both linacs; on Elekta linac for the smallest field 0.5 cm for 6 MV WFF and FFF beams as well as for 0.8 cm field for 10 MV WFF beam, whilst on Varian linac only for 10 MV WFF beam for field size of 0.8 cm.

Comparison of $k_{Q_{clin},Q_{ref}}^{f_{clin},f_{ref}}$ values for SN EDGE detector revealed statistically significant differences when 10 MV WFF beams are used on both linacs for small fields 0.8, 1.0, 1.5 and 2.0 cm with p-values of 0.033, 0.009, 0.013 and 0.024 for the Elekta linac and 0.033, 0.012, 0.026 and 0.034 for the Varian linac respectively. Comparison was not performed for 0.5 cm field since the data for this field are not provided in the TRS-483. One-tailed Student's t-test was used in this case for the statistical evaluation as the $k_{Q_{clin},Q_{ref}}^{f_{clin},f_{ref}}$ values from the present study were lower than the corresponding values from TRS-483 for all field sizes.

Similar differences were also observed when the values of $k_{Q_{clin},Q_{ref}}^{f_{clin},f_{ref}}$ from TRS-483 were compared with those obtained from the present study for the PTW 60019 microDiamond detector. For this case, however, statistically significant differences (see Tables 7.1 and 7.2) were found for all photon beams on the Elekta Versa HD linac for fields ranging from 0.5 to 1.0 cm; additionally, for the 10 MV WFF and FFF beams, this behavior was observed for fields up to 2.0 cm.

On the Varian linac statistically significant differences ($p < 0.05$) were found only for 10 MV WFF beam for small fields 0.8 and 1.0 cm with p-values of 0.033 and 0.022 respectively. Similar to the SN EDGE detector, the $k_{Q_{clin},Q_{ref}}^{f_{clin},f_{ref}}$ values of the PTW 60019 microDiamond detector from the present study were found to be always lower than the corresponding values given in TRS-483. A one-tailed Student's t-test was used to evaluate the statistical difference between the two sets of data.

Table 7.1. Output correction factors $k_{Q_{clin},Q_{ref}}^{f_{clin},f_{ref}}(S_{clin})$ published in the TRS-483 and those obatined in this study on Elekta Versa HD linac in four investigated megavoltage beams for PTW 60019 mD detector. Data represent „total" correction factors and include contributions from both, volume averaging effect as well as perturbation correction factors. TRS-483 data were obtained by linear interpolation of published data matching clinical field sizes S_{clin} from our study (see Table 6.1).

	Output correction factors $k_{Q_{clin},Q_{ref}}^{f_{clin},f_{ref}}$ for PTW 60019 microDiamond							
	TRS-483				THIS STUDY			
Field size[a] [cm]	6 MV WFF	6 MV FFF	10 MV WFF	10 MV FFF	6 MV WFF	6 MV FFF	10 MV WFF	10 MV FFF
0.5	0.968	0.967	0.969	0.967	0.922	0.925	0.906	0.905
0.8	0.979	0.979	0.979	0.979	0.964	0.962	0.936	0.946
1.0	0.985	0.985	0.986	0.985	0.968	0.966	0.955	0.963
1.5	0.993	0.993	0.993	0.993	0.984	0.983	0.977	0.979
2.0	0.997	0.997	0.997	0.997	0.991	0.985	0.984	0.984

[a]Field size is indicated as nominal square field side length. The relationship between the nominal size and the corresponding equivalent square small field sizes S_{clin} is provided in Table 6.1 for all investigated photon beams and field sizes.

Table 7.2 Statistical significance (p-values) of the differences between output correction factors $k_{Q_{clin},Q_{ref}}^{f_{clin},f_{ref}}$ for PTW 60019 mD detector given in TRS-483 and the corresponding values from the present study evaluated with one-tailed Student's t-test. Data for 6 and 10 MV beams from TRS-483 were compared with data from present study for both filtered (WFF) and unfiltered (FFF) 6 MV and 10 MV beams on Elekta Versa HD linac.

		p-values			
	Field size[a] (cm)	Elekta Versa HD			
		6 MV WFF	6 MV FFF	10 MV WFF	10 MV FFF
PTW 60019 mD	0.5	0.001	0.003	0.001	0.001
	0.8	0.027	0.025	0.001	0.004
	1.0	0.014	0.014	0.002	0.010
	1.5	0.070	0.059	0.016	0.027
	2.0	0.118	0.042	0.023	0.031

[a] Field size is indicated as nominal square field side length. The relationship between the nominal field size and the corresponding equivalent square field sizes S_{clin} is provided in Table 6.1 for all photon beams and field sizes.

7.2.2. Influence of beam filtration and collimating system on output correction factors

As stated earlier, TRS-483 provided tabulated data for output correction factors $k_{Q_{clin},Q_{ref}}^{f_{clin},f_{ref}}$ for several solid-state detectors as a function of the equivalent square small field size S_{clin}. These data do not distinguish between WFF and FFF beams for a given beam energy. Furthermore, the data also do not distinguish between the types of collimation that are used to create a small field, i.e., whether the fields are collimated using MLC, jaws or SRS cones. To investigate the validity of that approach, an analysis was done to determine the dependence of the $k_{Q_{clin},Q_{ref}}^{f_{clin},f_{ref}}$ values for different detectors on beam collimation and beam filtration for a given beam energy.

First, for given beam energy and a selected linac, all small field $k_{Q_{clin},Q_{ref}}^{f_{clin},f_{ref}}$ values for the investigated detectors for WFF and FFF beams were compared with each other to determine whether output correction factors differed significantly from each other or not. No significant differences were observed for measurements done with the IBA Razor, PTW 60012 E, and PTW 60019 mD detectors on both Versa HD and TrueBeam linacs using both

6 MV WFF/6MV FFF and 10 MV WFF/10MV FFF beams. For the other four detectors, significant differences ($p < 0.05$) were found for the smallest field sizes when measurements were done on the Elekta Versa HD linac. Measurements with IBA SFD diode showed significant differences using both 6 MV WFF/FFF and 10 MV WFF/FFF beams for field size 0.5 cm. In the case of PTW 60012 diode E, significant differences were found for 6 MV WFF/FFF beams for 0.5 cm field, while comparison of measurements performed with PTW 60018 Diode SRS and SN Edge detector showed significant differences for 10 MV WFF/FFF beams for field sizes 0.8 and 0.5 cm respectively. The PTW 60008 P diode showed a significant dependence on beam filtration for 10 MV beams on the Varian linac; statistically significant differences ($p < 0.05$) were found for field sizes 0.8 and 1.0 cm, and this was the only case where significant differences were found between WFF and FFF beams on Varian linac.

Second, $k_{Q_{clin},Q_{ref}}^{f_{clin},f_{ref}}$ values for selected beam energy and filtration on one linac was compared to the corresponding values on the second linac, e.g., $k_{Q_{clin},Q_{ref}}^{f_{clin},f_{ref}}$ values for 6 MV WFF beam on Elekta linac were compared to the corresponding values for 6 MV WFF beam on the Varian linac, etc. Analysis of the results show that statistically significant differences ($p < 0.05$) were found for all detectors but the IBA Razor diode, predominantly for the smallest clinical field 0.5 cm for 6 MV WFF (PTW 60008 Diode P, PTW 60008 Diode E, PTW 60008 Diode SRS, SN EDGE and PTW mD detectors) and 6MV FFF beams (IBA SFD, PTW 60012 E, PTW 60008 Diode SRS and PTW mD detectors).

For both, the 10MV WFF and 10MV FFF beams, significant differences in $k_{Q_{clin},Q_{ref}}^{f_{clin},f_{ref}}$ values were found between the two linacs when the PTW 60019 mD detector was used for measurements in the smallest field 0.5 cm. For this detector, observed differences for 0.5 cm field were 5.9% ($p = 0.009$), 5.5% ($p = 0.019$), 6.1% ($p = 0.017$) and 7.1% ($p = 0.004$) for 6 MV WFF, 6 MV FFF, 10 MV WFF and 10 MV FFF beam respectively. For all the other detectors, no statistically significant differences were observed for both the 10 MV WFF and 10 MV FFF beams.

It can then be concluded that different collimation system affects the output correction factors significantly for 6 MV WFF and 6 MV FFF beams for the smallest investigated field size 0.5 cm for all solid-state detectors included in the present study, with the only exception of IBA Razor diode for which no differences were seen. PTW 60019 mD detector showed differences in output correction factors for the smallest field also for 10 MV WFF and FFF

beams. The other detectors did not show any beam collimation dependence for the 10 MV WFF and 10 MV FFF beams. These results show that for given beam energy, the $k_{Q_{clin},Q_{ref}}^{f_{clin},f_{ref}}$ values obtained from different linacs (i.e., different collimation system) using different detectors can be different for $S_{clin} < 0.8$ cm.

7.2.3. PTW 60019 microDiamond detector

Properties of the PTW 60019 mD detector (mD) have been studied extensively, in particular, the determination of field output correction factors in small fields for combinations of various types of linacs, photon beam energies, and collimation systems. While the reported data for field output correction factors are reasonably consistent for field sizes of about 1 cm or larger, they diverge for field sizes below 1.0 cm.[58] Remarkably, published data show a specific pattern for the smallest fields around 0.5 cm. Monte Carlo (MC) studies and hybrid studies (partly Monte Carlo, partly experimental) report $k_{Q_{clin},Q_{ref}}^{f_{clin},f_{ref}}$ values which are close to unity or slightly higher,[22,39,44,56–58,84] indicating that an under-response (an increase of $k_{Q_{can\,lin},Q_{ref}}^{f_{clin},f_{ref}}$ values compared to the next larger field size) of the mD detector was observed for the smallest field size. On the contrary, in several experimental studies, authors have found a rather continuous increase of over-response of the mD detector down to the smallest field sizes, yielding $k_{Q_{clin},Q_{ref}}^{f_{clin},f_{ref}}$ values, which are always few percent below unity.[14,18,20,36]

Andreo et al. reported two different results within their MC study.[44] First, they calculated field output correction factors for the mD detector following the manufacturer's blueprints of its design and components. In this part of the study, they found a similar response of the mD detector for the smallest field sizes as it was reported in several other MC studies. [22,39,44,56–58,84] However, they found that the dimensions of the mD detector did not match those stated by the manufacturer, which brought them to repeat the calculations based on the new data for the active volume of the mD detector. Results from that part of the study were in close agreement with the experimental data. Interestingly, in the study by Marinelli et al.,[24] published shortly after the paper by Andreo et al., no differences between manufacturer's stated active volume and experimentally determined active volume were found, hence contradicting the approach and results from the second part of the study by Andreo et al. Nonetheless, we need to wait for new studies, experimental and MC, which might contribute to the understanding of the behavior of mD detector in small MV photon beams.

While it is not easy to understand neither to explain those differences between both approaches, experimental and MC, it seems that one of the poosible origins of observed differences in output correction factors could be a mismatch between real detector geometry and the geometry provided by the manufacturer or the geometry chosen for MC studies.

In our study $k_{Q_{clin},Q_{ref}}^{f_{clin},f_{ref}}$ values for the mD detector were below unity for all investigated clinical field sizes, regardless of the beam energy, filtration or linac used. Lowest $k_{Q_{clin},Q_{ref}}^{f_{clin},f_{ref}}$ values (largest corrections needed) were found for the Elekta Versa HD linac for 0.5 cm field size - 0.924 and 0.906 for 6 and 10 MV beams respectively, which represent an average of the data set for the WFF and FFF beams (see Table 6.7). For 6 MV beam, our values are around 3-4% lower than the corresponding values from TRS-483 and values from previously mentioned experimental studies,[14,18,20,36] while for the 10 MV beam, the present data for $k_{Q_{clin},Q_{ref}}^{f_{clin},f_{ref}}$ are lower than corresponding data reported in TRS-483 by close to 6% for 0.5 cm field size. These differences are outside the uncertainties reported in both studies. For the Varian TrueBeam, corresponding averaged values of $k_{Q_{clin},Q_{ref}}^{f_{clin},f_{ref}}$ are 0.983 and 0.973 for 6 and 10 MV beams respectively (Table 6.8), which is around 1-2% higher compared to data from TRS-483, however, within the reported uncertainties. On Elekta linac, we noticed continuous over-response ($k_{Q_{clin},Q_{ref}}^{f_{clin},f_{ref}} < 1$) of the mD detector down to the smallest field size, while it was not the case for the Varian linac, where $k_{Q_{clin},Q_{ref}}^{f_{clin},f_{ref}}$ for 0.5 cm field size were always higher than those for the 0.8 cm field size for all photon beams; we attributed this to the type of linac and different collimating systems used. It is important to note that for the mD detector, published values for $k_{Q_{clin},Q_{ref}}^{f_{clin},f_{ref}}$ in TRS-483 are exactly the same for the 6 and 10 MV beams, which clearly suggests, that there is no distinction in the field output correction factors for the mD detector regardless of the beam energy, filtration, collimation system and linac, an observation, which was not confirmed in our work.

In the present study, differences of up to 6% for 6 MV and close to 7% for 10 MV were observed for field output correction factors for 0.5 cm field size when measurements were made using the mD detector on Varian and Elekta linacs. This observation suggests that for field sizes below 1 cm, field output correction factors for the mD detector depend on the combination of linac type, photon beam energy and beam collimation system used. It is worth noting that similar but less pronounced differences of field output correction factors were also observed for

the smallest field size for two different collimation systems in the experimental study by Underwood et al.[18]

To summarize, the results of our experimental study show that $k_{Q_{clin},Q_{ref}}^{f_{clin},f_{ref}}$ values for the mD detector are below unity for field sizes below 1 cm, regardless of the linac type, beam collimation system, and beam energy or filtration used; this confirms observed over-response (regardless of the field size) from several experimental studies,[14,18,20,36] as well as form the second part of MC study by Andreo et al.[44] Moreover, present results also suggest that the mD detector cannot be considered as an almost correction-less detector for small field dosimetry; additionally, the field output correction factors for this detector depend on the type of linac, beam energy and collimations used.

7.3. Detector specific output correction factors for ionization chambers

7.3.1. Comparison with data given in TRS-483

TRS-483 has recommended values for output correction factors $k_{Q_{clin},Q_{ref}}^{f_{clin},f_{ref}}$ for nine mini and micro ionization chambers down to the minimal field size for which detector specific output correction factors fall within the interval 0.95 – 1.05. Absence of data for output correction factors for smaller fields is intended to prevent measurements with a large chamber and then apply correction factors which are unreliable.[11] Data for $k_{Q_{clin},Q_{ref}}^{f_{clin},f_{ref}}$ are provided only for perpendicular orientation of the ionization chambers, which is also recommended orientation in the TRS-483, since at the time of publishing TRS-483 CoP there were not enough data available for ionization chambers in parallel orientation.[12] From that reason, we did the comparison of output correction factors for perpendicular orientation only. Similar as for solid-state detectors, TRS-483 CoP does not make a distinction between the fields collimated by MLC, jaws or SRS cones.

Among seven chambers from our study set, data for only three of them are available in the TRS-483 CoP.

Since we did not observe any apparent one-sided difference between the data from TRS-483 CoP and those from our study, we have applied two-tailed Student's t-test to verify the statistical significance of differences between both sets of output correction factors. Data from TRS-483 CoP were compared separately for each photon beam energy, filtration, and

linac. No statistically significant differences ($P > 0.05$) were found regardless of the beam energy, linac, filtration or field size being evaluated. However, we have to note that output correction factors were compared only for the field sizes given in the TRS-483: for IBA CC04 and PTW 31016 PinPoint 3D chambers down to 1.0 cm, while for SI Exradin A16 chambers the smallest field in the comparison was 0.8 cm. The only exception (among 24 compared sets) was noticed for SI Exradin A16 chamber for 0.8 cm field in 6 MV WFF beam on Elekta linac, where the statistically significant difference ($P < 0.05$) was found between the value for output correction factor published in TRS-483 CoP and value obtained in our study.

We can conclude that detector specific output correction factors obtained in our study for three ionization chambers (IBA CC04, PTW 31016 PinPoint 3D and SI Exradin A16) confirm the corresponding data published in TRS-483 CoP. Output correction factor data presented in this experimental study for the remaining four ionization chambers, IBA Razor IC, PTW 31021 3D Semiflex, PTW 31022 PinPoint 3D and PTW 31023 PinPoint is considered to be a valuable supplement to the literature and the TRS-483 dataset.

7.3.2. The orientation of ionization chambers

Following the advice from IAEA TRS-483 CoP, the determination of field output factors using ionization chambers should be performed in the perpendicular orientation, i.e., orienting chamber's axis perpendicular to the central beam axis (see Figure 3.1 and Table 3.1). On the other hand, in the recently published ICRU Report 91 we can find a general statement on the orientation of detectors: *"In small fields, output correction factors is typically performed by orienting the detector with its longest axis parallel to the beam axis."*[9] In the case of ionization chamber, longest axis usually coincides with the central electrode, therefore the above statement from ICRU Report means that ionization chamber is supposed to be positioned in the parallel orientation, i.e., with its long axis parallel to the central axis of the beam, which contradicts to the advice from the TRS-483 CoP. Authors of the IAEA TRS-483 CoP have additionally explained their stand regarding the recommendation on the orientation of the ionization chambers in their correspondence published in Medical Physics journal.[12] They state that perpendicular orientation was recommended in the CoP only because of a lack of data for parallel orientation, which is true. Indeed, only a few studies report experimental results for $k_{Q_{clin},Q_{ref}}^{f_{clin},f_{ref}}$ in small fields determined with only a few small or micro ionization chambers in both orientations.[85–87] Further, lack of homogeneity regarding the size of the normalization field, differences in the definition of field sizes, variations in set-up (SSD or SDD used), among

others, make the potential analysis very difficult and unreliable. Therefore, we will keep the discussion in this section predominantly within the limits of the results obtained in our study.

While the orientation of ionization chamber is not crucial for the accuracy of relative measurements in large fields where LCPE exists, it is becoming an important issue when we conduct relative dosimetry studies in small fields below 2.0 cm, where lack of LCPE steps in. Since some ionization chambers show considerable stem effect, parallel orientation is advantageous also from this point of view, since stem effect can be minimized if the chamber is oriented with its stem parallel to the beam. In this work, as presented earlier (chapter Methods and materials Figure 5.2), we utilize two orientations for the determination of field output factors, perpendicular and parallel, aiming to resolve the ambiguity concerning the orientation of ionization chambers in megavoltage photon beams.[12,82,10,9]

In the chapter Results, we have shown that our experimental data support the hypothesis that output correction factors determined with our set of ionization chambers are smaller if the chamber is positioned with its axis parallel to the central beam axis compared to the output correction factors obtained in a perpendicular orientation. (Tables 6.9 to 6.12, Figures 6.7 to 6.10 and Appendixes 10.1 and 10.3). Since the output correction factors $k_{Q_{clin},Q_{ref}}^{f_{clin},f_{ref}}$ were always lower for parallel orientation compared to the perpendicular, the significance of differences was tested with one-tailed Student's t-test. We found statistically significant differences ($p < 0.05$) in the output correction factors $k_{Q_{clin},Q_{ref}}^{f_{clin},f_{ref}}$, depending upon the orientation of the ionization chamber in the beam; $k_{Q_{clin},Q_{ref}}^{f_{clin},f_{ref}}$ values were almost always significantly higher for perpendicular orientation compared to the parallel one for smallest fields as presented in Tables 7.3 and 7.4, which means, that corrections needed to correct the readings of the ionization chambers are larger for perpendicular orientation.

Detailed analysis reveals that only for IBA CC04 ionization chamber we did not find any statistically significant differences in $k_{Q_{clin},Q_{ref}}^{f_{clin},f_{ref}}$ with respect to the orientation in the beam, regardless of the photon beam energy, linac or field size used. Such finding is not surprising and can be attributed to the dimensions of the cavity. Comparable dimensions of the chamber's cavity in two main axis – the diameter of the cavity is 4.0 mm, while the length of the cavity is 3.6 mm (Table 5.2) - result in a very similar volume averaging effect for perpendicular and parallel orientation, which is the main contributing factor for $k_{Q_{clin},Q_{ref}}^{f_{clin},f_{ref}}$ in that case.

Similarly, for PTW 31021 Semiflex 3D we found statistically significant differences ($p < 0.05$) only for two photon beams (10 MV WFF and FFF) on Elekta linac for the smallest field size of 0.5 cm, while no significant differences were found on Varian linac concerning the orientation. Also in this case, constructional characteristics of the chamber are the reason for a similar response in both utilized orientations, since the length of the cavity of 4.8 mm is equal to the cavity diameter (Table 5.2). This chamber has the largest active volume V = 0.07 cm^3 among all investigated chambers. Thus it's under response due to the volume averaging is most pronounced.

Two more ionization chambers in our study, PTW 31016 3D PinPoint and its successor PTW 31022 3D PinPoint, are classified as 3D chambers implying that there should be no or negligible difference in their response regardless of the orientation in the beam. Both chambers have a cavity length of 2.9 mm which is identical to their cavity diameters. However, in this case, differences between the two orientations are more noticeable than in the previous two examples. Namely, in some beams, we found significant differences also for field size 0.8 cm: for PTW 31016 chamber on Varian linac in both 10 MV beams, while on Elekta linac similar difference was found in 10 MV WFF beam. Detailed data are presented in Tables 6.9 to 6.12. We can conclude that for these two ionization chambers, equivalency concerning the orientation was not proven for smallest fields up to 0.8 cm, despite their 3D construction.

We have also studied the response of two ionization chambers which have elongated cavities, having a cavity dimension in the principal chamber's axis (direction of the central electrode) larger than the diameter of the cavity. To this group belong ionization chambers IBA Razor and PTW 31023 PinPoint. Both chambers have a cavity diameter of 2.0 mm. However, they have different cavity lengths: IBA Razor has a cavity length of 3.6 mm, while the PTW 31023 PinPoint chamber has a cavity of length 5.0 mm. (Table 5.2) For IBA Razor chamber significant differences were found only for 0.5 cm field size in all photon beams on both linacs, while for PTW 31023 chamber, significant differences in the response were found for three smallest fields (up to 1.0 cm) on Elekta linac and two smallest fields 0.5 and 0.8 cm on Varian linac. Among all chambers included in the study, most pronounced differences, concerning the orientation, were found for PTW 31023 PinPoint chamber, which was expected, since this chamber has most elongated cavity geometry, thus most expressed volume averaging effect in the perpendicular orientation.

Table 7.2 Statistical significance (p-values) of the differences between output correction factors $k_{Q_{clin},Q_{ref}}^{f_{clin},f_{ref}}$ for seven ionization chambers for two investigated orientations: perpendicular, when chamber's main axis was placed perpendicular to the central beam axis, and parallel, when chamber's main axis was placed parallel to the central beam axis. Data obtained on Elekta Versa HD linac for 6 and 10 MV filtered (WFF) and unfiltered (FFF) beams were compared and evaluated with one-tailed Student's t-test. Since no significant differences were observed for field sizes above 1.0 cm, p-values for those fields are omitted.

p-values					
	Field size[a] [cm]	Elekta Versa HD			
		6 MV WFF	6 MV FFF	10 MV WFF	10 MV FFF
IBA CC04	0.5	0.236	0.101	0.217	0.161
	0.8	0.171	0.148	0.106	0.148
	1.0	0.247	0.354	0.167	0.096
IBA Razor IC	0.5	0.011	0.016	0.008	0.012
	0.8	0.065	0.114	0.047	0.063
	1.0	0.127	0.171	0.103	0.127
PTW 31016 3D PinPoint	0.5	0.006	0.012	0.007	0.046
	0.8	0.008	0.167	0.035	0.093
	1.0	0.014	0.100	0.021	0.122
PTW 31021 3D Semiflex	0.5	0.061	0.226	0.016	0.024
	0.8	0.211	0.339	0.229	0.252
	1.0	0.430	0.485	0.423	0.404
PTW 31022 3D PinPoint	0.5	0.010	0.106	0.008	0.019
	0.8	0.127	0.111	0.038	0.066
	1.0	0.176	0.115	0.420	0.089
PTW 31023 PinPoint	0.5	0.001	0.004	0.000	0.003
	0.8	0.004	0.006	0.008	0.019
	1.0	0.034	0.032	0.021	0.043
SI Exradin A16	0.5	0.085	0.029	0.034	0.080
	0.8	0.065	0.102	0.074	0.080
	1.0	0.069	0.145	0.256	0.153

[a] Field size is indicated as a nominal square small field side length. The relationship between the nominal field size and the corresponding equivalent square small field sizes S_{clin} is provided in Table 6.1 for all energies and field sizes.

Table 7.3 Statistical significance (p-values) of the differences between output correction factors $k_{Q_{clin},Q_{ref}}^{f_{clin},f_{ref}}$ for seven ionization chambers for two investigated orientations: perpendicular and parallel (see also Fig. 5.2). Data obtained on Varian TrueBeam linac for 6 and 10 MV filtered (WFF) and unfiltered (FFF) beams were compared and evaluated with one-tailed Student's t-test. No significant differences were observed for field sizes above 1.0 cm.

p-values					
	Field size[a] [cm]	Varian TrueBeam			
		6 MV WFF	6 MV FFF	10 MV WFF	10 MV FFF
IBA CC04	0.5	0.143	0.151	0.185	0.105
	0.8	0.285	0.345	0.275	0.230
	1.0	0.439	0.463	0.367	0.348
IBA Razor IC	0.5	0.018	0.024	0.029	0.011
	0.8	0.141	0.182	0.110	0.092
	1.0	0.332	0.345	0.240	0.205
PTW 31016 3D PinPoint	0.5	0.030	0.042	0.038	0.017
	0.8	0.053	0.090	0.041	0.031
	1.0	0.110	0.185	0.082	0.066
PTW 31021 3D Semiflex	0.5	0.220	0.186	0.230	0.129
	0.8	0.469	0.478	0.467	0.491
	1.0	0.441	0.471	0.447	0.473
PTW 31022 3D PinPoint	0.5	0.086	0.123	0.085	0.047
	0.8	0.168	0.403	0.134	0.154
	1.0	0.281	0.419	0.218	0.244
PTW 31023 PinPoint	0.5	0.003	0.004	0.007	0.002
	0.8	0.017	0.052	0.020	0.016
	1.0	0.072	0.172	0.064	0.054
SI Exradin A16	0.5	0.058	0.073	0.079	0.040
	0.8	0.183	0.209	0.154	0.150
	1.0	0.316	0.359	0.273	0.259

[a] Field size is indicated as a nominal square small field side length. The relationship between the nominal field size and the corresponding equivalent square small field sizes S_{clin} is provided in Table 6.1 for all energies and field sizes.

Smallest chamber in our study, SI Exradin A16, showed significant differences in $k_{Q_{clin},Q_{ref}}^{f_{clin},f_{ref}}$ with respect to the orientation for 0.5 cm field, however, only in 6 MV FFF and 10 MV WFF beams on Elekta linac and in 10 MV FFF beam on Varian linac. Exradin A16

chamber has cavity dimensions equal in both principal chamber's axis, similar as PTW 31016 and PTW 31022 3D PinPoint chambers discussed earlier, which qualifies this chamber to the group of "3D chambers", although its name does not suggest that. On the other hand, its cavity volume of 0.007 cm^3 is two time smaller than corresponding volumes of the PTW 31016 and PTW 31022 3D chambers, which additionally minimize volume averaging effect in both orientations.

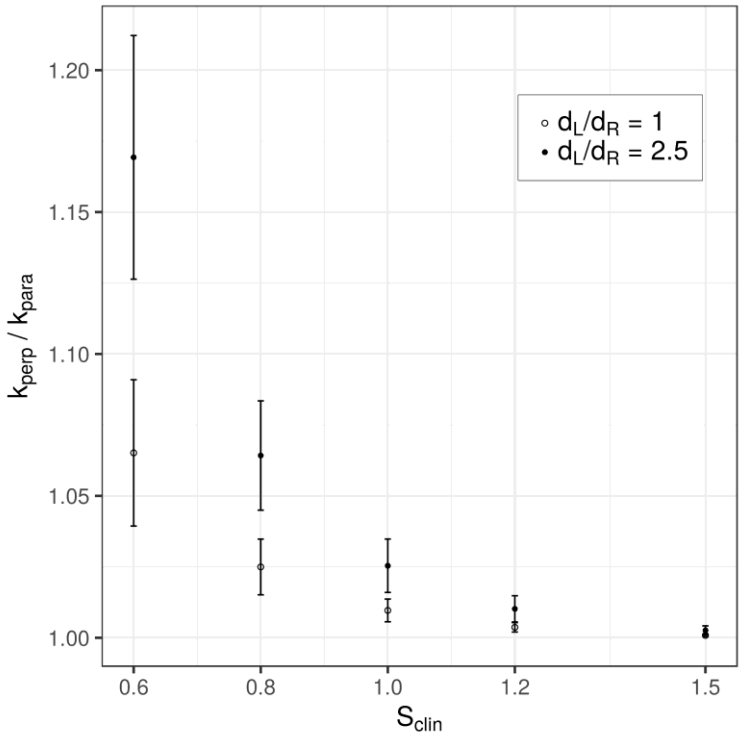

Figure 7.1. Ratios k_{perp}/k_{para} of output correction factors determined in two orientations (perpendicular and parallel) for two ionization chambers, PTW 31022 3D PinPoint and PTW 31023 PinPoint, having different dimensions of their cavities (active volumes) in the longitudinal and radial direction. $d_L/d_R = 1$ correspond to the PTW 31022 3D PinPoint chamber, while $d_L/d_R = 2.5$ corresponds to the PTW 31023 Pinpoint chamber. Average values for output correction factors for all investigated beams were considered for the determination of k_{perp}/k_{para} values. Error bars represent standard deviations of mean values.

The response of two small ionization chambers, PTW 31022 3D PinPoint and PTW 31023 PinPoint, was analyzed more in detail. Those two chambers have almost equal active volumes (cavity volumes). However, they differ considerably in their cavity dimensions, d_L and d_R, along longitudinal and radial axes respectively (see also Figure 2.6 and Table 5.2): PTW 31022 3D PinPoint chamber has equal cavity dimensions in its longitudinal and radial directions,

$d_L = d_R = 2.9\,mm$, while PTW 31023 PinPoint chamber is more elongated, having $d_L = 5.0\,mm$ and $d_R = 2.0\,mm$. Plot in Figure 7.1 shows a dependence of ratios between output correction factors determined in perpendicular and parallel orientations (k_{perp}/k_{para}) on clinical field size S_{clin} for two different ratios d_L/d_R; one corresponds to the PTW 31022 3D PinPoint chamber ($d_L/d_R = 1$), while the other to the PTW 31023 Pinpoint chamber ($d_L/d_R = 2.5$). Ratios k_{perp}/k_{para} were determined from average values determined in all megavoltage beams on both linear accelerators using analytical function from Eq. (5.15) and fitting coefficients from Appendixes 10.2 and 10.4. In the case of ionization chambers, fitting parameter d is equal to -1.

From the graph in Figure 7.1 we clearly identify three main characteristics:

- k_{perp}/k_{para} values strongly depend on the d_L/d_R ratio;
- k_{perp}/k_{para} values are higher for a more elongated chamber having larger d_L/d_R ratio;
- k_{perp}/k_{para} values gradually approach to 1 as S_{clin} are becoming larger.

However, all mentioned characteristics are expected and have a solid physical background, mostly within the concept of volume averaging effect. Also, they were explicitly or implicitly encompassed in our second hypothesis of the thesis.

To summarize, output correction factors for ionization chambers included in the study are lower if they are oriented with their main axis parallel to the central axis of the beam even if the length of the cavity is equal to the cavity diameter as it is in the case of 3D ionization chambers. Therefore, to minimize the output correction factors $k_{Q_{clin},Q_{ref}}^{f_{clin},f_{ref}}$, we recommend to use ionization chambers in parallel orientation for the determination of field output factors in small fields.

However, considering the construction and size of the ionization chambers, we do not recommend to use ionization chambers below certain minimum field size. The minimal field size is such that output correction factors $k_{Q_{clin},Q_{ref}}^{f_{clin},f_{ref}}$ comply with the requirement $0.95 < k_{Q_{clin},Q_{ref}}^{f_{clin},f_{ref}} < 1.05$.[11] At this point, we highlight that two ionization chambers from our set fulfil this requirement down to the smallest field size of 0.5 cm, IBA Razor IC and PTW 31023 PinPoint, if they are positioned parallel to the beam axis, and are therefore suitable detectors for relative small field dosimetry even for very small fields below 1.0 cm.

7.3.3 Clinical relevance of the thesis results

While there is no rule about the magnitude of systematic dosimetry errors above which we would face with unacceptable clinical outcome of the radiotherapy treatment, it seems reasonable to make every effort to keep systematic dosimetric errors (i.e., systematic difference between prescribed and delivered dose) within the range of about 1 – 2%.[88] Therefore, systematic errors in the determination of field output factors should be minimized as much as reasonably achievable, as those inaccuracies affect a large group of patients and can remain undetectable for a longer period.

Although we have obtained rather small output correction factors for some of the solid-state detectors included in the study even for very small fields, we focus our discussion on the ionization chambers since we have determined $k_{Q_{clin},Q_{ref}}^{f_{clin},f_{ref}}$ values for two orientation. Latter is an important contribution to the dosimetry of small fields. Detector specific output correction factors $k_{Q_{clin},Q_{ref}}^{f_{clin},f_{ref}}$ determined in our study for micro and mini ionization chambers, have revealed that we can be more confident in the accuracy of field output factors if they were determined in the parallel orientation. While there is practically no difference between $k_{Q_{clin},Q_{ref}}^{f_{clin},f_{ref}}$ values determined in either of orientations down to the field size of 2 × 2 cm^2, the differences between both orientations become more apparent for smaller fields, the fact, that deserves a consideration in the scope of clinical relevance of our findings.

From the radiobiological point of view and the analysis of dose-response curves, we can expect 10 – 20% change in the tumor control probability (TCP) for a 5% change in the delivered dose, at a 50% TCP. A similar change in the dose may result in a 20 – 30% change in the normal tissue complication probability (NCTP).[88,89] Radiobiological aspects of dosimetric errors are known for decades. However, they were not closely related to the dosimetry of small fields, as the use of large static fields was the most common approach in the radiotherapy until recently. In the last two decades, widespread use of new radiotherapy techniques, such as intensity modulated radiotherapy (IMRT), volumetric arc therapy (VMAT), stereotactic radiosurgery (SRS), and stereotactic body radiotherapy (SBRT) have raised the importance of small field dosimetry. Lastly mentioned techniques have in common the use of single or multiple small fields for which we need to import and define accurate data in the treatment planning system, in particular field output factor values for small fields. Also, some radiotherapy units can form

only very small fields below 2.0 cm, such as the GammaKnife, which increase the importance of accurate small field dosimetry.

A closer look at the $k_{Q_{clin},Q_{ref}}^{f_{clin},f_{ref}}$ values in the Tables 6.9 – 6.12 and figures in the Appendix 10.1 and 10.3 for the smallest field of 0.5 × 0.5 cm^2 reveals that they are well below 1.05 (5%) for ionization chambers PTW 31023 PinPoint and IBA Razor, if they have been determined in the parallel orientation. Latter lead us to the conclusion that we could expect a change in TCP below 10% and a change in NTCP below 20% even if we would not take output correction factors into consideration. However, since dosimetry errors, also systematic, can be introduced at various levels of the radiotherapy process, such an assumption would be imprudent. Also, previously mentioned techniques IMRT, VMAT, SRS, and SBRT do not use exclusively small fields or small beam segments during radiation treatment delivery. In fact, usually, only a portion of radiotherapy treatment consists of very small fields or beam segments, which fortunately minimize the possibility of severe dosimetric errors due to incorrectly determined or modelled small field output factors.

Nonetheless, the advantage of parallel orientation of the ionization chambers for the determination of field output factors over the perpendicular one, have been clearly and unambiguously shown for all micro and mini ionization chambers used in the present work.

8 CONCLUSIONS

The thesis presents the results of field output factors for small photon fields determined by two reference detectors, radiochromic films EBT3 and Exradin W1 plastic scintillator, which are perturbation free except for volume averaging. Results are presented as analytical functions as well as discrete values for nine clinical fields, ranging from 0.5 cm to 10 cm. Measurements were performed at a Varian TrueBeam and Elekta Versa HD linear accelerators using 6 MV WFF, 6 MV FFF, 10 MV WFF and 10 MV FFF photon beams. Only volume averaging correction factors k_{vol} were applied to the measured datasets; these were calculated from 2D dose matrices obtained from EBT3 films for each small field and photon beam individually, which were fitted to bivariate Gaussian function. This is a novel approach for the determination of field output factors in small static fields in megavoltage photon beams. Field output factor data presented in this study can be used as a reference data sets on linacs with same collimation of the fields as was used in the present study. First hypothesis of the thesis was confirmed, since our novel method for the determination of field output factors in small megavoltage beams was proven as appropriate.

Additionally, based on calculated field output factors, detector specific output correction factors $k_{Q_{clin},Q_{ref}}^{f_{clin},f_{ref}}$ were determined for six diodes, a microDiamond detector, and seven small and micro ionization chambers, which are widely used detectors for performing relative dosimetry in the clinics.

A large set of field output factor and output correction factor data for 16 detectors and four photon beams were determined/measured on two linacs by a single group; this is considered to be a valuable supplement to the literature and the TRS-483 dataset. Data are presented in graphical form using an analytical function from TRS-483 as well as in the form of discrete values. To the best of our knowledge, no similar comprehensive study on the orientation of ionization chambers in MV photon beams has been published until present.

Comparison between the output correction factors reported in the present work and those published in TRS-483 show statistically significant difference ($p < 0.05$) when an SN EDGE detector is used for measurements made with 10 MV WFF beams at both Varian TrueBeam and Elekta Versa HD linacs for field sizes < 2.0 cm. Statistically significant differences ($p < 0.05$) were also found when a PTW 60019 mD detector was used with 6 MV WFF,

6 MV FFF and 10 MV FFF beams on Elekta Versa HD linac. Those findings do not confirm entirely the approach in the TRS-483 CoP.

For most combinations of field size, beam energy, and beam collimation, no significant differences were found between TRS-483 data set and the present results for output correction factors for WFF and FFF beams; a few exceptions were found for the smallest field sizes.

Results of the present study also show that different collimation systems can significantly influence the output correction factors for the smallest field size of 0.5 cm for 6 MV WFF and 6 MV FFF beams regardless of the detector used. For PTW 60019 mD detector this effect was also observed for the 10 MV WFF and 10 MV FFF beams. The only exception was IBA Razor diode for which dependence of output correction factors on beam collimating system was not observed. These results show that for given beam energy, the $k_{Q_{clin},Q_{ref}}^{f_{clin},f_{ref}}$ values obtained from different linacs (i.e., different collimation system) can be different for $S_{clin} < 0.8$ cm.

Our second hypothesis was mainly directed toward the problem connected to the orientation of small and micro ionization chambers when determining field output factors and output correction factors in small fields. While TRS-483 recommends perpendicular orientation, we were hypothesizing that parallel orientation is advantageous since detector specific correction factors are smaller compared to those obtained in a perpendicular orientation. We have used seven small and micro ionization chambers to test the hypothesis in four megavoltage photon beams on two linear accelerators. Results of our study confirm the second hypothesis without exceptions: output correction factors were lower if they were determined in a parallel orientation of ionization chambers compared to those obtained in a perpendicular orientation. This observation has been confirmed for all seven ionization chambers regardless of the photon beam energy or linear accelerator being used. As a consequence, if the parallel orientation is utilized for the determination of output correction factors, they can be determined for field sizes smaller than those reported in the TRS-483 CoP, since the requirement $0.95 < k_{Q_{clin},Q_{ref}}^{f_{clin},f_{ref}} < 1.05$ is not violated even for field sizes below 1.0 cm for five ionization chambers used in our study: three PTW PinPoint chambers, IBA Razor chamber and Exradin A16 chamber. Even more, output correction factors $k_{Q_{clin},Q_{ref}}^{f_{clin},f_{ref}}$ determined with IBA Razor and PTW 31023 PinPoint ionization chambers in parallel orientation were always within the specified interval 0.95 – 1.05 regardless of the photon beam energy or linac used down to the smallest investigated field of 0.5 cm. Therefore, to minimize

corrections in the experimental determination of field output factors, we recommend to use ionization chambers in parallel orientation. Latter is considered as a valuable and vindicated upgrade to the present recommendations given in the IAEA TRS-483 CoP, where perpendicular orientation is advised.

TRS-483 recommends the use of two (or more) detectors for the determination of field output factors.[10,11] In such combination, detectors should have individual correction factors $k_{Q_{clin},Q_{ref}}^{f_{clin},f_{ref}}$ above and below unity, yielding to the combined $k_{Q_{clin},Q_{ref}}^{f_{clin},f_{ref}}$ values close to 1.00. Nonetheless, we have to accept the fact, that the lastly mentioned recommendation given in the TRS-483 is in principal general only. Namely, no such pair of detectors has been specifically recommended or identified yet, neither from the authors of the TRS-483, nor from any other research group. Importantly, our large set of output correction factors determined for seven solid stated detectors and seven small ionization chambers under the same experimental conditions, allows us quantitative approach in finding most suitable pairs of detectors for which no correction factors would be necessary to apply, even for the smallest fields down to 0.5 × 0.5 cm^2. Latter remains a challenge and motivation for our future work.

9 BIBLIOGRAPHY

1. Andreo P, Burns DT, Hohlfeld K, et al. Absorbed Dose Determination in External Beam Radiotheraphy: An International Code of Practice for Dosimetry based on Standards of Absorbed Dose to Water. *Iaea Trs-398*. 2006;2006(June):183. doi:10.1097/00004032-200111000-00017.
2. Almond PR, Biggs PJ, Hanson WF. AAPM ' s TG – 51 Protocol for Clinical Reference Dosimetry of High-Energy Photon and Electron Beams b) a) dose. *Med Phys*. 1999;26(1999):1-9.
3. McEwen M, Dewerd L, Ibbott G, et al. Addendum to the AAPM's TG-51 protocol for clinical reference dosimetry of high-energy photon beams. *Med Phys*. 2014;41(4):1-20. doi:10.1118/1.4866223.
4. Derreumaux S, Etard C, Huet C, et al. Lessons from recent accidents in radiation therapy in France. *Radiat Prot Dosim*. 2008;131:130-135.
5. Bogdanich W, Rebelo K. A pinpoint beam strays invisibly, harming instead of healing. *New York Times*. 2010.
6. Das IJ, Downes MB, Kassaee A, Tochner Z. Choice of Radiation Detector in Dosimetry of Stereotactic Radiosurgery–Radiotherapy. *J Radiosurgery*. 2000;3(4):177-186.
7. Aspradakis MM, Byrne JP, Palmans H, et al. *IPEM Report Number 103: Small Field MV Photon Dosimetry*. IPEM; 2010.
8. Alfonso R, Andreo P, Capote R, et al. A new formalism for reference dosimetry of small and nonstandard fields. *Med Phys*. 2008;35(11):5179-5186. doi:10.1118/1.3005481.
9. ICRU. *ICRU 91 - Prescribing, Recording, and Reporting of Stereotactic Treatments with Small Photon Beams*. Vol 10.; 2017. doi:10.1093/jicru/ndn032.
10. Palmans H, Andreo P, Huq S, Seuntjens J. Dosimetry of small static fields used in external beam radiotherapy: An IAEA-AAPM International Code of Practice for reference and relative dose determination. Technical Report Series No. 483. *Iaea Trs483*. 2017;(November).
11. Palmans H, Andreo P, Huq MS, Seuntjens J, Christaki KE, Meghzifene A. Dosimetry of small static fields used in external photon beam radiotherapy: Summary of TRS-483, the IAEA-AAPM international Code of Practice for reference and relative dose determination. *Med Phys*. 2018;45(11):e1123-e1145. doi:10.1002/mp.13208.
12. Palmans H, Andreo P, Huq MS, Seuntjens J, Meghzifene A, Christaki KE. Reply to " Comments on the TRS-483 Protocol on Small fi eld Dosimetry ." *Med Phys*. 2018.
13. Sauer OA, Wilbert J. Measurement of output factors for small photon beams. *Med Phys*. 2007;34(6):1983-1988. doi:10.1118/1.2734383.
14. Azangwe G, Grochowska P, Georg D, et al. Detector to detector corrections: A comprehensive experimental study of detector specific correction factors for beam output measurements for small radiotherapy beams. *Med Phys*. 2014;41(7):072103.
15. Gonzales-Lopez A, Vera-Sanches J, Lago-Martin J. Small fields measurements with radiochromic films. *J Med Phys*. 2015;40(2):61-67.

16. Dieterich S, Sherouse G. Experimental comparison of seven commercial dosimetry diodes for measurement of stereotactic radiosurgery cone factors. *Med Phys*. 2011;38(7):4166-4173.

17. Liu PZY, Suchowerska N, McKenzie DR. Can small field diode correction factors be applied universally? *Radiother Oncol*. 2014;112(3):442-446. doi:10.1016/j.radonc.2014.08.009.

18. Underwood TSA, Rowland BC, Ferrand R, Vieillevigne L. Application of the Exradin W1 scintillator to determine Ediode 60017 and microDiamond 60019 correction factors for relative dosimetry within small MV and FFF fields. *Phys Med Biol*. 2015;60(17):6669-6683. doi:10.1088/0031-9155/60/17/6669.

19. Bassinet C, Huet C, Derreumaux S, et al. Small fields output factors measurements and correction factors determination for several detectors for a CyberKnife®and linear accelerators equipped with microMLC and circular cones. *Med Phys*. 2013;40(7). doi:10.1118/1.4811139.

20. Ralston A, Tyler M, Liu P, McKenzie D, Suchowerska N. Over-response of synthetic microDiamond detectors in small radiation fields. *Phys Med Biol*. 2014;59(19):5873-5881. doi:10.1088/0031-9155/59/19/5873.

21. Ralston A, Liu P, Warrener K, McKenzie D, Suchowerska N. Small field diode correction factors derived using an air core fibre optic scintillation dosimeter and EBT2 film. *Phys Med Biol*. 2012;57(9):2587-2602. doi:10.1088/0031-9155/57/9/2587.

22. O'Brien DJ, León-Vintró L, McClean B. Small field detector correction factors kQclin,Qmsrfclin,fmsr for silicon-diode and diamond detectors with circular 6 MV fields derived using both empirical and numerical methods. *Med Phys*. 2015;43(1):411-423. doi:10.1118/1.4938584.

23. Poppinga D, Meyners J, Delfs B, et al. Experimental determination of the lateral dose response functions of detectors to be applied in the measurement of narrow photon-beam dose profiles. *Phys Med Biol*. 2015;60(24):9421-9436. doi:10.1088/0031-9155/60/24/9421.

24. Marinelli M, Prestopino G, Verona C, Verona-Rinati G. Experimental determination of the PTW 60019 microDiamond dosimeter active area and volume. *Med Phys*. 2016;43(9):5205-5212. doi:10.1118/1.4961402.

25. Papaconstadopoulos P, Archambault L, Seuntjens J. Experimental investigation on the accuracy of plastic scintillators and of the spectrum discrimination method in small photon fields: *Med Phys*. 2017;44(2):654-664. doi:10.1002/mp.12064.

26. Pasquino M, Cutaia C, Radici L, et al. Dosimetric characterization and behaviour in small X-ray fields of a microchamber and a plastic scintillator detector. *Br J Radiol*. 2017;90(1069). doi:10.1259/bjr.20160596.

27. Godson HF, Ravikumar M, Ganesh KM, Sathiyan S, Ponmalar YR. Small field output factors: Comparison of measurements with various detectors and effects of detector orientation with primary jaw setting. *Radiat Meas*. 2016;85:99-110.

28. Bruggmoser G, Saum R, Kranzer R. Determination of recombination and polarity correction factors, kS and kP, for small cylindrical ionization chambers PTW 31021 and PTW 31022 in pulsed filtered and unfiltered beams. *Z Med Phys*. 2018;28(3):247-253. doi:10.1016/j.zemedi.2017.09.010.

29. Delfs B, Kapsch RP, Chofor N, Looe HK, Harder D, Poppe B. A new reference-type ionization chamber with direction-independent response for use in small-field photon-beam dosimetry – An experimental and Monte Carlo study. *Z Med Phys*. 2018;(2017):1-10. doi:10.1016/j.zemedi.2018.05.001.

30. Pantelis E, Moutsatsos A, Zourari K, et al. On the output factor measurements of the CyberKnife iris collimator small fields: Experimental determination of the [bold k][sub [bold Q][sub clin],[bold Q][sub msr]][sup [bold f][sub clin],[bold f][sub msr]] correction factors for microchamber and diode . *Med Phys*. 2012;39(8):4875-4885. doi:10.1118/1.4736810.

31. Pantelis E, Moutsatsos A, Zourari K, et al. On the implementation of a recently proposed dosimetric formalism to a robotic radiosurgery system. *Med Phys*. 2010;37(5):2369-2379. doi:10.1118/1.3404289.

32. Reggiori G, Stravato A, Pimpinella M, et al. Use of PTW-microDiamond for relative dosimetry of unflattened photon beams. *Phys Medica*. 2017;38:45-53. doi:10.1016/j.ejmp.2017.05.046.

33. Cranmer-Sargison G, Weston S, Sidhu NP, Thwaites DI. Experimental small field 6 MV output ratio analysis for various diode detector and accelerator combinations. *Radiother Oncol*. 2011. doi:10.1016/j.radonc.2011.09.002.

34. Qin Y, Zhong H, Wen N, Snyder K, Huang Y, Chetty IJ. Deriving detector-specific correction factors for rectangular small fields using a scintillator detector. *J Appl Clin Med Phys*. 2016;17(6):379-391. doi:10.1120/jacmp.v17i6.6433.

35. Poppinga D, Delfs B, Meyners J, Harder D, Poppe B, Looe HK. The output factor correction as function of the photon beam field size - direct measurement and calculation from the lateral dose response functions of gas-filled and solid detectors. *Z Med Phys*. 2017. doi:10.1016/j.zemedi.2017.07.006.

36. Lechner W, Palmans H, Sölkner L, Grochowska P, Georg D. Detector comparison for small field output factor measurements in flattening filter free photon beams. *Radiother Oncol*. 2013;109(3):356-360. doi:10.1016/j.radonc.2013.10.022.

37. Wegener S, Sauer OA. Separation of scatter from small MV beams and its effect on detector response. *Med Phys*. 2017;44(3):1139-1148. doi:10.1002/mp.12091.

38. Morales JE, Butson M, Crowe SB, Hill R, Trapp J V. An experimental extrapolation technique using the Gafchromic EBT3 film for relative output factor measurements in small x-ray fields. *Med Phys*. 2016;43(8):4687-4692. doi:10.1118/1.4958679.

39. Francescon P, Kilby W, Noll JM, Masi L, Satariano N, Russo S. Monte Carlo simulated corrections for beam commissioning measurements with circular and MLC shaped fields on the CyberKnife M6 System: A study including diode, microchamber, point scintillator, and synthetic microdiamond detectors. *Phys Med Biol*. 2017;62(3):1076-1095. doi:10.1088/1361-6560/aa5610.

40. Francescon P, Cora S, Satariano N. Calculation of k Q clin, Q msr f clin, f msr for several small detectors and for two linear accelerators using Monte Carlo simulations. *Med Phys*. 2011;38(12):6513-6527. doi:10.1118/1.3660770.

41. Czarnecki D, Zink K. Monte Carlo calculated correction factors for diodes and ion chambers in small photon fields. *Phys Med Biol*. 2013;58(8):2431-2444. doi:10.1088/0031-9155/58/8/2431.

42. Moignier C, Huet C, Barraux V, et al. Determination of small field output factors and correction factors using a Monte Carlo method for a 1000 MU/min CyberKnife® system equipped with fixed collimators. *Radiat Meas*. 2014;71:287-292. doi:10.1016/j.radmeas.2014.05.009.

43. Zoros E, Pappas EP, Moutsatsos A, et al. Monte carlo determination of correction factors for dosimetric measurements in gamma knife perfexion small fields. *Phys Medica*. 2016;32:237. doi:10.1016/j.ejmp.2016.07.494.

44. Andreo P, Palmans H, Marteinsdóttir M, Benmakhlouf H, Carlsson-Tedgren Å. On the Monte Carlo simulation of small-field micro-diamond detectors for megavoltage photon dosimetry. *Phys Med Biol*. 2015;61(1):L1-L10. doi:10.1088/0031-9155/61/1/L1.

45. Crop F, Reynaert N, Pittomvils G, et al. The influence of small field sizes, penumbra, spot size and measurement depth on perturbation factors for microionization chambers. *Phys Med Biol*. 2009;54(9):2951-2969. doi:10.1088/0031-9155/54/9/024.

46. Scott AJD, Kumar S, Nahum AE, Fenwick JD. Characterizing the influence of detector density on dosimeter response in non-equilibrium small photon fields. *Phys Med Biol*. 2012;57(14):4461-4476. doi:10.1088/0031-9155/57/14/4461.

47. Park K, Bak J, Park S, Choi W, Park SW. Determination of small-field correction factors for cylindrical ionization chambers using a semiempirical method. *Phys Med Biol*. 2016;61(3):1293-1308. doi:10.1088/0031-9155/61/3/1293.

48. Papaconstadopoulos P, Tessier F, Seuntjens J. On the correction, perturbation and modification of small field detectors in relative dosimetry. *Phys Med Biol*. 2014;59(19):5937-5952. doi:10.1088/0031-9155/59/19/5937.

49. Zoros E, Moutsatsos A, Pappas EP, et al. Monte Carlo and experimental determination of correction factors for gamma knife perfexion small field dosimetry measurements. *Phys Med Biol*. 2017;62(18):7532-7555.

50. García-Garduño OA, Lárraga-Gutiérrez JM, Rodríguez-Villafuerte M, Martínez-Dávalos A, Celis MA. Small photon beam measurements using radiochromic film and Monte Carlo simulations in a water phantom. *Radiother Oncol*. 2010;96(2):250-253. doi:10.1016/j.radonc.2010.03.016.

51. Andreo P. The physics of small megavoltage photon beam dosimetry. *Radiother Oncol*. 2018;126(2):205-213. doi:10.1016/j.radonc.2017.11.001.

52. Casar B, Gershkevitsh E, Mendez I, Jurković S, Huq MS. A novel method for the determination of field output factors and output correction factors for small static fields for six diodes and a microdiamond detector in megavoltage photon beams. *Med Phys*. December 2018:mp.13318. doi:10.1002/mp.13318.

53. Das IJ, Ding GX, Ahnesjö A. Small fields: Nonequilibrium radiation dosimetry. *Med Phys*. 2008;35(1):206-215. doi:10.1118/1.2815356.

54. Wuerfel JU. Dose measurements in small fields. *Med Phys Int*. 2013;1(1):81-90.

55. McKerracher C, Thwaites DI. Notes on the construction of solid-state detectors. *Radiother Oncol*. 2006;79(3):348-351. doi:10.1016/j.radonc.2006.05.008.

56. Lárraga-Gutiérrez JM, Ballesteros-Zebadúa P, Rodríguez-Ponce M, García-Garduno OA, De La Cruz OOG. Properties of a commercial PTW-60019 synthetic diamond detector for the dosimetry of small radiotherapy beams. *Phys Med Biol*. 2015;60(2):905-924. doi:10.1088/0031-9155/60/2/905.

57. Masi L, Russo S, Francescon P, et al. CyberKnife beam output factor measurements: A multi-site and multi-detector study. *Phys Medica*. 2016;32(12):1637-1643. doi:10.1016/j.ejmp.2016.08.001.

58. De Coste V, Francescon P, Marinelli M, et al. Is the PTW 60019 microDiamond a suitable candidate for small field reference dosimetry? *Phys Med Biol*. 2017;62(17):7036-7055. doi:10.1088/1361-6560/aa7e59.

59. Ravichandran R, Binukumar JP, Al Amri I, Davis CA. Diamond detector in absorbed dose measurements in high-energy linear accelerator photon and electron beams. *J Appl Clin Med Phys*. 2016;17(2):291-303. doi:10.1120/jacmp.v17i2.5690.

60. Laub WU, Crilly R. Clinical radiation therapy measurements with a new commercial synthetic single crystal diamond detector. *J Appl Clin Med Phys*. 2014;15(6):92-102. doi:10.1120/jacmp.v15i6.4890.

61. Butson MJ, Yu PKN, Cheung T, Alnawaf H. Energy response of the new EBT2 Radiochromic film to X-ray radiation. *Radiat Meas*. 2010;45(7):836-839. doi:10.1016/j.radmeas.2010.02.016.

62. Massillon-JL G, Chiu-Tsao S-T, Domingo-Munoz I, Chan MF. Energy Dependence of the New Gafchromic EBT3 Film:Dose Response Curves for 50 KV, 6 and 15 MV X-Ray Beams. *Int J Med Physics, Clin Eng Radiat Oncol*. 2012;01(02):60-65. doi:10.4236/ijmpcero.2012.12008.

63. Crijns W, Maes F, Van Der Heide UA, Van Den Heuvel F. Calibrating page sized Gafchromic EBT3 films. *Med Phys*. 2013;40(1). doi:10.1118/1.4771960.

64. Carrasco P, Jornet N, Jordi O, et al. Characterization of the Exradin W1 scintillator for use in radiotherapy. *Med Phys*. 2015;42(1):297-304. doi:10.1118/1.4903757.

65. Méndez I, Šljivić Ž, Hudej R, Jenko A, Casar B. Grid patterns, spatial inter-scan variations and scanning reading repeatability in radiochromic film dosimetry. *Phys Medica*. 2016;32(9). doi:10.1016/j.ejmp.2016.08.003.

66. Méndez I, Peterlin P, Hudej R, Strojnik A, Casar B. On multichannel film dosimetry with channel-independent perturbations.

67. Vera-Sanches J, Ruis-Morales C, Gonzales-Lopez A. Monte Carlo uncertainty analysis of dose estimates in radiochromic film dosimetry with single-channel and multichannel algorithms. *Phys Medica*. 2018;47:23-33.

68. van Battum L, Huizenga H, Verdaasdonk R, Heukelom S. How flatbed scanners upset accurate film dosimetry. *Phys Med Biol*. 2016;61(2):625-649.

69. Mendez I, Polšak A, Hudej R, Casar B. The multigaussian method: a new approach to mitigating spatial heterogeneities with multichannel radiochromic film dosimetry. *Phys Med Biol*. 2018;accepted m.

70. https://radiochromic.com.

71. R Core Team. R: A language and environment for statistical computing. 2014:3-36.

72. Cranmer-Sargison G, Charles PH, Trapp J V., Thwaites DI. A methodological approach to reporting corrected small field relative outputs. *Radiother Oncol*. 2013;109(3):350-355. doi:10.1016/j.radonc.2013.10.002.

73. Dimitriadis A, Patallo IS, Billas I, Duane S, Nisbet A, Clark CH. Characterisation of a plastic scintillation detector to be used in a multicentre stereotactic radiosurgery dosimetry audit. *Radiat Phys Chem*. 2017;140(February):373-378. doi:10.1016/j.radphyschem.2017.02.023.

74. Garnier N, Amblard R, Villeneuve R, et al. Detectors assessment for stereotactic radiosurgery with cones. *J Appl Clin Med Phys*. 2018;19(6):88-98. doi:10.1002/acm2.12449.

75. Beaulieu L, Beddar S. Review of plastic and liquid scintillation dosimetry for photon, electron, and proton therapy. *Phys Med Biol*. 2016;61(20):R305-R343. doi:10.1088/0031-9155/61/20/R305.

76. Frelin A, Fontbonne J, Ban G, et al. Spectral discrimination of Cerenkov radiation in scintillating dosimeters. *Med Phys*. 2005;32(9):3000-3006.

77. Guillot M, Gingras L, Archambault L, Beddar S, Beaulieu L. Spectral method for the correction of the Cerenkov light effect in plastic scintillation detectors: a comparison study of calibration procedures and validation in Cerenkov light-dominated situations. *Med Phys*. 2011;38(4):2140-2150.

78. Morin J, Béliveau-Nadeau D, Chung E, et al. A comparative study of small field total scatter factors and dose profiles using plastic scintillation detectors and other stereotactic dosimeters: The case of the CyberKnife. *Med Phys*. 2013;40(1). doi:10.1118/1.4772190.

79. Burke E, Poppinga D, Schönfeld A, Harder D, Poppe B, Looe HK. The practical application of scintillation dosimetry in small-field photon-beam radiotherapy. *Z Med Phys*. 2017;27(4):324-333.

80. Francescon P, Beddar S, Satariano N, Das IJ. Variation of kQclin,Qmsrfclin,fmsr for the small-field dosimetric parameters percentage depth dose, tissue-maximum ratio, and off-axis ratio. *Med Phys*. 2014;41(10):1-15.

81. Francescon P, Kilby W, Satariano N, Cora S. Monte Carlo simulated correction factors for machine specific reference field dose calibration and output factor measurement using fixed and iris collimators on the CyberKnife system. 3741. doi:10.1088/0031-9155/57/12/3741.

82. Das IJ, Francescon P. Comments on the TRS-483 protocol on small fi eld dosimetry. *Med Phys*. 2018;45(12):5666-5668.

83. Bouchard H, Seuntjens J, Palmans H. On charged particle equilibrium violation in external photon fields. *Med Phys*. 2012;39(3):1473-1480. doi:10.1118/1.3684952.

84. Veselsky T, Jr JN, Pastykova V. Assessment of basic physical and dosimetric parameters of synthetic single-crystal diamond detector and its use in Leksell Gamma Knife and CyberKnife small radiosurgical fields. 2018;16(1). doi:10.18869/acadpub.ijrr.16.1.7.

85. Tanny S, Sperling N, Parsai EI. Correction factor measurements for multiple detectors used in small field dosimetry on the Varian Edge radiosurgery system. *Med Phys*. 2015;42(9):5370-5376. doi:10.1118/1.4928602.

86. Francescon P, Kilby W, Satariano N. Monte Carlo simulated correction factors for output factor measurement with the CyberKnife system - Results for new detectors and correction factor dependence on measurement distance and detector orientation. *Phys Med Biol*. 2014;59(6). doi:10.1088/0031-9155/59/6/N11.

87. Benmakhlouf H, Sempau J, Andreo P. Output correction factors for nine small detectors in 6 MV radiation therapy photon beams: A PENELOPE Monte Carlo study. *Med Phys*. 2014;41(4):pp 12.

88. IAEA Human Health Series No.31. *Accuracy Requirements and Uncertainties in Radiotherapy*. Vienna: International Atomic energy Agency; 2016.

89. Van Dyk J, ed. *The Modern Technology of Radiation Oncology – A Compendium for Medical Physicists and Radiation Oncologists*. Medical Physics Publishing, Madison, Wisconsin; 2006.

10 APPENDIX

1 Output correction factors for perpendicular and parallel orientation of ionization chambers on Elekta Versa HD linac

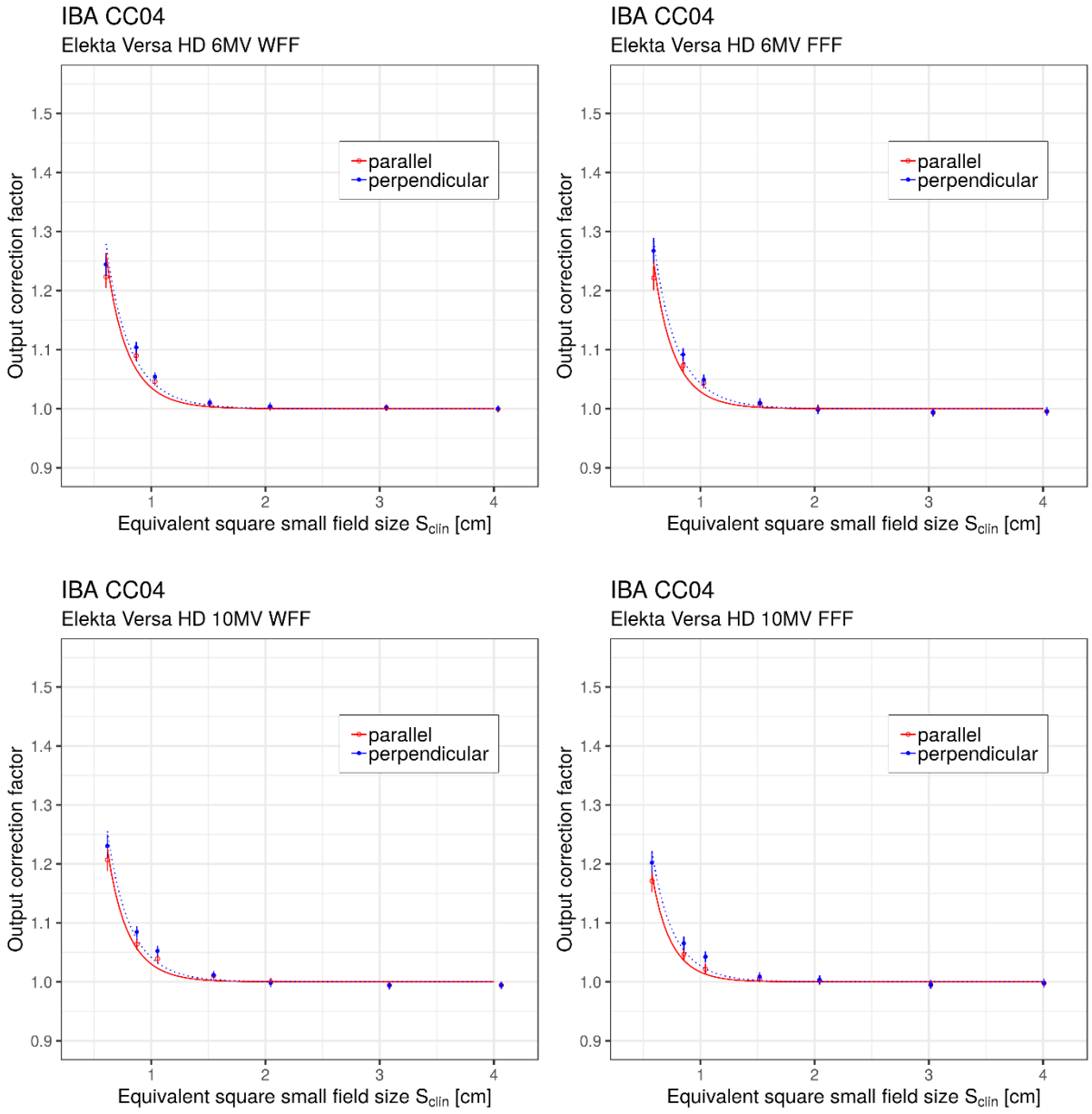

Figure I. Detector specific output correction factors $k_{Q_{clin},Q_{ref}}^{f_{clin},f_{ref}}$ for IBA CC04 ionization chamber for two orientation with respect to the central beam axis; perpendicular (blue symbols and blue dotted lines) and (red symbols and red full lines) for four photon beams on Elekta Versa HD linac. Output correction factors are presented as individual values/points and as curves of analytical function applying Eq. (5.14) and Eq. (5.15) respectively.

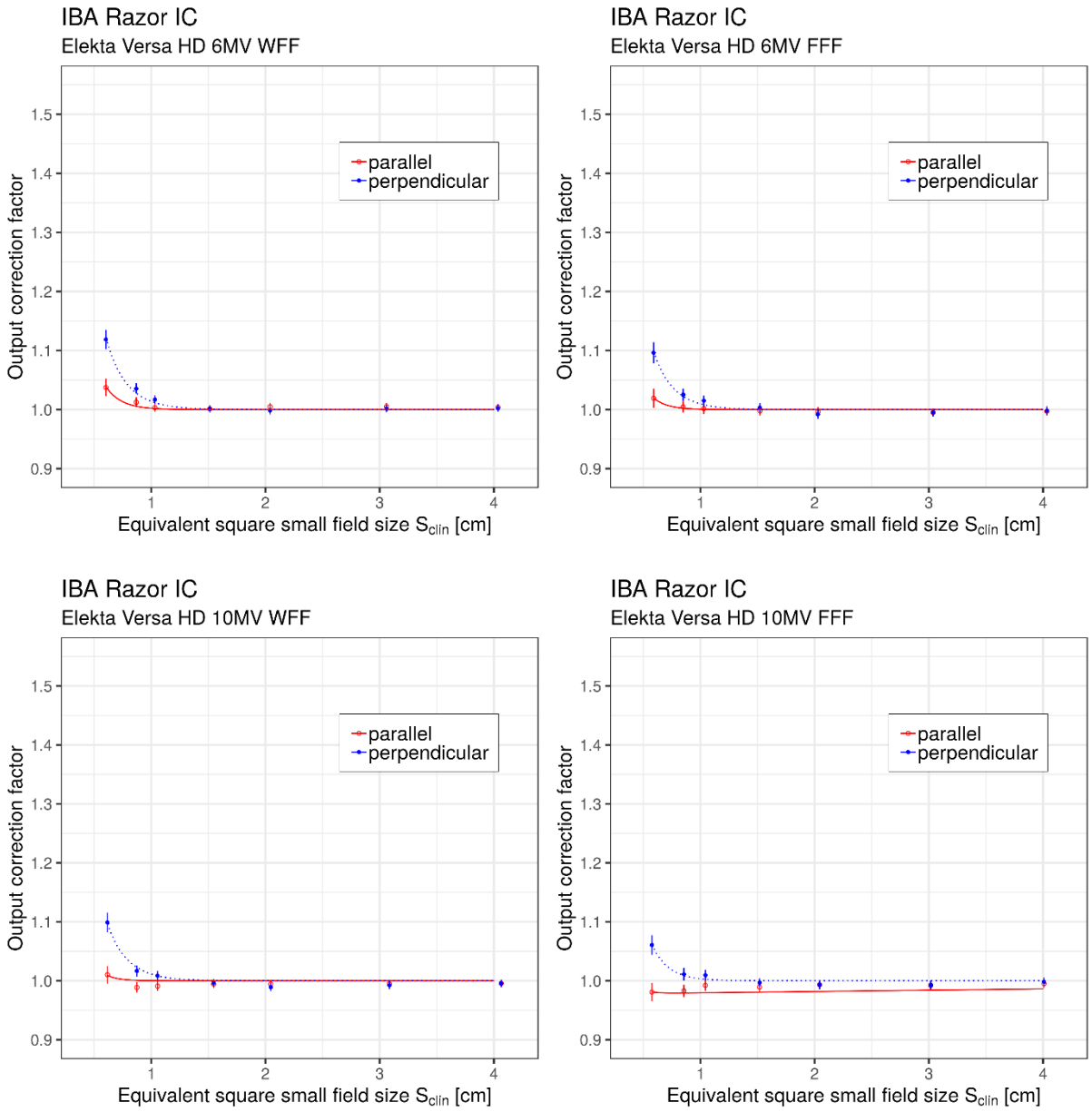

Figure II. Detector specific output correction factors $k_{Q_{clin},Q_{ref}}^{f_{clin},f_{ref}}$ for IBA Razor ionization chamber for two orientation with respect to the central beam axis; perpendicular (blue symbols and blue dotted lines) and (red symbols and red full lines) for four photon beams on Elekta Versa HD linac. Output correction factors are presented as individual values/points and as curves of analytical function applying Eq. (5.14) and Eq. (5.15) respectively.

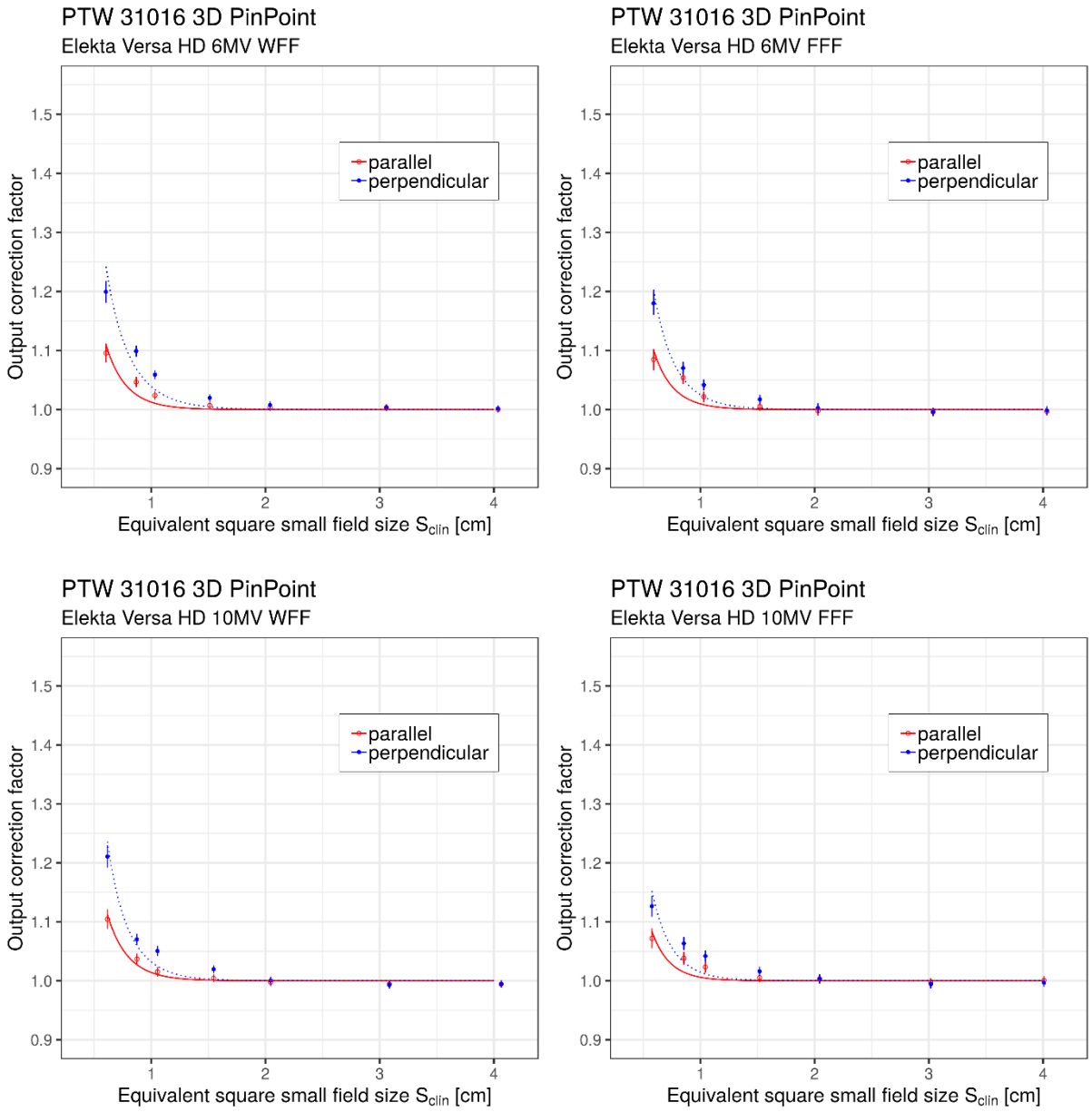

Figure III. Detector specific output correction factors $k_{Q_{clin},Q_{ref}}^{f_{clin},f_{ref}}$ for PTW 31016 3D PinPoint ionization chamber for two orientation with respect to the central beam axis; perpendicular (blue symbols and blue dotted lines) and (red symbols and red full lines) for four photon beams on Elekta Versa HD linac. Output correction factors are presented as individual values/points and as curves of analytical function applying Eq. (5.14) and Eq. (5.15) respectively.

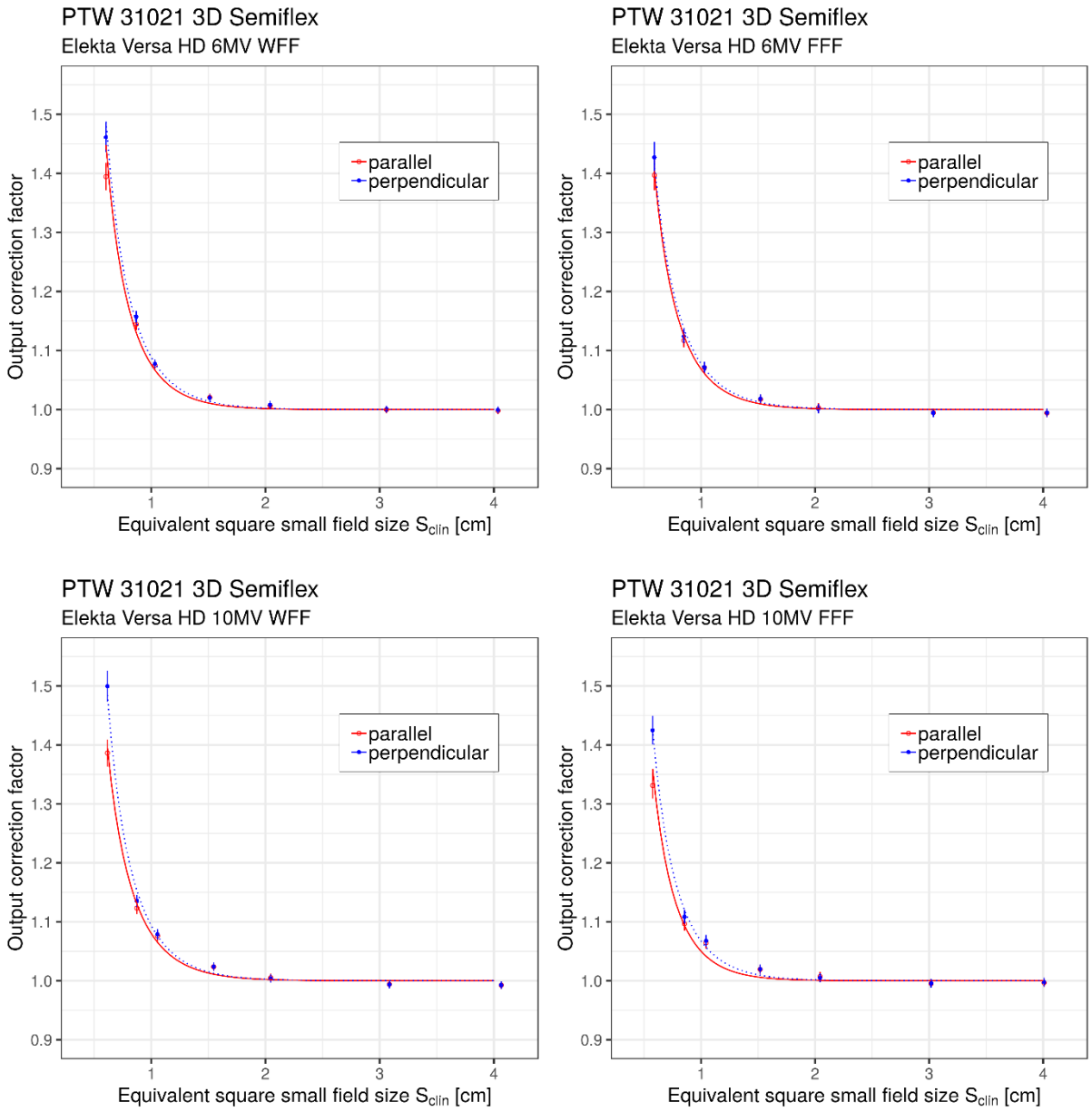

Figure IV. Detector specific output correction factors $k_{Q_{clin},Q_{ref}}^{f_{clin},f_{ref}}$ for PTW 31021 3D Semiflex ionization chamber for two orientation with respect to the central beam axis; perpendicular (blue symbols and blue dotted lines) and (red symbols and red full lines) for four photon beams on Elekta Versa HD linac. Output correction factors are presented as individual values/points and as curves of analytical function applying Eq. (5.14) and Eq. (5.15) respectively.

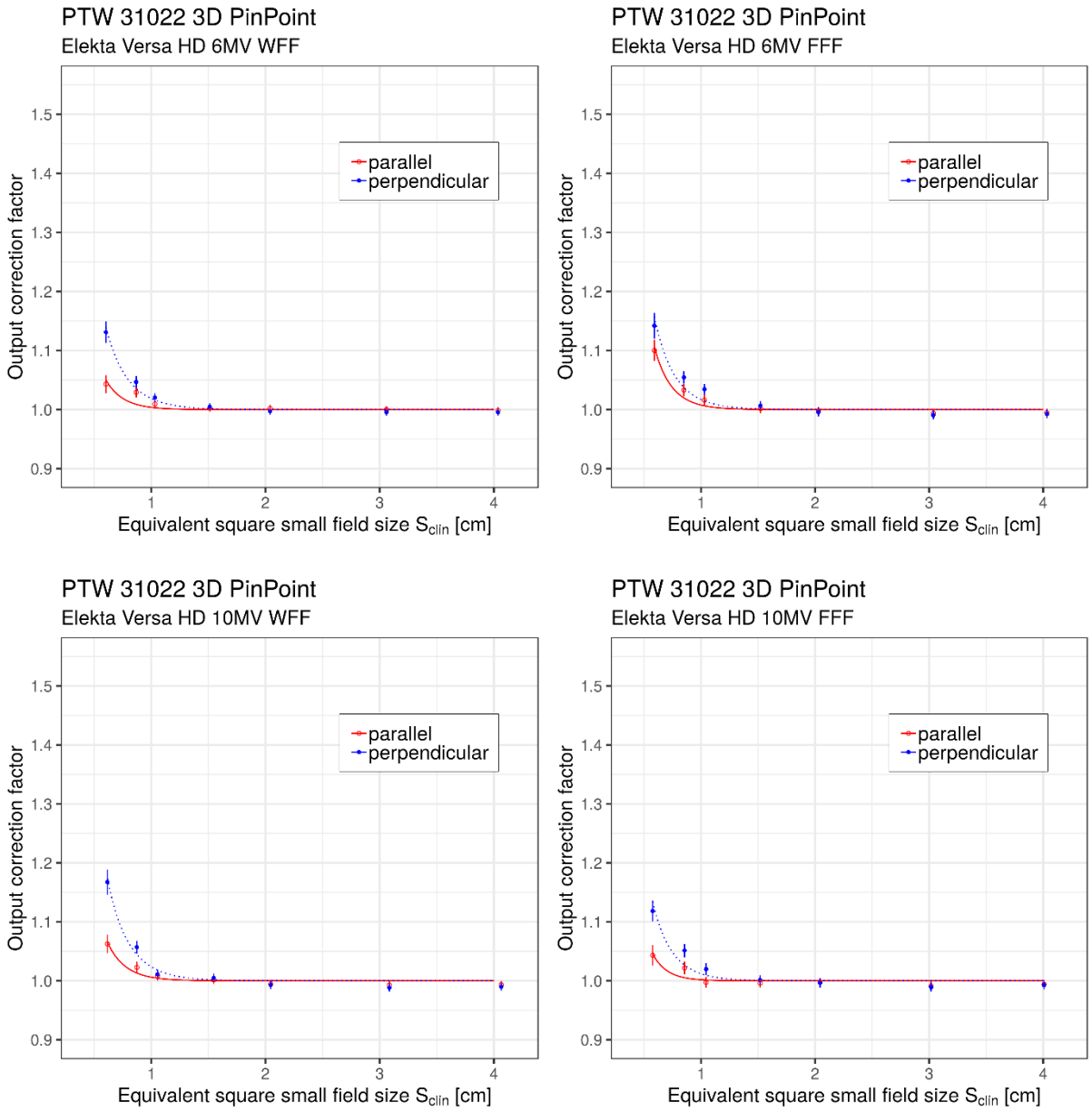

Figure V. Detector specific output correction factors $k_{Q_{clin},Q_{ref}}^{f_{clin},f_{ref}}$ for PTW 31022 3D PinPoint ionization chamber for two orientation with respect to the central beam axis; perpendicular (blue symbols and blue dotted lines) and (red symbols and red full lines) for four photon beams on Elekta Versa HD linac. Output correction factors are presented as individual values/points and as curves of analytical function applying Eq. (5.14) and Eq. (5.15) respectively.

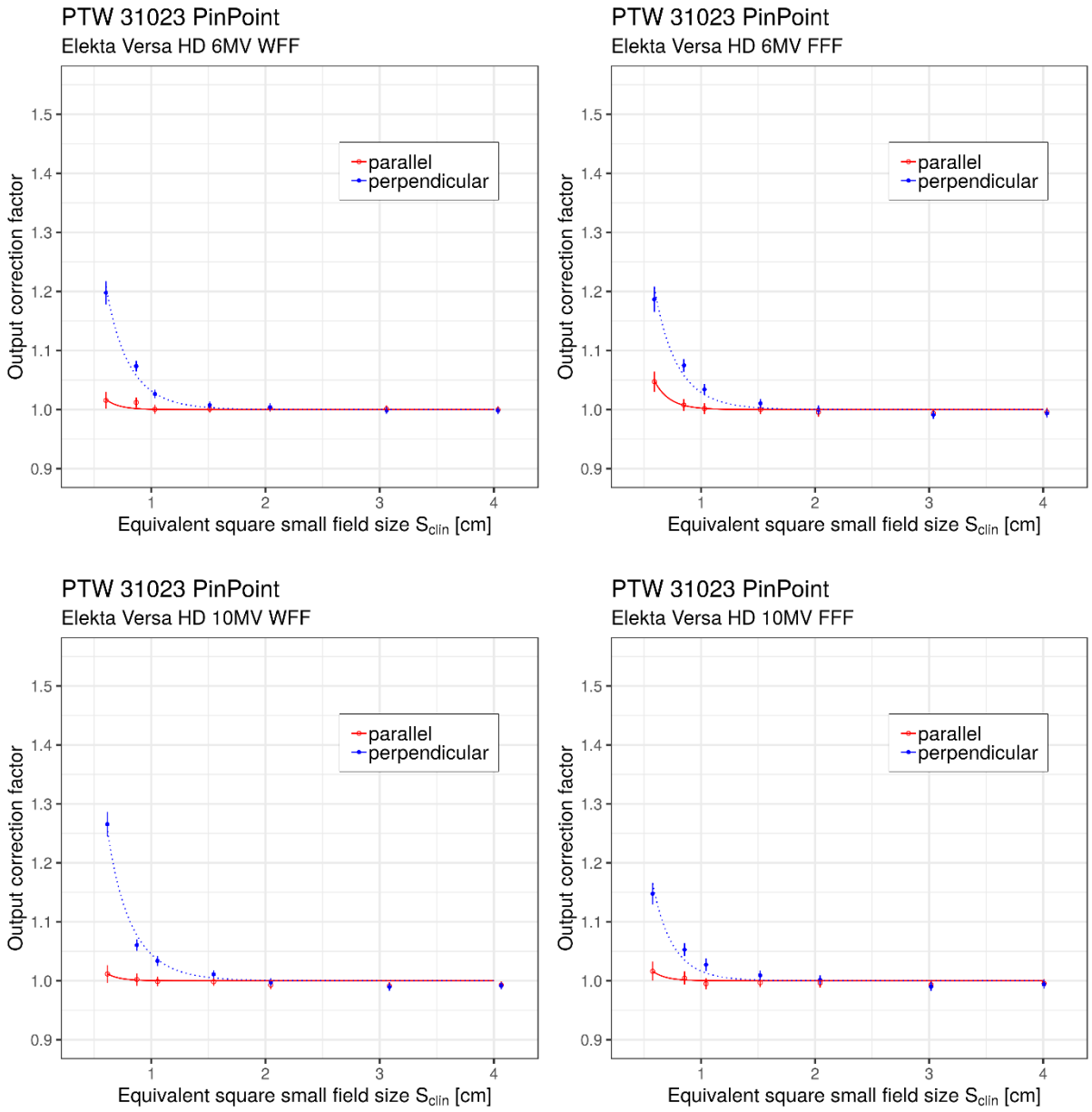

Figure VI. Detector specific output correction factors $k_{Q_{clin},Q_{ref}}^{f_{clin},f_{ref}}$ for PTW 31023 PinPoint ionization chamber for two orientation with respect to the central beam axis; perpendicular (blue symbols and blue dotted lines) and (red symbols and red full lines) for four photon beams on Elekta Versa HD linac. Output correction factors are presented as individual values/points and as curves of analytical function applying Eq. (5.14) and Eq. (5.15) respectively.

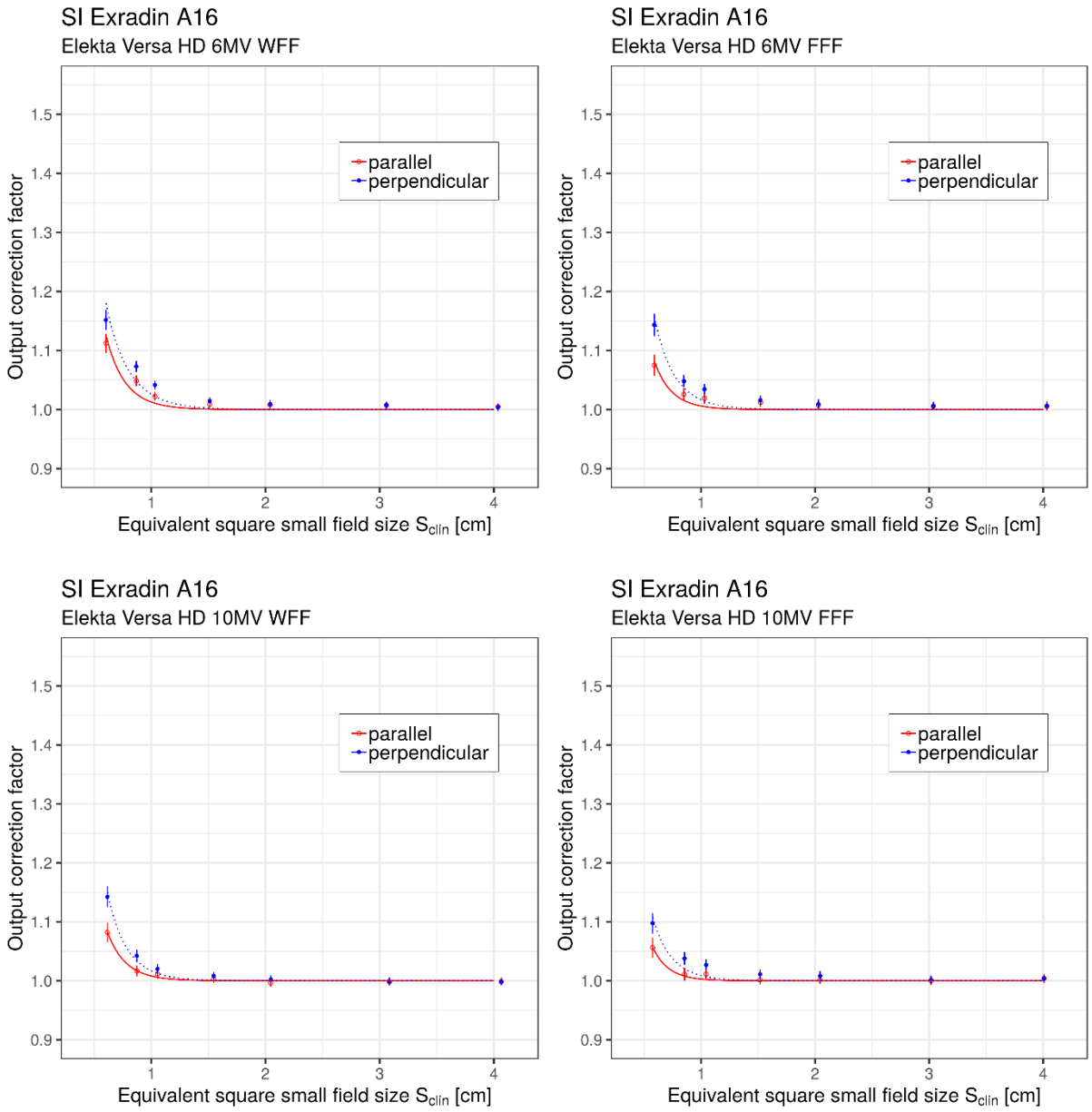

Figure VII. Detector specific output correction factors $k_{Q_{clin},Q_{ref}}^{f_{clin},f_{ref}}$ for SI Exradin A16 ionization chamber for two orientation with respect to the central beam axis; perpendicular (blue symbols and blue dotted lines) and (red symbols and red full lines) for four photon beams on Elekta Versa HD linac. Output correction factors are presented as individual values/points and as curves of analytical function applying Eq. (5.14) and Eq. (5.15) respectively.

2 Fitting parameters for the analytical function for output correction factors for ionization chambers on Elekta Versa HD linac

Table I Values of fitting parameters for the analytical function given in Eq. (5.15) shown graphically in Figure I (Appendix 1) for output correction factors for IBA CC04 ionization chamber for two utilized orientations with respect to the beam's central axis.

IBA CC04	perpendicular			parallel		
E	a	b	c	a	b	c
6 MV WFF	0.2502	0.2366	0	0.2411	0.2275	0
6 MV FFF	0.2434	0.2343	0	0.2047	0.2320	0
10 MV WFF	0.2297	0.2411	0	0.2116	0.2343	0
10 MV FFF	0.2047	0.2184	0	0.1979	0.2002	0

Table II Values of fitting parameters for the analytical function given in Eq. (5.15) shown graphically in Figure II (Appendix 1) for output correction factors for IBA Razor ionization chamber for two utilized orientations with respect to the beam's central axis.

IBA Razor IC	perpendicular			parallel		
E	a	b	c	a	b	c
6 MV WFF	0.1774	0.1934	0	0.1524	0.1388	0
6 MV FFF	0.1729	0.1729	0	0.1342	0.1160	0
10 MV WFF	0.1524	0.1911	0	0.1228	0.1046	0
10 MV FFF	0.1342	0.1547	0	0.0819	0.0819	0.0023

Table III Values of fitting parameters for the analytical function given in Eq. (5.15) shown graphically in Figure III (Appendix 1) for output correction factors for PTW 31016 3D PinPoint ionization chamber for two utilized orientations with respect to the beam's central axis.

PTW 31016 3D PinPoint	perpendicular			parallel		
E	a	b	c	a	b	c
6 MV WFF	0.2206	0.2366	0	0.1592	0.1911	0
6 MV FFF	0.2070	0.2161	0	0.1865	0.1706	0
10 MV WFF	0.2320	0.2297	0	0.1661	0.1956	0
10 MV FFF	0.1615	0.2047	0	0.1410	0.1683	0

Table IV Values of fitting parameters for the analytical function given in Eq. (5.15) shown graphically in Figure IV (Appendix 1) for output correction factors for PTW 31021 3D Semiflex ionization chamber for two utilized orientations with respect to the beam's central axis.

PTW 31021 3D Semiflex	perpendicular			parallel		
E	a	b	c	a	b	c
6 MV WFF	0.2730	0.2912	0	0.2752	0.2752	0
6 MV FFF	0.2457	0.2843	0	0.2707	0.2593	0
10 MV WFF	0.2934	0.2866	0	0.2639	0.2798	0
10 MV FFF	0.2661	0.2593	0	0.2730	0.2320	0

Table V Values of fitting parameters for the analytical function given in Eq. (5.15) shown graphically in Figure V (Appendix 1) for output correction factors for PTW 31022 3D PinPoint ionization chamber for two utilized orientations with respect to the beam's central axis.

PTW 31022 3D PinPoint	perpendicular			parallel		
E	a	b	c	a	b	c
6 MV WFF	0.2161	0.1865	0	0.1365	0.1524	0
6 MV FFF	0.1911	0.2002	0	0.1774	0.1774	0
10 MV WFF	0.2229	0.2070	0	0.1547	0.1661	0
10 MV FFF	0.1592	0.1934	0	0.1456	0.1388	0

Table VI Values of fitting parameters for the analytical function given in Eq. (5.15) shown graphically in Figure VI (Appendix 1) for output correction factors for PTW 31023 PinPoint ionization chamber for two utilized orientations with respect to the beam's central axis.

PTW 31023 PinPoint	perpendicular			parallel		
E	a	b	c	a	b	c
6 MV WFF	0.2479	0.2070	0	0.1251	0.1183	0
6 MV FFF	0.1979	0.2229	0	0.1319	0.1479	0
10 MV WFF	0.2138	0.2525	0	0.1092	0.1137	0
10 MV FFF	0.2002	0.1911	0	0.1183	0.1115	0

Table VII Values of fitting parameters for the analytical function given in Eq. (5.15) shown graphically in Figure VII (Appendix 1) for output correction factors for SI Exradin A16 ionization chamber for two utilized orientations with respect to the beam's central axis.

SI Exradin A16	perpendicular			parallel		
E	a	b	c	a	b	c
6 MV WFF	0.2320	0.2002	0	0.1911	0.1888	0
6 MV FFF	0.2206	0.1865	0	0.1820	0.1570	0
10 MV WFF	0.2343	0.1865	0	0.1774	0.1706	0
10 MV FFF	0.1797	0.1706	0	0.1501	0.1456	0

3 Output correction factors for perpendicular and parallel orientation of ionization chambers on Varian TrueBeam linac

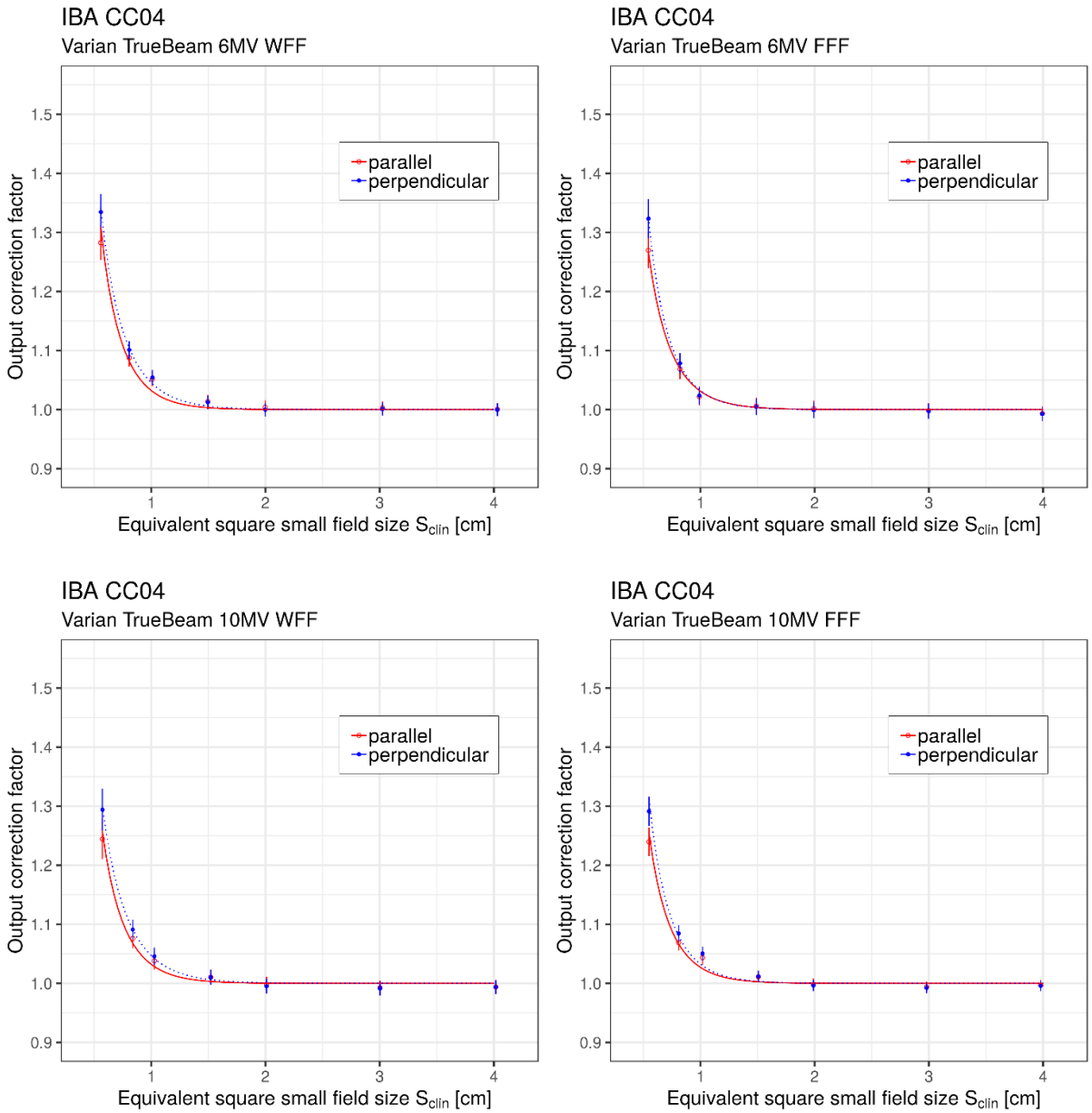

Figure VIII. Detector specific output correction factors $k_{Q_{clin},Q_{ref}}^{f_{clin},f_{ref}}$ for IBA CC04 ionization chamber for two orientation with respect to the central beam axis; perpendicular (blue symbols and blue dotted lines) and (red symbols and red full lines) for four photon beams on Varian TrueBeam linac. Output correction factors are presented as individual values/points and as curves of analytical function applying Eq. (5.14) and Eq. (5.15) respectively.

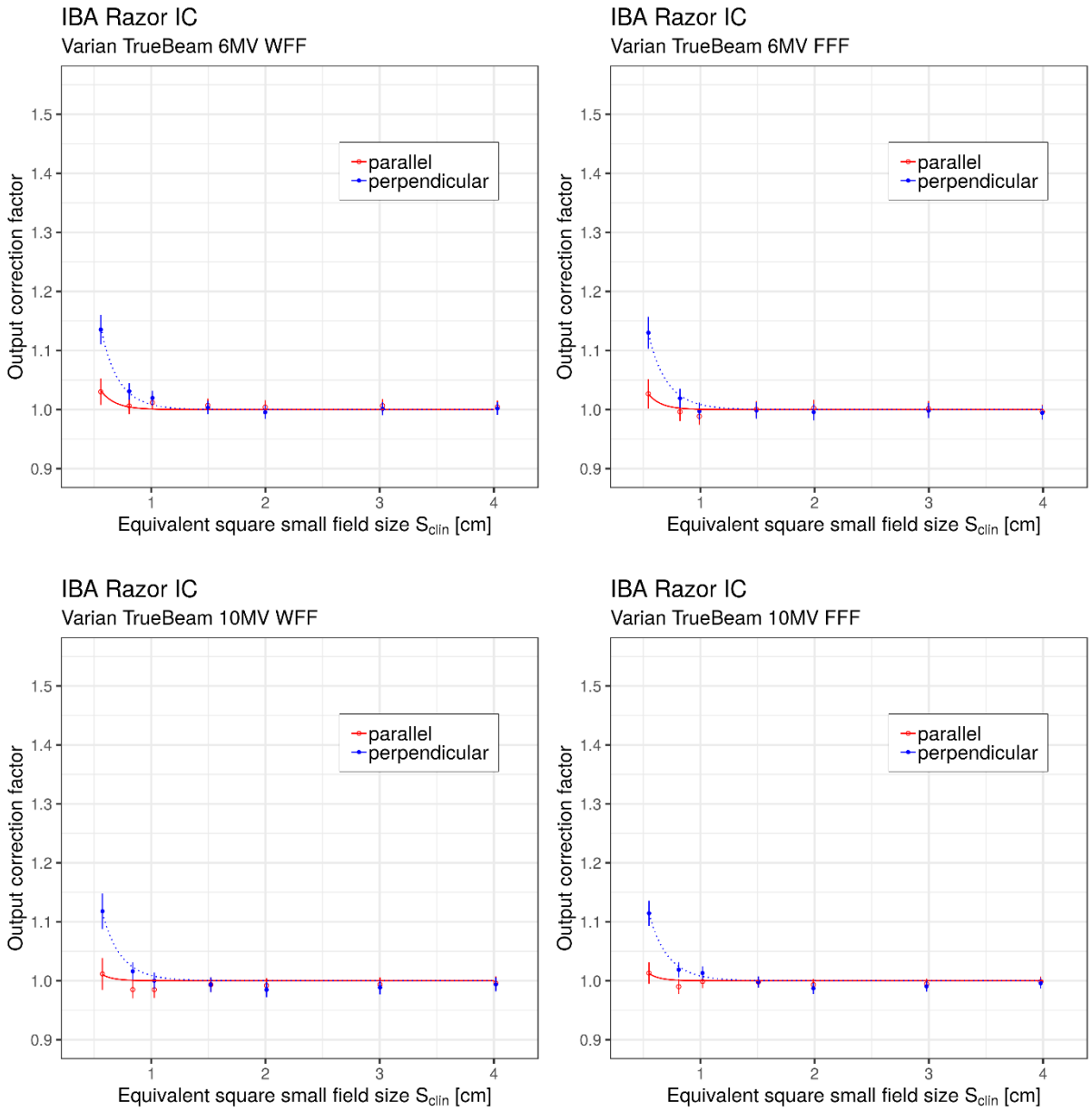

Figure IX. Detector specific output correction factors $k_{Q_{clin},Q_{ref}}^{f_{clin},f_{ref}}$ for IBA Razor ionization chamber for two orientation with respect to the central beam axis; perpendicular (blue symbols and blue dotted lines) and (red symbols and red full lines) for four photon beams on Varian TrueBeam linac. Output correction factors are presented as individual values/points and as curves of analytical function applying Eq. (5.14) and Eq. (5.15) respectively.

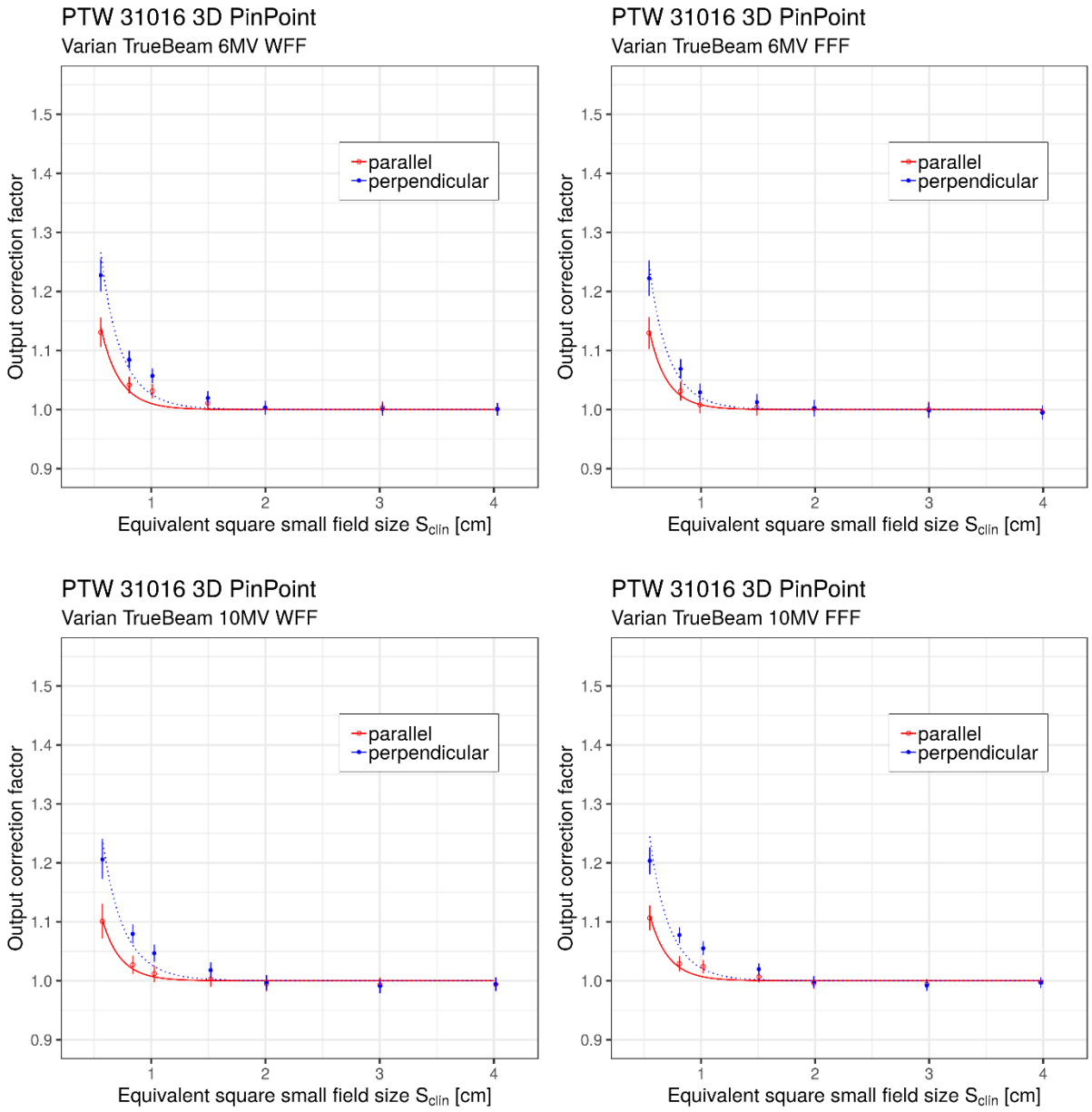

Figure X. Detector specific output correction factors $k_{Q_{clin},Q_{ref}}^{f_{clin},f_{ref}}$ for PTW 31016 3D PinPoint ionization chamber for two orientation with respect to the central beam axis; perpendicular (blue symbols and blue dotted lines) and (red symbols and red full lines) for four photon beams on Varian TrueBeam linac. Output correction factors are presented as individual values/points and as curves of analytical function applying Eq. (5.14) and Eq. (5.15) respectively.

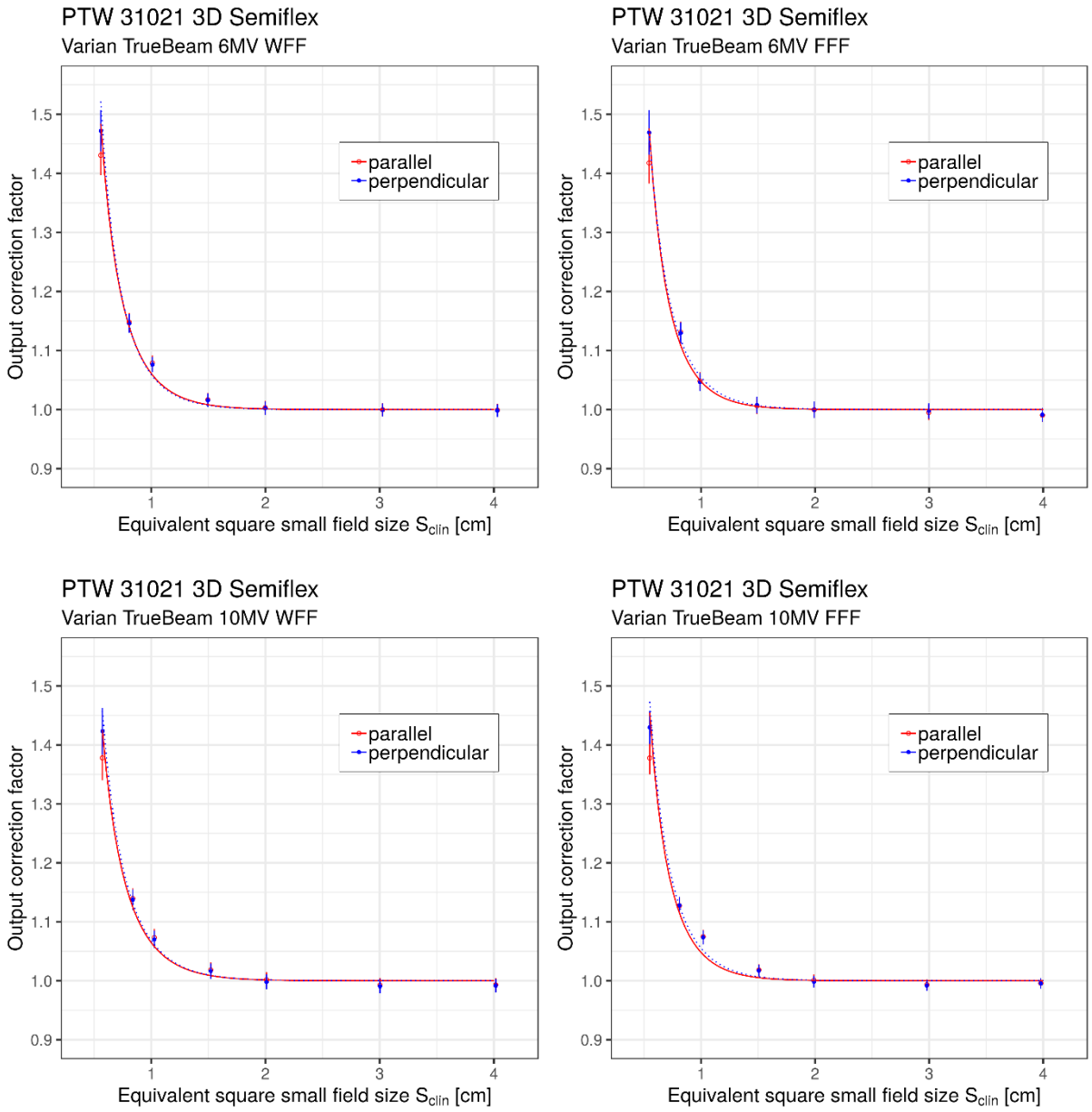

Figure XI. Detector specific output correction factors $k_{Q_{clin},Q_{ref}}^{f_{clin},f_{ref}}$ for PTW 31021 3D Semiflex ionization chamber for two orientation with respect to the central beam axis; perpendicular (blue symbols and blue dotted lines) and (red symbols and red full lines) for four photon beams on Varian TrueBeam linac. Output correction factors are presented as individual values/points and as curves of analytical function applying Eq. (5.14) and Eq. (5.15) respectively.

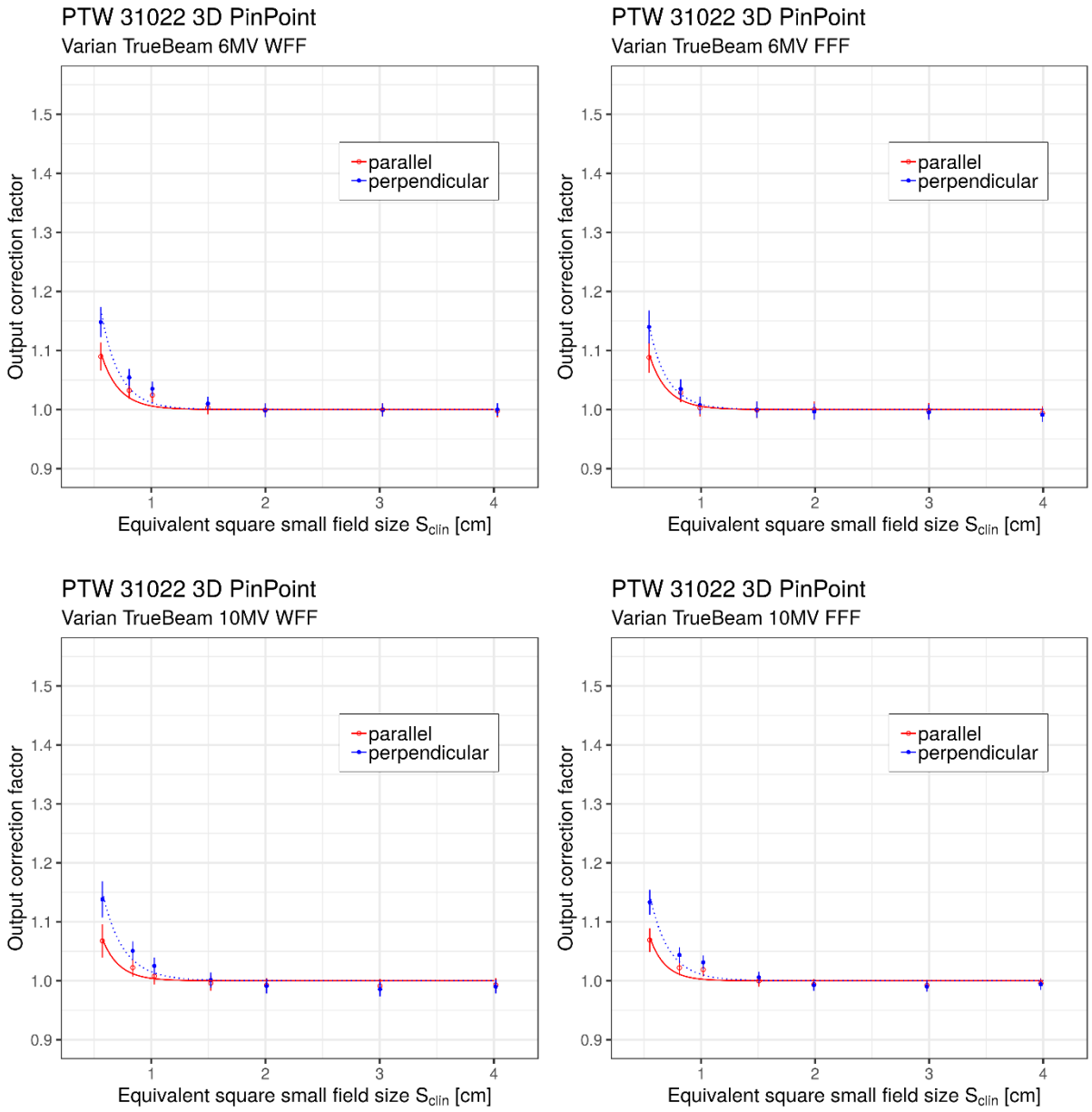

Figure XII. Detector specific output correction factors $k_{Q_{clin},Q_{ref}}^{f_{clin},f_{ref}}$ for PTW 31022 3D PinPoint ionization chamber for two orientation with respect to the central beam axis; perpendicular (blue symbols and blue dotted lines) and (red symbols and red full lines) for four photon beams on Varian TrueBeam linac. Output correction factors are presented as individual values/points and as curves of analytical function applying Eq. (5.14) and Eq. (5.15) respectively.

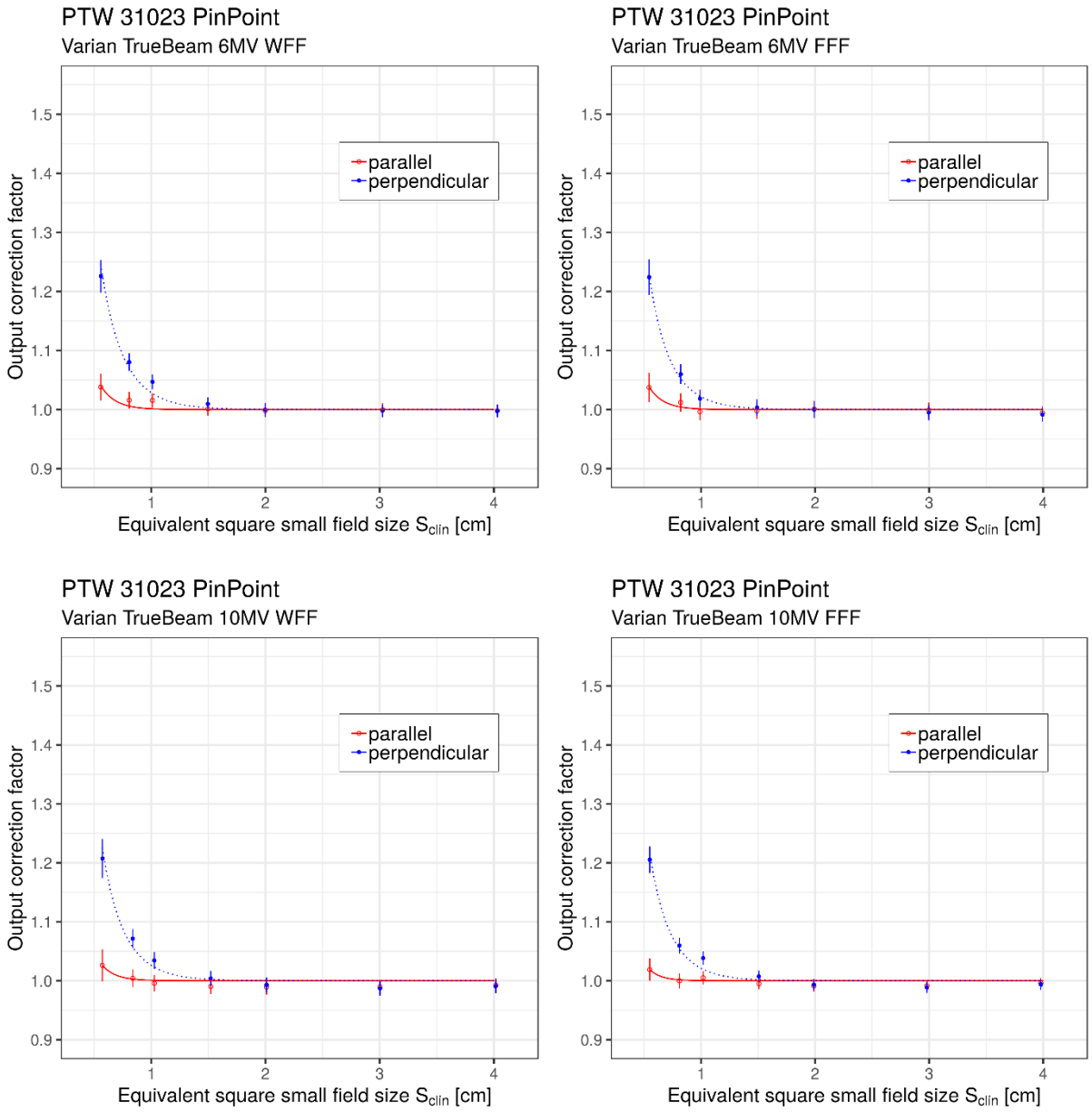

Figure XIII. Detector specific output correction factors $k_{Q_{clin},Q_{ref}}^{f_{clin},f_{ref}}$ for PTW 31023 PinPoint ionization chamber for two orientation with respect to the central beam axis; perpendicular (blue symbols and blue dotted lines) and (red symbols and red full lines) for four photon beams on Varian TrueBeam linac. Output correction factors are presented as individual values/points and as curves of analytical function applying Eq. (5.14) and Eq. (5.15) respectively.

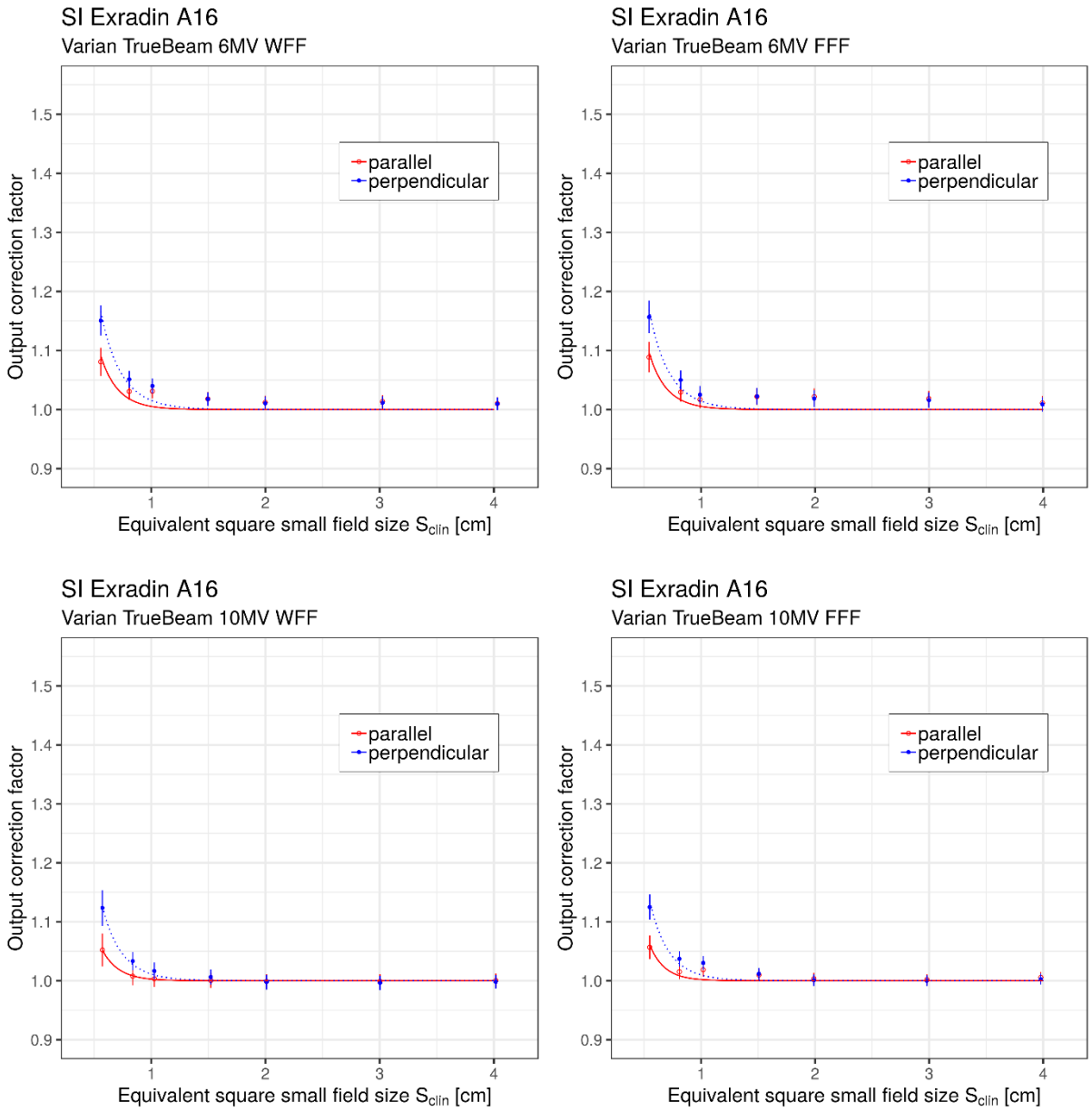

Figure XIV. Detector specific output correction factors $k_{Q_{clin},Q_{ref}}^{f_{clin},f_{ref}}$ for SI Exradin A16 ionization chamber for two orientation with respect to the central beam axis; perpendicular (blue symbols and blue dotted lines) and (red symbols and red full lines) for four photon beams on Varian TrueBeam linac. Output correction factors are presented as individual values/points and as curves of analytical function applying Eq. (5.14) and Eq. (5.15) respectively.

4 Fitting parameters for the analytical function for output correction factors for ionization chambers on Varian TrueBeam linac

Table VIII Values of fitting parameters for the analytical function given in Eq. (5.15) shown graphically in Figure VIII (Appendix 3) for output correction factors for IBA CC04 ionization chamber for two utilized orientations with respect to the beam's central axis.

IBA CC04	perpendicular			parallel		
E	a	b	c	a	b	c
6 MV WFF	0.2252	0.2457	0	0.2093	0.2366	0
6 MV FFF	0.2457	0.2138	0	0.2229	0.2093	0
10 MV WFF	0.2411	0.2320	0	0.2116	0.2275	0
10 MV FFF	0.2388	0.2184	0	0.2297	0.2025	0

Table IX Values of fitting parameters for the analytical function given in Eq. (5.15) shown graphically in Figure IX (Appendix 3) for output correction factors for IBA Razor ionization chamber for two utilized orientations with respect to the beam's central axis.

IBA Razor IC	perpendicular			parallel		
E	a	b	c	a	b	c
6 MV WFF	0.1729	0.1820	0	0.1433	0.1183	0
6 MV FFF	0.1524	0.1797	0	0.1092	0.1183	0
10 MV WFF	0.1479	0.1865	0	0.1024	0.1024	0
10 MV FFF	0.1774	0.1638	0	0.1069	0.1001	0

Table X Values of fitting parameters for the analytical function given in Eq. (5.15) shown graphically in Figure X (Appendix 3) for output correction factors for PTW 31016 3D PinPoint ionization chamber for two utilized orientations with respect to the beam's central axis.

PTW 31016 3D PinPoint	perpendicular			parallel		
E	a	b	c	a	b	c
6 MV WFF	0.2161	0.2184	0	0.1683	0.1865	0
6 MV FFF	0.2047	0.2070	0	0.1956	0.1638	0
10 MV WFF	0.2070	0.2206	0	0.1547	0.1774	0
10 MV FFF	0.2047	0.2093	0	0.1820	0.1615	0

Table XI Values of fitting parameters for the analytical function given in Eq. (5.15) shown graphically in Figure XI (Appendix 3) for output correction factors for PTW 31021 3D Semiflex ionization chamber for two utilized orientations with respect to the beam's central axis.

PTW 31021 3D Semiflex	perpendicular			parallel		
E	a	b	c	a	b	c
6 MV WFF	0.2639	0.2661	0	0.2570	0.2639	0
6 MV FFF	0.2593	0.2502	0	0.2388	0.2570	0
10 MV WFF	0.2752	0.2593	0	0.2730	0.2548	0
10 MV FFF	0.2457	0.2616	0	0.2343	0.2593	0

Table XII Values of fitting parameters for the analytical function given in Eq. (5.15) shown graphically in Figure XII (Appendix 3) for output correction factors for PTW 31022 3D PinPoint ionization chamber for two utilized orientations with respect to the beam's central axis.

PTW 31022 3D PinPoint	perpendicular			parallel		
E	a	b	c	a	b	c
6 MV WFF	0.2138	0.1774	0	0.1843	0.1547	0
6 MV FFF	0.1615	0.1843	0	0.1410	0.1638	0
10 MV WFF	0.1774	0.1956	0	0.1433	0.1592	0
10 MV FFF	0.1911	0.1752	0	0.1388	0.1547	0

Table XIII Values of fitting parameters for the analytical function given in Eq. (5.15) shown graphically in Figure XIII (Appendix 3) for output correction factors for PTW 31023 PinPoint ionization chamber for two utilized orientations with respect to the beam's central axis.

PTW 31023 PinPoint	perpendicular			parallel		
E	a	b	c	a	b	c
6 MV WFF	0.2070	0.2184	0	0.1433	0.1297	0
6 MV FFF	0.2002	0.2047	0	0.1388	0.1228	0
10 MV WFF	0.1979	0.2206	0	0.1297	0.1206	0
10 MV FFF	0.2184	0.1956	0	0.1046	0.1115	0

Table XIV Values of fitting parameters for the analytical function given in Eq. (5.15) shown graphically in Figure XIV (Appendix 3) for output correction factors for SI Exradin A16 ionization chamber for two utilized orientations with respect to the beam's central axis.

SI Exradin A16	perpendicular			parallel		
E	a	b	c	a	b	c
6 MV WFF	0.2116	0.1797	0	0.1592	0.1592	0
6 MV FFF	0.1479	0.2047	0	0.1342	0.1683	0
10 MV WFF	0.1888	0.1774	0	0.1274	0.1479	0
10 MV FFF	0.1934	0.1683	0	0.1365	0.1433	0

11 BIOGRAPHY

Božidar Casar is internationally recognized medical physicists born in Murska Sobota, Slovenia, and presently the only medical physicist in Slovenia awarded as Medical Physics Expert by the European Examination Board of European Federation of Organizations for Medical Physics (EFOMP). He graduated from Physics at the University of Ljubljana, Faculty of Mathematics and Physics. Since 1993 he is employed as a medical physicist at the Institute of Oncology Ljubljana. From 2000 to 2016 he was heading the Department for Radiation Physics, and from 2016 until the present, he is a Head of the Department for Dosimetry and Quality of Radiological Procedures. Since 2010, he is involved in the postgraduate educational program as a teaching assistant for the course Experimental Medical Physics at the Department of Physics, Faculty of Mathematics and Physics in Ljubljana.

Casar's clinical, scientific and research work encompass complex radiotherapy dosimetry, stereotactic radiosurgery and introduction of proton therapy in Slovenia. In 1999 he pioneered stereotactic radiosurgery in Slovenia with the equipment of his design, the achievement, which was recognized among the most important achievements of Slovenian scientists in the field of biotechnology in medicine in 2013. For his contribution to the development of medical physics in Bosnia and Herzegovina, he has been awarded the honorary membership of the Association of Medical Physicists in Bosnia and Herzegovina, among only three non-Bosnian medical physicists.

In the past, Božidar Casar has been involved in the activities of many national and international organizations and societies, among others he was a member of EFOMP Scientific Committee and Committee for Education and Training and was cofounder of Medical Physics Section of the Slovenian Biophysical Society in 1997. However, his professional career has been most notably marked by the cooperation with the International Atomic Energy Agency (IAEA) where he has served as a member and leader of several scientific projects and has been nominated as an IAEA expert in more than ten international expert missions.

12 LIST OF SELECTED PUBLISHED WORKS

10.1 Original scientific article

1. SMILOVIĆ RADOJČIĆ, Đeni, ŠVABIĆ KOLACIO, Manda, RADOJČIĆ, Milan, RAJLIĆ, David, **CASAR, Božidar**, FAJ, Dario, JURKOVIĆ, Slaven. Comparison of calculated dose distributions reported as dose-to-water and dose-to-medium for intensity-modulated radiotherapy of nasopharyngeal cancer patients. *Medical dosimetry*, 2018, 43(4), 363-369, doi: 10.1016/j.meddos.2017.11.008.

2. **CASAR, Božidar**, GERSHKEVITSH, Eduard, MÉNDEZ CAROT, Ignasi, JURKOVIĆ, Slaven, SAIFUL HUQ, M. A novel method for the determination of field output factors and output correction factors for small static fields for six diodes and a microdiamond detector in megavoltage photon beams. *Medical physics*, 2018, 1-20, doi: 10.1002/mp.13318.

3. MÉNDEZ CAROT, Ignasi, POLŠAK, Aljoša, HUDEJ, Rihard, **CASAR, Božidar**. The Multigaussian method: a new approach to mitigating spatial heterogeneities with multichannel radiochromic film dosimetry. *Physics in medicine & biology*, 2018, 63, 175013, doi: 10.1088/1361-6560/aad9c1.

4. SMILOVIĆ RADOJČIĆ, Đeni, RAJLIĆ, David, **CASAR, Božidar**, ŠVABIĆ KOLACIO, Manda, OBAJDIN, Nevena, FAJ, Dario, JURKOVIĆ, Slaven. Evaluation of two-dimensional dose distributions for pre-treatment patient-specific IMRT dosimetry. *Radiology and oncology*, 2018, 52(3), 346-352, doi: 10.2478/raon-2018-0019.

5. **CASAR, Božidar**, PASLER, Marlies, WEGENER, Sonja, HOFFMAN, David, TALAMONTI, Cinzia, QIAN, Jianguo, MÉNDEZ CAROT, Ignasi, BROJAN, Denis, PERRIN, Bruce, KUSTERS, Martijn, PETERLIN, Primož, et al. Influence of the Integral Quality Monitor transmission detector on high energy photon beams: a multi-centre study. *Zeitschrift für medizinische Physik*, 2017, 27(3), 232-242, doi: 10.1016/j.zemedi.2016.10.001.

6. MÉNDEZ CAROT, Ignasi, ŠLJIVIĆ, Željko, HUDEJ, Rihard, JENKO, Aljaša, **CASAR, Božidar**. Grid patterns, spatial inter-scan variations and scanning reading repeatability in radiochromic film dosimetry. *Physica medica*, 2016, 32(9), 1072-1081, doi: 10.1016/j.ejmp.2016.08.003.

7. **CASAR, Božidar**, CARMO LOPES, Maria do, DRLJEVIĆ, Advan, GERSHKEVITSH, Eduard, PESZNYÁK, Csilla. Medical physics in Europe following recommendations of the International Atomic Energy Agency. *Radiology and oncology*, 2016, 50(1), 64-72, doi: 10.1515/raon.2016.0004.

8. MÉNDEZ CAROT, Ignasi, PETERLIN, Primož, HUDEJ, Rihard, STROJNIK, Andrej, **CASAR, Božidar**. On multichannel film dosimetry with channel-independent perturbations. *Medical physics*, 2014, 41(1), 011705-1-011705-10, doi: 10.1118/1.4845095.

9. MÉNDEZ CAROT, Ignasi, HARTMAN, Vida, HUDEJ, Rihard, STROJNIK, Andrej, **CASAR, Božidar**. Gafchromic EBT2 film dosimetry in reflection mode with a novel plan-based calibration method. *Medical physics*, 2013, 40(1), 011720-1-011720-9, doi: 10.1118/1.4772075.

10. **CASAR, Božidar**, ŠARVARI, Attila. Experimental verification of the calculated dose for stereotactic radiosurgery with specially designed white polystyrene phantom. V: JARM, Tomaž (ur.), KRAMAR, Peter (ur.), ŽUPANIČ, Anže (ur.). *11th Mediterranean Conference on Medical and Biological Enginering and Computing 2007: [also] MEDICON 2007, 26-30 June, 2007, Ljubljana, Slovenia*, (IFMBE proceedings, ISSN 1727-1983, vol. 16). New York: Springer: International Federation for Medical and Biological Engineering. 2007, 887-890.

11. **CASAR, Božidar**, ZDEŠAR, Urban, ROBAR, Vlado. Evaluation of water equivalency of Plastic waterTM for high-energy electron beams using IAEA TRS-398 code of practice. *Radiology and oncology*, 2004, 38(1), 55-60.

12. **CASAR, Božidar**. Tertiary collimator system for stereotactic radiosurgery with linear accelerator = Tarciarni kolimatorski sistem za stereotaktično radiokirurgijo z linearnim pospeševalnikom. *Radiology and oncology*, 1998, 32(1), 125-128.

13. VELNAR, Tomaž, SMRDEL, Uroš, **CASAR, Božidar**, BOŠNJAK, Roman, BUNC, Gorazd. Kratek pregled stereotaktičnih radiokirurških tehnik = A short review of stereotactic radiosurgery techniques. *Medicinski razgledi*, 2010, 49(3), 307-315.

10.2 Professional article

14. CYGLER, Joanna, **CASAR, Božidar**, JERAJ, Robert. AAPM - ISEP/IOMP therapy course: challenges in modern radiation therapy physics. *AAPM Newsletter*, 2019, 44(1), 1-7. https://w3.aapm.org/newsletter/posts/2019/jan-feb/.

15. CYGLER, Joanna, **CASAR, Božidar**, JERAJ, Janez. 2018 AAPM/IOMP - ISEP therapy course challenges in modern radiation therapy physics. *Medical physics international*, 2018, 6(2), 268-271.

16. **CASAR, Božidar**, STROJAN, Primož. Radioterapija s protonskimi žarki = Proton beam therapy. *Onkologija : strokovni časopis za zdravnike*, 2018, 22(1), 12-16.

17. BURGAR, Janko, STROJAN, Primož, **CASAR, Božidar**. Napredno zdravljenje raka s protonsko terapijo in izzivi uvajanja v Sloveniji. *NOVIS: novice, obvestila, vesti, informacije združenja*, 2017, 44(10), 6-8.

18. **CASAR, Božidar**. IAEA regional meeting on medical physics in Europe. *European medical physics news*, 2015, 2(2), 7. http://www.efomp.org/index.php/efomp-publications/finish/3/862.

19. **CASAR, Božidar**, STROJAN, Primož. Stereotaktična tehnika v radioterapiji. *Onkologija: strokovni časopis za zdravnike*, 2003, 7(1), 12-14.

10.3 Published scientific conference contribution or abstract

20. **CASAR, Božidar**, ZDEŠAR, Urban. Clinical reference dosimetry: experimental comparison between IAEA TRS-277 and IAEA TRS-398 dosimetry protocols for high energy photon beams and 60 Co gamma rays. V: SCHMIDT, Werner (ur.), CASAR, Božidar (ur.). *Physics contribution to radiation therapy*. Udine: Associazione Italiana di Fisica in Medicina (AIFM): Austrian Society for Medical Physics (ÖGMP): Slovenian Biophysical Society (SBS). 2003. (Invited lecture).

21. RAJLIĆ, David, SMILOVIĆ RADOJČIĆ, Deni, **CASAR, Božidar**, ŠVABIĆ KOLACIO, Manda, FAJ, Dario, JURKOVIĆ, Slaven. Evaluation of dose planes using 2D detector array: patient specific dosimetry or accelerator performance assessment. V: PETROVIC, Borislava (Ed.). *Proceedings*, 8th AAMP [Alpe-Adria Medical Phisics] Conference, Novi Sad, Serbia 25-27 May 2017. [Beograd]: Serbian Association of Medical Physicists: Society for Radiation Protection of Serbia and Montenegro: Vinca Institute of Nuclear Sciences. 2017, 198-201.

22. **CASAR, Božidar**. Medical physicists: clinical scientists or hospital wizards. V: HRŠAK, Hrvoje (Ed.), BUDANEC, Mirjana (Ed.). *Proceedings*, 7th AAMP Meeting, Zagreb, Croatia, May 19-21, 2016. [Zagreb: CROMBES: CRPA]. 2016, 1-4.

23. **CASAR, Božidar**, ČUGURA, David, MÉNDEZ CAROT, Ignasi, VOJVODIĆ, Ilija, REBERŠEK, Stanislav. Measuring system for testing the mechanical isocenter accuracy of medical linear accelerators. V: *World Congress on Medical Physics and Biomedical Engineering, 7-12 September, 2009, Munich, Germany*, (IFMBE proceedings, ISSN 1680-0737, vol. 25). Heidelberg: Springer. 2009, 989-992.

24. **CASAR, Božidar**, VOJVODIĆ, Ilija, ROBAR, Vlado, SMRDEL, Uroš, MÉNDEZ CAROT, Ignasi. New system for TBI with translation method at the Institute of Oncology Ljubljana. V: *World Congress on Medical Physics and Biomedical Engineering, 7-12 September, 2009, Munich, Germany*, (IFMBE proceedings, ISSN 1680-0737, vol. 25). Heidelberg: Springer. 2009, 996-997.

25. VRTAČNIK, Danilo, **CASAR, Božidar**, RESNIK, Drago, ALJANČIČ, Uroš, MOŽEK, Matej, AMON, Slavko. Radiation hardness of composite nitride-oxide films. V: SMOLE, Franc (Ed.), TOPIČ, Marko (Ed.), ŠORLI, Iztok (Ed.). *Proceedings*, 37th International Conference on Microelectronics, Devices and Materials and the Workshop on Optoelectronic Devices and Applications, October 10. - 12. 2001, Bohinj, Slovenia. Ljubljana: MIDEM - Society for Microelectronics, Electronic Components and Materials. 2001, 285-290.

26. VRTAČNIK, Danilo, KRIŽAJ, Dejan, MALI, Tadej, **CASAR, Božidar**, RESNIK, Drago, ALJANČIČ, Uroš, MOŽEK, Matej, AMON, Slavko. Influence of radiation on characteristics of FOXFET biased silicon microstrip detector. V: HROVAT, Marko (Ed.), KOSEC, Marija (Ed.), ŠORLI, Iztok (Ed.). *Proceedings*, 36th International Conference on Microelectronics, Devices and Materials and the Workshop on Analytical Methods in Microelectronics and Electronic Materials, October 18. - 20. 2000, Postojna, Slovenia. Ljubljana: MIDEM - Society for Microelectronics, Electronic Components and Materials. 2000, 117-122.

27. **CASAR, Božidar**, MILOŠEVIČ, Z..., SEKEREŠ, Boris. Simulation of stereotactic radiosurgery with a specially designed polystyrene phantom and radiochromic films. V: *Programme & Abstract Book*, 4th International Stereotactic Radiosurgery Social Congress, 23 - 26 February 1999, Sydney, Australia. Sydney: The Prince of Wales Hospital. 1999, 55.

28. **CASAR, Božidar**, PREGELJ, Andrej, SEKEREŠ, Bogdan, VERK, T.... Collimator system for sterotactic radiosurgery with linear accelerator. *Radiotherapy and oncology*, 1998, vol. 48, suppl. 1.

29. **CASAR, Božidar**. Public procurement of medical radiological equipment: starting point of patient safety. V: *Tudományos program és absztrakt könyv*. Budapest: Sugárvédelem. 2016, str. 6-7. (Invited lecture).

30. MÉNDEZ CAROT, Ignasi, **CASAR, Božidar**. Big data in radiochromic film dosimetry. *Physica medica*, 2018, 52, suppl. 159-60, doi: 10.1016/j.ejmp.2018.06.227.

31. **CASAR, Božidar**, GERSHKEVITSH, Eduard, MÉNDEZ CAROT, Ignasi. Dosimetrical properties of the new IBA RAZOR NanoChamber ionization chamber in MV photon beams. *Radiotherapy and oncology*, 2018, 127, suppl. 1, S919.

32. **CASAR, Božidar**. Cost-effective public procurements of equipment for radiotherapy: starting point of patient's safety. V: *Book of synopses*, International Conference on Advances in Radiation Oncology, Vienna, 20-23 June 2017. Vienna: IAEA. 2017, 81-82.

33. **CASAR, Božidar**, MÉNDEZ CAROT, Ignasi, PETERLIN, Primož. Beam hardening and attenuation of photon beams using integral quality monitor in radiotherapy. *Medical physics*, 2016, 43(6), 3590, doi: 10.1118/1.4956736.

34. MÉNDEZ CAROT, Ignasi, ŠLJIVIĆ, Željko, HUDEJ, Rihard, JENKO, Aljaša, **CASAR, Božidar**. The repeatability of the scanner in radiochromic film dosimetry. *Physica medica*, 2016, 32, suppl. 3, 203, doi: 10.1016/j.ejmp.2016.07.690.

35. **CASAR, Božidar**. Numerical evaluation of offers for medical radiological equipment. *Physica medica*, 2016, vol. 32, suppl. 3, str. 282.

36. **CASAR, Božidar**. How to become a medical physicist in Slovenia. V: *Scientific programme and abstract book*, Alpe-Adria Medical Physics Meeting, Budapest, Hungary, May 29-31, 2014. Budapest: Hungarian Society of Medical Physicists. 2014, 20.

37. SMRDEL, Uroš, **CASAR, Božidar**. Stereotactic and image guided techniques in treatment of central nervous system tumours. V: *Fourth International Medical Congress, 11-15 September 2013, Portoroz, Slovenia*. 2013, 48.

38. **CASAR, Božidar**, ŠARVARI, Attila, MÉNDEZ CAROT, Ignasi. Dosimetrical comparison of pencil beam and Monte Carlo algorithms for the iPlan treatment planning system using gamma analysis. V: *An international meeting dedicated to advanced brain and body radiosurgery*, (Journal of radiosurgery and SBRT, 2, suppl. 1. Toronto: Old City Publishing. 2013, 101-102.

39. MÉNDEZ CAROT, Ignasi, HARTMAN, Vida, HUDEJ, Rihard, PETERLIN, Primož, STROJNIK, Andrej, ŠARVARI, Attila, **CASAR, Božidar**. A novel method for EBT2 radiochromic film dosimetry. V: *Estro 31, 9-13 May, 2012, Barcelona, Spain*, (Radiotherapy and oncology, ISSN 0167-8140, vol. 103, suppl. 1). Amsterdam: Elsevier. 2012, S506.

40. **CASAR, Božidar**, VOJVODIĆ, Ilija, ROBAR, Vlado, SEKEREŠ, Boris. System for TBI with translation method on linear accelerator. V: BREGANT, Paola (ur.), DE DENARO, Mario (ur.), FORNASIER, Maria Rosa (ur.). *Proceedings of V Alpe-Adria Medical Physics Meeting, Trieste, Italy, May 3-5, 2012*. Trieste: ICTP. 2012, 33-34.

41. ŠARVARI, Attila, **CASAR, Božidar**, MÉNDEZ CAROT, Ignasi. Dosimetric verification of iPlan RT dose treatment planning system for Novalis TX linear accelerator. V: CASAR, Božidar (ur.), et al. *Proceedings of 4th Austrian, Italian, Slovenian and Croatian Medical Physics Meeting [also] Alpe Adria Medical Physics Conference, Ljubljana, Slovenia, May 20-22, 2010*. Ljubljana: Institute of Occupational Safety. 2010, 46-47.

42. MÉNDEZ CAROT, Ignasi, ŠARVARI, Attila, HUDEJ, Rihard, ROBAR, Vlado, **CASAR, Božidar**. Measuring small photon beams output factors - application of linear correction factors. V: CASAR, Božidar (ur.), et al. *Proceedings of 4th Austrian, Italian, Slovenian and Croatian Medical Physics Meeting [also] Alpe Adria Medical Physics Conference, Ljubljana, Slovenia, May 20-22, 2010*. Ljubljana: Institute of Occupational Safety. 2010, 79.

43. **CASAR, Božidar**, ŠARVARI, Attila. Experimental verification of the calculated dose for stereotactic radiosurgery with specially designed white polystyrene phantom. V: KRAMAR, Peter (Ed.), et al. *Conference programme & book of abstracts*, 11th Mediterranean Conference on Medical and Biological Engineering and Computing - Medicon 2007, Ljubljana, June 26-30, 2007. Ljubljana: Fakulteta za elektrotehniko. 2007, 277.

44. **CASAR, Božidar**, ŠARVARI, Attila, SEKEREŠ, Boris, VERK, Tomaž. Dosimetrical verification of the calculated dose for stereotactic radiosurgery. *Radiotherapy and oncology*, 2007, 84, suppl. 1, S290.

45. **CASAR, Božidar**, ZDEŠAR, Urban. Determination of fluence scaling factors for plastic water for high-energy electron beams using IAEA TRS-398 code of practice. V: *8th Biennial ESTRO meeting on physics and radiation technology for clinical radiotherapy, Amsterdam, October 24-28, 2004*, (Radiotherapy and oncology, 73, suppl. 1). Amsterdam: Elsevier. 2004, S114.

46. **CASAR, Božidar**, ZDEŠAR, Urban. Clinical reference dosimetry: comparison between IAEA TRS-398 and IAEA TRS-277 dosimetry protocols for high energy photon beams. *Physica medica*, 2003, 19(1), 73.

47. **CASAR, Božidar**, ZDEŠAR, Urban. Medical physics in Slovenia. V: CASAR, Božidar (ur.), SCHMIDT, Werner (ur.), ZDEŠAR, Urban (ur.). *Role and status of medical physicists, diagnostics & nuclear medicine, new developments in teletherapy: [course book]*. Ljubljana: Onkološki inštitut: = Institute of Oncology. 2002, 34.

48. **CASAR, Božidar**, MILOŠEVIČ, Zoran, SEKEREŠ, Boris. Polystyrene phantom for simulation of stereotactic radiosurgery using radiochromic films. V: CASAR, Božidar (Ed.), JERAJ, Robert (Ed.). *Book of abstracts*, Research Meeting on Andvances in Cancer Therapy, Ljubljana, 19th May 2000. Ljubljana: Institute of Oncology. 2000, 10.

49. IKIĆ, Vojislav, NINKOVIĆ, Z., KOLAR, M., **CASAR, Božidar**. Monitoring the movements of the prostate during irradiation. *Radiotherapy and oncology*, 2000, 56, suppl. 1, S169.

50. VERK, Tomaž, **CASAR, Božidar**, UMEK, Bogdan, SEKEREŠ, Boris. Dose dispersion in total body irradiation with translation method. *Physica medica*, 1999, 15(3), 158.

10.4 Book or a chapter in a monography

51. **CASAR, Božidar**. Osnove radiofizike in sevanja. V: HOČEVAR, Marko (ur.), STROJAN, Primož (ur.). *Onkologija: učbenik za študente medicine*. 1. Edition, Ljubljana: Onkološki inštitut: = Institute of Oncology. 2018, 205-224. https://www.onko-i.si/fileadmin/onko/datoteke/Dejavnosti/Raziskovalna_in_izobrazevalna_dejavnost/onkologija/Onkologija_ucbenik_april2018. pdf.

52. STROJAN, Primož, **CASAR, Božidar**, PETRIČ, Primož, SERŠA, Gregor. Radioterapija. V: NOVAKOVIĆ, Srdjan (Ed.), et al. *Onkologija : raziskovanje, diagnostika in zdravljenje raka*. 1. Edition. Ljubljana: Mladinska knjiga. 2009, 120-155. ISBN 978-961-01-0744-6.

53. BOŠNJAK, Roman, BUNC, Gorazd, **CASAR, Božidar**, CHUDY, Darko, DOLENC, Vinko V., KOCIJANČIČ, Igor, KORŠIČ, Marjan, LIPOVŠEK, Matej, MILOJKOVIČ, Vojin, PREGELJ, Rado, PRESTOR, Borut, RAVNIK, Janez, SMRDEL, Uroš, STROJNIK, Tadej, ŠERUGA, Tomaž, VORŠIČ, Matjaž, STROJNIK, Tadej (editor in chief). *Izbrana poglavja iz nevrokirurgije*. 1. izd. Maribor: Medicinska fakulteta, 2010. 340 pp., ilustr. ISBN 978-961-6739-15-3.

54. **CASAR, Božidar**. *Praktikum iz radioterapevtske fizike*. Ljubljana: Zdravstvena fakulteta, 2015. 40 pp. ISBN 978-961-6808-58-3.

55. AFFONSECA, M., ANDREO, P., ARIB, M., BJERKE, H., **CASAR, Božidar**, CZAP, L., DUANE, S., FERREIRA, H., GRINDBORG, J-E., HARTMANN, G.H., et al. *Implementation of the International Code of Practice on Dosimetry in Radiotheraphy (TRS 398) : review of testing results*, (IAEA-Tecdoc, 1455). Vienna: IAEA - International Atomic Energy Agency, cop. 2005. 102 pp. ISBN 92-0-105005-4.